PHILOSOPHICAL TRANSACTIONS OF THE ROYAL SOCIETY A MATHEMATICAL, PHYSICAL & ENGINEERING SCIENCES

Kinetic Mechanism, Structure and Properties of Premixed Flames in Hydrogen-Oxygen-Nitrogen Mixtures

G. Dixon-Lewis

Phil. Trans. R. Soc. Lond. A 1979 **292**, 45-99
doi: 10.1098/rsta.1979.0045

KINETIC MECHANISM, STRUCTURE AND PROPERTIES OF PREMIXED FLAMES IN HYDROGEN–OXYGEN–NITROGEN MIXTURES

By G. DIXON-LEWIS

Department of Fuel and Combustion Science, The University, Leeds LS2 9JT, U.K.

(*Communicated by T. M. Sugden, F.R.S. – Received* 10 *May* 1978)

CONTENTS

Vol. 292. A 1388. 6 [Published 24 August 1979

The composite flux method described by Dixon-Lewis, Goldsworthy & Greenberg (1975*a*) for the computation of detailed temperature and composition profiles in suitable flames has been applied to the simulation of the properties of a number of fuel-rich and fuel-lean hydrogen–oxygen–nitrogen flame systems. The reaction mechanism proposed by Day, Dixon-Lewis & Thompson (1972), extended to include all the reverse reactions, has been used in the simulation, together with assumed sets of reaction rate and transport parameters. The computed profiles have then been compared with published measurements in flames, covering a wide range of experimental conditions, in order to arrive iteratively at an optimum, self-consistent set of rate parameters which also takes full account of the available elementary reaction rate data from sources other than flames. The flame properties considered in this part of the investigation were (*a*) radical recombination profiles in both fuel-rich and fuel-lean flames, and (*b*) the burning velocities and properties of the main reaction zones of several low temperature, slow burning, fuel-rich flames. Three sets of rate parameters which satisfy all the constraints, and which differ only in detail, are given as sets 1, 2 and 3 in table 4 of the paper.

Measurements by Kaskan (1958*b*) of radical recombination in the hydrogen-lean systems have used the (0, 0) band ultraviolet absorption of the hydroxyl radical in order to measure its concentration. The interpretation of the measurements so as also to be consistent with the remaining flame measurements by other methods additionally allows a determination of the oscillator strength associated with the transition. A band oscillator strength $f_{00} = 9.5 \times 10^{-4}$ was found.

Following the establishment of the reaction rate parameters, one set of these (table 9) was used to calculate the expected properties of the whole composition range of hydrogen–air premixed flames. In these cases, as well as in the calculations already summarized, either partial equilibrium or kinetic quasi-steady state assumptions must be used in conjunction with the composite flux method. Partial equilibrium assumptions on the reactions

$$OH + H_2 \rightleftharpoons H_2O + H, \quad \text{(i)}$$

$$H + O_2 \rightleftharpoons OH + O, \quad \text{(ii)}$$

$$O + H_2 \rightleftharpoons OH + H, \quad \text{(iii)}$$

may be employed to relate the concentrations of H, OH, O and O_2 in calculations where only the concentration profiles in the recombination regions of the flames are required. In the calculation of complete flame properties, quasi-steady state assumptions must be used to relate the concentrations either of O, OH and HO_2 with that of H (rich flame formulation), or of H, O and HO_2 with that of OH (lean flame formulation). Subsequent investigation showed that the quasi-steady state assumptions were not completely valid for oxygen atoms everywhere in the flames. Nevertheless, further calculations on several flames by the completely different approach of implicit finite difference solution of the time-dependent flame equations, which does not involve any quasi-steady state assumptions, led to results essentially identical with the original computations. The departures from the quasi-steady state do not therefore significantly affect the flame properties computed by the composite flux method.

The general pattern of flame structure which emerges from the complete flame calculations is one in which radicals are produced by chain branching reactions in the hotter regions of the flames, while the major heat releasing reactions occur at lower temperatures. Ahead of the heat release zone there is only a very small preheat zone where heating occurs purely by thermal conduction. This behaviour is different from that of flame models which assume a large preheat zone coupled with a single global exothermic reaction of high activation energy.

Comparison of the results of calculations which employed respectively the partial equilibrium and quasi-steady state assumptions showed that the former were valid in the 'recombination zones' of the flames for predicting the concentrations of those species which are present in significant amounts. Except in lower temperature flames, for example the 15% hydrogen–air flame and to some extent the 70% hydrogen–air

flame, the 'recombination zones' extend almost back from the hot boundaries of the flames to the maxima in the hydrogen atom mole fraction profiles.

On continuing the flame integrations back from the recombination zones into the main reaction zones, the quasi-steady state overall radical concentrations, represented by $X_H + 2X_O + X_{OH}$, where X is mole fraction, fall below those calculated with the partial equilibrium assumptions. On the other hand, the distribution of the radical pool between H, O and OH is such that in fuel-rich flames the comparatively small quasi-steady state oxygen atom concentration, and to a lesser extent also the hydroxyl radical concentration, appreciably overshoot their partial equilibrium values. This is referred to as *kinetic overshoot*. It is observable only in sufficiently fuel-rich flames, and for example, there is no observable hydroxyl radical kinetic overshoot in hydrogen–air flames containing less than about 50% hydrogen, and no similar oxygen atom overshoot in those with less than 30% hydrogen.

A fundamental feature of the flame model used is that it assumes a state of thermal equilibrium to exist at each point in the flames, so that the properties of the gas at each point can be represented by a single temperature. This assumption may not be valid in faster flames, because of the finite velocities of relaxation of thermal disequilibrium between the various degrees of freedom in the system. Properly carried out, a comparison of the computed burning velocities of the hydrogen–air flames with experimental observation should throw light on the possible effect of such slow relaxation on the flame properties. However, an attempt at such a comparison initially raised several questions about the interpretation of burning velocity measurements. These are fully discussed. The hydrogen–air flame having the maximum burning velocity is that containing 41% hydrogen. At this composition it is concluded that the true burning velocity lies in the range (285 ± 10) cm s^{-1}, and hence is not more than 4 or 5% above the computed value.

Finally, the effect on the computed flame properties of (*a*) changes in the diffusion coefficient and (*b*) neglect of thermal diffusion of hydrogen atoms was investigated. Other conditions being equal in fuel-rich hydrogen–air flames near stoichiometric, the neglect of thermal diffusion caused an increase of 5–6% in the computed burning velocity.

1. Introduction

Although studies of the structure and properties of a number of low temperature, fuel-rich hydrogen–oxygen supported flames (Dixon-Lewis, Sutton & Williams 1970; Dixon-Lewis 1970*a*; Day, Dixon-Lewis & Thompson 1972; Day, Thompson & Dixon-Lewis 1973) have established the participation of the reactions

	ΔH°_{298}/(kJ mol^{-1}) (forward reaction)	
$OH + H_2 \rightleftharpoons H_2O + H$	−63.30	(i)
$H + O_2 \rightleftharpoons OH + O$	+70.67	(ii)
$O + H_2 \rightleftharpoons OH + H$	+8.26	(iii)
$H + O_2 + M \rightleftharpoons HO_2 + M$	−197.07	(iv)
$H + HO_2 \rightleftharpoons OH + OH$	−159.98	(vii)
$H + HO_2 \rightleftharpoons O + H_2O$	−231.54	(vii*a*)
$H + HO_2 \rightleftharpoons H_2 + O_2$	−238.91	(xii)
$OH + HO_2 \rightleftharpoons H_2O + O_2$	−302.21	(xiii)
$O + HO_2 \rightleftharpoons OH + O_2$	−230.65	(xiv)

$$H + H + M \rightleftharpoons H_2 + M \qquad -435.97 \qquad \text{(xv)}$$

$$H + OH + M \rightleftharpoons H_2O + M \qquad -499.28 \qquad \text{(xvi)}$$

$$H + O + M \rightleftharpoons OH + M \qquad -427.72 \qquad \text{(xvii)}$$

$$OH + OH \rightleftharpoons O + H_2O \qquad -71.56, \qquad \text{(xviii)}$$

in the flame mechanism, the rate parameters of many of these steps are only very imperfectly known. The same elementary processes also form an important group of reactions in hydrocarbon–air flames, and reliable information about the rate parameters therefore becomes doubly important, not only in connection with hydrogen–oxygen supported flames themselves, but also as an aid to the elucidation of the more complex hydrocarbon–air flame mechanisms. Following the development of the composite flux method for the computation of flame properties (Dixon-Lewis, Goldsworthy & Greenberg 1975*a*), both species concentration profiles in the recombination regions of certain hydrogen–oxygen–nitrogen flames, and complete flame properties in others, covering a wide range of experimental conditions, have been calculated by assuming sets of reaction rate and other parameters. The computed properties have then been compared with published measurements on flames in order to test the validity of the assumed sets of data, and to construct a satisfactory flame model.

The earlier sections of the present paper are concerned with discussion of radical recombination in both fuel-rich and fuel-lean hydrogen–oxygen–nitrogen flames, and of the overall properties and main reaction zones of some low temperature, slow burning, fuel-rich flames. In addition to the flame velocities, a number of flame profiles which have been measured in these situations are used to contribute to the establishment of certain of the unknown rate parameters. A complete set of rate parameters from these studies has then been used to calculate the expected properties of a number of premixed hydrogen–air flames, covering the whole flammable range of composition at atmospheric pressure. In addition to providing burning velocities for comparison with experiment, these calculations also provide an insight into the mechanism of propagation of the flames. In all cases the heat release extends over the whole of the temperature range, and occurs principally by the low activation energy reaction (iv) of hydrogen atoms with molecular oxygen, followed by one of the reactions (vii), (vii*a*), (xii), (xiii) or (xiv) of HO_2 with H, OH or O, and then where appropriate by one or both of reactions (i) and (iii) to re-form the hydrogen atom. These heat releasing cycles are effectively either chain propagating or chain terminating. The atoms responsible for them are produced by the chain branching cycle consisting of reactions (i), (ii) and (iii) in the hotter regions of the flames, and they diffuse upstream to meet the incoming oxygen and react with it by the lower activation energy cycles via reaction (iv). Superimposed on all this are the effects of the radical recombination steps (xv), (xvi) and (xvii), but because of competition with reaction (iv) these only become dominant in situations where molecular oxygen is more or less absent, for example in the recombination zones of fuel-rich flames. The approaches to the determination of the rate coefficients described in the earlier parts of the paper have involved more detailed assessments of the dominant reactions in various flame situations.

Since the faster hydrogen–air flames studied in the later parts of the paper are all too narrow for measurements to be possible within the main reaction zones, the computations here provide the only avenue of approach to the determination of the flame structures. They also allow an assessment to be made of the ranges of applicability of the partial equilibrium and quasi-steady state assumptions in relation to the distribution of the radical populations within the flames.

To conclude this general discussion of the flame reaction mechanism, there are two features

which require additional comment. The first of these is the omission of a group of elementary steps which involve the participation of hydrogen peroxide. Such a group is an essential part of the mechanism controlling certain characteristics of the slow reaction and explosion limit behaviour under isothermal conditions. The reason for its omission here is that the occurrence of all the reactions of the group depends on the initial formation of hydrogen peroxide by one or both of the steps

$$HO_2 + HO_2 \longrightarrow H_2O_2 + O_2, \qquad (x)$$

$$HO_2 + H_2 \longrightarrow H_2O_2 + H. \qquad (xi)$$

Because the combined concentrations of H, OH and O in the flames at atmospheric pressure and below are very much higher than the concentration of HO_2 at all positions except a very small region at the start of the reaction zone, reactions (vii), (xii), (xiii) and (xiv) dominate reaction (x) almost throughout. Details of the argument with respect to both reactions (x) and (xi) have been given for lower temperature flames by Dixon-Lewis (1970*a*), and the omission may be justified in similar manner for hotter flames.

The second feature requiring comment is the introduction of the whole series of reverse reactions into the mechanism. Although many of these only become significant in limited regions of the flames, they are nevertheless essential for the representation of the approach to full equilibrium in the hot gases. Reactions (−i), (−ii), (−iii) and (−xviii) further play a significant role in the whole of the recombination zones of the flames.

2. Methods of computation

All but a few of the calculations described in the paper followed in detail the methods described by Dixon-Lewis *et al.* (1975*a*), and they employed either the partial equilibrium assumptions or appropriate quasi-steady state assumptions in order to divide the overall radical pool consisting of H, O and OH (and also HO_2 in the quasi-steady state cases) into its constituent species. Integration was carried out backwards from the hot sides of the flames, starting from perturbed full equilibrium situations. Initially, both the partial equilibrium and quasi-steady state assumptions were used separately to calculate the radical recombination profiles in the flames discussed in §§4 and 7. Comparison of the two sets of computed profiles, discussed in §8, then showed the extents of the burnt gas regions of the flames over which the two methods gave identical results. Following this some of the later *complete* flame calculations were started as before from a perturbed full equilibrium situation, but treated the appropriate burnt gas region by means of the partial equilibrium assumptions. Such initial calculations evaluated the diffusional fluxes of all the flame species at a position further into the flame. At this position the partial equilibrium profiles were then themselves given small perturbations in order to introduce the quasi-steady state assumptions; and the diffusional fluxes, already calculated, were introduced artificially into the newly started quasi-steady state calculation.

As a test of the validity of the quasi-steady state approach, a single calculation is also discussed in §8, in which the oxygen atom flux and concentration changes were treated from first principles, their separate reaction rate expressions being used explicitly. The calculation was carried out for a 30% hydrogen–air flame. The composite flux method of Dixon-Lewis *et al.* (1975*a*), was again employed, but the effective radical pool now consisted only of H, OH and HO_2, with the oxygen

atom treated as a separate species. The net reaction rates q^*, given by equations (32) of Dixon-Lewis *et al.*, are now replaced by

$$\left.\begin{aligned} q^*_{\mathrm{H}} &= q_{\mathrm{H}} + \tfrac{1}{17} q_{\mathrm{OH}} (+ \tfrac{1}{33} q_{\mathrm{HO_2}}), \\ q^*_{\mathrm{H_2}} &= q_{\mathrm{H_2}} - \tfrac{2}{17} q_{\mathrm{OH}}, \\ q^*_{\mathrm{H_2O}} &= q_{\mathrm{H_2O}} + \tfrac{18}{17} q_{\mathrm{OH}}, \\ q^*_{\mathrm{O}} &= q_{\mathrm{O}}, \\ q^*_{\mathrm{O_2}} &= q_{\mathrm{O_2}} (+ \tfrac{32}{33} q_{\mathrm{HO_2}}), \\ q^*_{\mathrm{OH}} &= q^*_{\mathrm{HO_2}} = 0, \\ q^*_{\mathrm{N_2}} &= q_{\mathrm{N_2}} = 0. \end{aligned}\right\} \qquad (1)$$

The stoichiometry of the recombination steps (xii), (xiii), (xv) and (xvi) become, on this formulation

$$\mathrm{H} + \mathrm{H} \rightleftharpoons \mathrm{H_2},$$

while the stoichiometries of reactions (ii), (iii), (vii), (vii*a*), (xiv), (xvii) and (xviii) become

$$\mathrm{H} + \mathrm{O_2} (+ \mathrm{H_2}) \rightleftharpoons \mathrm{H} + \mathrm{H_2O} + \mathrm{O}, \qquad (\mathrm{ii}')$$

$$\mathrm{O} + \mathrm{H_2} (+ \mathrm{H_2}) \rightleftharpoons \mathrm{H_2O} + 2\mathrm{H}, \qquad (\mathrm{iii}')$$

$$\mathrm{H} + \mathrm{O_2} + \mathrm{M} (+ \mathrm{H} + 2\mathrm{H_2}) \rightleftharpoons 2\mathrm{H_2O} + 2\mathrm{H} + \mathrm{M}, \qquad (\mathrm{vii}')$$

$$\mathrm{H} + \mathrm{O_2} + \mathrm{M} (+ \mathrm{H}) \rightleftharpoons \mathrm{O} + \mathrm{H_2O} + \mathrm{M}, \qquad (\mathrm{vii}a')$$

$$\mathrm{H} + \mathrm{O_2} + \mathrm{M} (+ \mathrm{O} + \mathrm{H_2}) \rightleftharpoons \mathrm{H} + \mathrm{O_2} + \mathrm{H_2O} + \mathrm{M}, \qquad (\mathrm{xiv}')$$

$$\mathrm{H} + \mathrm{O} + \mathrm{M} (+ \mathrm{H_2}) \rightleftharpoons \mathrm{H} + \mathrm{H_2O} + \mathrm{M}, \qquad (\mathrm{xvii}')$$

$$\mathrm{H} + \mathrm{H} + \mathrm{H_2O} \rightleftharpoons \mathrm{O} + 2\mathrm{H_2}. \qquad (\mathrm{xviii}')$$

The quasi-steady state condition (35) of Dixon-Lewis *et al.* (1975*a*) is now dispensed with, but conditions (34) and (36) remain.

The problem of matching the working hot boundary values is, of course, more difficult than usual, since an extra value now needs to be matched. A satisfactory approach for the single flame was developed by means of a three stage calculation. In the stage closest to the full equilibrium hot boundary of the flame, partial equilibration of reactions (i), (ii) and (iii) was assumed. Next, in an intermediate range of integration, the complete set of quasi-steady state conditions was employed in the manner described above for the standard calculations. Integration through the whole flame on this basis also allowed approximate matching of the boundary value for the overall radical pool (consisting of H, OH, HO_2 *and* O atoms) with that for molecular oxygen. Lastly, after the short intermediate range in the final calculations, a third perturbation exactly similar to the second one was introduced, in order to allow the full kinetic treatment of the oxygen atom concentrations and fluxes. It was then necessary further to match the second and third perturbations in order to obtain the complete solution.

Finally, a few computations were carried out at a later stage by implicit finite difference solution of the time-dependent equations for some of the flames. The results from these computations, which employed no quasi-steady state assumptions, are given in §§ 8 and 9. The collaboration of Dr Ing. G. Tsatsaronis in this phase of the work is gratefully acknowledged.

3. Recombination regions of some fuel-rich flames

The composite flux method with partial equilibrium assumptions was applied first to the simulation of recombination in a series of fuel-rich hydrogen–oxygen–nitrogen flames which have been studied experimentally by Halstead & Jenkins (1969, 1970), Kaskan (1958*a*) and Dixon-Lewis, Sutton & Williams (1962). The equilibrium constants K_1, K_2 and K_3 were represented during the calculations by the expressions due to Del Greco & Kaufman (1963):

$$K_1 = 0.21 \exp(+7640/T),$$
$$K_2 = 300.0\,T^{-0.372} \exp(-8565/T),$$
$$K_3 = 2.27 \exp(-938/T).$$

These and other thermodynamic data were taken from JANAF (1971). For the remaining independent equilibrium constants the expressions used (cm mol s units) were

$$K_4 = 0.745 \exp(+23\,380/T),$$
$$K_{15} = 0.24 \exp(+52\,590/T),$$
$$K_{16} = 0.0594 \exp(+59\,910/T),$$
$$K_{17} = 0.565 \exp(+51\,570/T).$$

The latter were deduced by simple parametric fitting of the van't Hoff isochore to equilibrium constants determined at 1500 and 2500 K from the tabulations. The fitting for K_4, K_{15}, K_{16} and K_{17} was restricted to this temperature range since the reverse reactions (−iv), (−xv), (−xvi) and (−xvii) only become of significance near full equilibrium in higher temperature flames. Del Greco & Kaufman (1963) claim 3% accuracy for their expressions for K_1, K_2 and K_3 over the whole temperature range from 300 to 2400 K.

Most of the data for the transport property calculations have been given by Dixon-Lewis (1968). Interactions involving H, OH and O were represented here by the Lennard–Jones (12:6) potential, the following force constants given by Svehla (1962), except for σ_H, being used:

$$(eps)_H/k = 37.0\,\mathrm{K}, \qquad \sigma_H = 0.35\,\mathrm{nm},$$
$$(eps)_{OH}/k = 79.8\,\mathrm{K}, \qquad \sigma_{OH} = 0.3147\,\mathrm{nm},$$
$$(eps)_O/k = 106.7\,\mathrm{K}, \qquad \sigma_O = 0.305\,\mathrm{nm}.$$

The value for σ_H is some 25–30% higher than the value of 0.271 nm recommended by Svehla. The precise value is not too important in the present context of rather fast flames, and it will be discussed further in §§4 and 9.

Because H_2O is the polar component present in major concentration in all the mixtures studied, and because the theory will deal only with mixtures containing not more than one polar component, the hydroxyl radical was considered as a non-polar molecule. The collision number $\zeta_{OH,j}$ for rotational relaxation of OH on colliding with any other species j was taken to be 4.5 collisions.

Table 1 lists the properties of twelve flames studied by Halstead & Jenkins (1969, 1970), Kaskan (1958*a*) and Dixon-Lewis *et al.* (1962). With hindsight, given values of all the rate parameters which fit the body of results discussed in the paper, the last three columns of table 1 show the

relative importance of the different recombination reactions in these flames. The approximate percentages of primary removal by reactions (xv), (xvi) and (iv) are given for points lying roughly midway through the recombination zones. In the rich flames these percentages do not alter much over the whole region. In all the flames the concentration of oxygen atoms in the recombination region is at least an order of magnitude less than the concentration of hydroxyl; so that for reasonable values of k_{17}, the contribution of reaction (xvii) may be neglected. Clearly the major recombination steps in the rich flames are reactions (xv) and (xvi) only. Analysis of the recombination in these flames thus involves optimization of the rate coefficients k_{15} and k_{16} so as to give the best overall agreement with experiment. The values assigned to the remaining rate parameters in the overall scheme are not critical in this context, though they were finally given values derived from an iterative process covering the complete set of results discussed in the paper.

TABLE 1. PROPERTIES OF FUEL-RICH HYDROGEN–OXYGEN–NITROGEN FLAMES IN RECOMBINATION REGION

flame	p/atm	$(H_2/O_2)_u$	$(N_2/O_2)_u$	V_b†/(cm s^{-1})	approx. temp. range of study / K	approx. percentage primary recombination by (xv) H+H+M	(xvi) H+OH+M	(iv) H+O$_2$+M
				(*a*) Halstead & Jenkins (1969, 1970)				
A	1.0	4.16	4.59	133	1680–1825	74	26	v. small
B	1.0	4.19	3.865	157	1750–1840	74	26	v. small
C	1.0	3.30	5.48	118	1825–1850	60	40	0.2
D	1.0	2.70	6.09	107	1740–1840	45	53.5	1.5
E	1.0	5.22	4.97	88	1580–1660	87	13	v. small
F	1.0	4.44	5.77	76	1540–1650	83	17	v. small
G	1.0	2.93	7.37	65	1540–1640	65	35	0.5
				(*b*) Kaskan (1958*a*)				
H	1.0	2.05	3.76	27.5	1600–1685	4	60	36
I	0.5	3.48	3.76	51.0	1225–1340	90	10	v. small
J	0.5	2.38	3.76	35.3	1460–1540	45	52	3
				(*c*) Dixon-Lewis *et al.* (1962)				
K	1.0	2.57	18.17	6.35	1030–1080	93.1	6.9	v. small
L	1.0	4.09	16.65	9.0	1030–1080	98.0	2.0	v. small
M	1.0	5.62	15.11	10.75	1030–1080	98.5	1.5	v. small

† V_b gives linear burnt gas velocity corrected to standard conditions of 298 K and p atm pressure.

During the early part of the investigation it was assumed that all the chaperon molecules H_2, N_2, O_2 and H_2O have the same efficiency in reaction (xv). On this basis Dixon-Lewis, Greenberg & Goldsworthy (1975*b*) found that $k_{15,M} = 1.5 \times 10^{15} \exp(+250/T)$ cm^6 mol^{-2} s^{-1} gave a reasonable parametric Arrhenius fit to a whole series of results between 300 and 1800 K. However, the initial assumption regarding chaperon efficiency has now been shown to be incorrect at lower temperatures. Ham, Trainor & Kaufman (1970, 1973) and Walkauskas & Kaufman (1975) have studied hydrogen atom recombination in a discharge-flow system at 77–295 K with H_2, N_2, He, Ar and certain other species as chaperon molecules, and have obtained reproducible results ($\pm 10\%$) over an extended period. Near 300 K their results with H_2 as chaperon agree well with those of Larkin & Thrush (1964, 1965), and with recent results of

Aldred & Dixon-Lewis (unpublished work). For H_2, N_2 and Ar as chaperons, Walkauskas & Kaufman (1975) find (cm mol s units):

$$k_{15,\,H_2} = 9.2 \times 10^{16}\, T^{-0.6}, \tag{2a}$$

$$k_{15,\,N_2} = 5.65 \times 10^{18}\, T^{-1.3}, \tag{2b}$$

$$k_{15,\,Ar} = 3.26 \times 10^{17}\, T^{-0.8}, \tag{2c}$$

i.e. not only are the chaperon efficiencies not equal, but also the *relative* efficiences change with temperature. The expression for $k_{15,\,H_2}$ extrapolates fairly accurately towards the shock tube results of Rink (1962), Sutton (1962), Hurle (1967), and Jacobs, Giedt & Cohen (1967). For argon, expression (2*c*) predicts somewhat high values of $k_{15,\,Ar}$ compared with the shock tube expressions from the same four papers. Jacobs *et al.* (1967) give

$$k_{15,\,Ar} = 1.0 \times 10^{18}\, T^{-1.0},$$

and this expression is found to fit both the shock tube work and the room temperature results of Walkauskas & Kaufman (1975). The situation is discussed more fully by Dixon-Lewis & Williams (1977).

Both the shock tube results of Getzinger & Blair (1969) and the flame results of Halstead & Jenkins (1970) suggest $k_{15,\,N_2} \approx k_{15,\,Ar}$ at around 2000 K. The fast flow results of Walkauskas & Kaufman (1975) give $k_{15,\,N_2} = k_{15,\,Ar} = 3.4 \times 10^{15}$ cm^6 mol^{-2} s^{-1} at room temperature. A good approximation for both gases between 300 and 2000 K is therefore likely to be given by the expression of Jacobs *et al.* (1967):

$$k_{15\ M=Ar,\,N_2} = 1.0 \times 10^{18}\, T^{-1.0}. \tag{2d}$$

For flames containing a large excess of hydrogen, reaction (xvi) is of little importance. Its importance increases as the composition approaches stoichiometric from the rich side. However, the occurrence of reaction (xvi) always creates difficulties in the analysis of recombination results when the partial equilibrium assumptions are employed, since it becomes impossible to separate $k_{15,\,H_2O}$ from $k_{16,\,H_2}$. The observed recombination depends on the combined parameter $(k_{15,\,H_2O} + k_{16,\,H_2}/K_1)$, together with the remaining four rate coefficients $k_{15,\,H_2}$, $k_{15,\,N_2}$, $k_{16,\,H_2O}$ and $k_{16,\,N_2}$. To resolve this difficulty regarding $k_{15,\,H_2O}$ and $k_{16,\,H_2}$, it has been assumed here (i) that $k_{16,\,H_2} = k_{16,\,N_2}$ and (ii) that $k_{16,\,H_2O} = 5k_{16,\,N_2}$. The second assumption is close to the evaluation of Baulch, Drysdale, Horne & Lloyd (1972).

No reliable information on k_{17} is available. Because of the low oxygen atom concentrations in the rich flames, reaction (xvii) is likely to be much less important than either (xv) or (xvi). The relative chaperon efficiencies of H_2, N_2 and H_2O in reaction (xvii) were assumed to be the same as for reaction (xvi), and k_{17} was arbitrarily assigned the expression $k_{17,\,H_2} = 6.2 \times 10^{16}\, T^{-0.6}$.

With the assumptions stated regarding k_{16} and k_{17}, there remain two unknown parameters, $(k_{15,\,H_2O} + k_{16,\,H_2}/K_1)$ and $k_{16,\,N_2}$, which may be determined by experiment, and which, once known, permit all six rate coefficients associated with reactions (xv) and (xvi) to be derived. For a range of compositions for which the contribution of reaction (xvi) to the recombination varied between approximately 25 and 50 %, the optimum values of $(k_{15,\,H_2O} + k_{16,\,H_2}/K_1)$ and $k_{16,\,N_2}$ at 1900 K were estimated from the results of Halstead & Jenkins (1969, 1970) to be 5.2×10^{15} and 4.9×10^{15}, respectively. The assumptions above then lead to $k_{15,\,H_2O} = 4.8 \times 10^{15}$, i.e. $k_{15,\,H_2O}/k_{15,\,H_2} = 4.8$, at 1900 K; and combination of this result with a second value of $k_{15,\,H_2O}$ obtained at

1050 K from recombination measurements in the lower temperature flames K, L and M of table 1 gives

$$k_{15,\mathrm{H_2O}} = 6.0 \times 10^{19}\, T^{-1.25}. \qquad (2e)$$

The results from these lower temperature flames will be discussed in §4.

At 300 K, equation (2*e*) predicts $k_{15,\mathrm{H_2O}} = 4.8 \times 10^{16}$, in excellent agreement with the value of $(4.5 \pm 1.0) \times 10^{16}$ reported by Eberius, Hoyermann & Wagner (1969). The shock tube results of Gay & Pratt (1971) also suggest a high chaperon efficiency of water vapour in reaction (xv).

Using the values of k_{15} given by equations (2*a*), (2*d*) and (2*e*), together with the expressions

$$k_{16,\mathrm{M=N_2,\,H_2}} = 9.77 \times 10^{17}\, T^{-0.71}, \qquad (3a)$$

$$k_{16,\mathrm{H_2O}} = 4.89 \times 10^{18}\, T^{-0.71}, \qquad (3b)$$

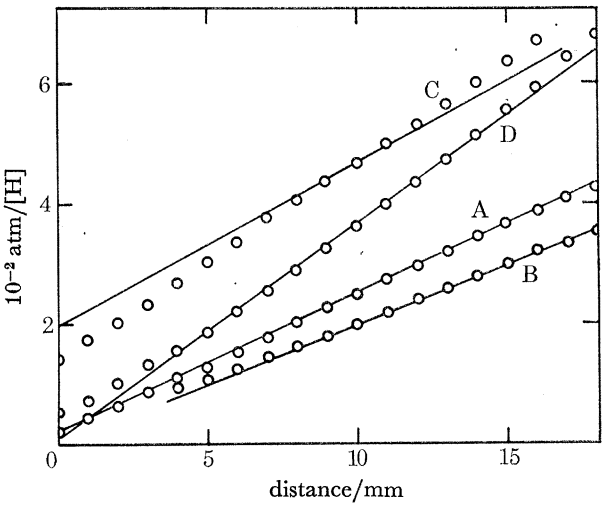

FIGURE 1. Recombination in fuel-rich hydrogen–oxygen–nitrogen flames. Comparison of measured points of Halstead & Jenkins (1969, 1970) with computed lines. Letters refer to flames of table 1. Reaction rate parameters as in table 9.

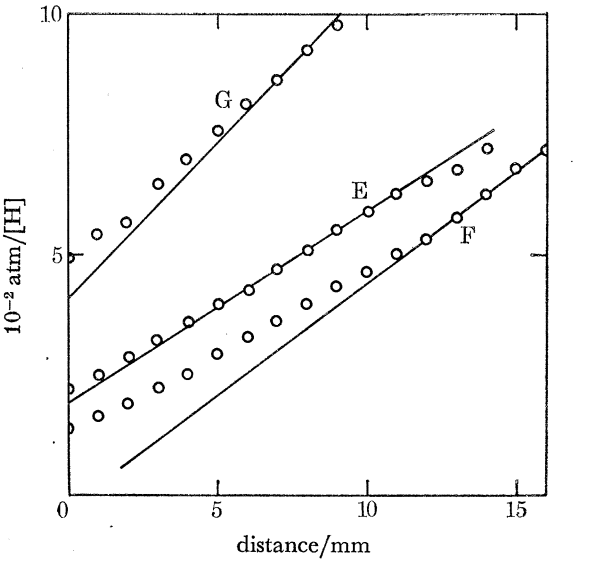

FIGURE 2. Recombination in fuel-rich hydrogen–oxygen–nitrogen flames. Comparison of measured points of Halstead & Jenkins (1969, 1970) with computed lines. Letters refer to flames of table 1. Reaction rate parameters as in table 9.

recombination profiles were calculated by the composite flux method for flames A–G of table 1. Figures 1 and 2 compare the computed profiles of the reciprocal of the hydrogen atom concentration with the measurements of Halstead & Jenkins (1969, 1970) in the temperature ranges 1750–1850 and 1550–1650 K. Agreement is satisfactory, particularly for those flames in which reaction (xv) is dominant. In this connection it may be observed that the discrepancies in flames F and G are in the direction which would be expected if the measurements had been taken far enough back into the main flame to cause the partial equilibrium assumptions to break down.

Kaskan (1958*a*) used ultraviolet absorption to measure concentrations of hydroxyl radicals in the recombination regions of several fuel-rich hydrogen–air flames, and he later (Kaskan 1958*b*) examined a number of lean flames in the same way. Discussion of Kaskan's available rich flame results is complicated by the need for discussion also of the calibration of the OH absorption measurements, and will be deferred until §5. His recombination results for flame I of table 1 are quite

consistent with the expressions (2*a*), (2*d*) and (2*e*) for k_{15}. Between 300 and 3000 K, suggested error limits for all the k_{15} are ± 0.1 in lg k.

The temperature dependence of k_{16} will also be discussed later.

4. Burning velocities, main reaction zones and recombination regions in low temperature, fuel-rich flames

(*a*) *Relevant flame data*

The flame measurements considered in this section include

(i) The burning velocity, temperature profile and profiles of the mole fraction ratios X_{H_2}/X_{N_2}, X_{O_2}/X_{N_2} and X_{H_2O}/X_{N_2} for flame L of table 1 (Dixon-Lewis *et al.* 1970). The measured profiles of the temperature and the mole fraction ratios are shown by the points in figures 3 and 4.

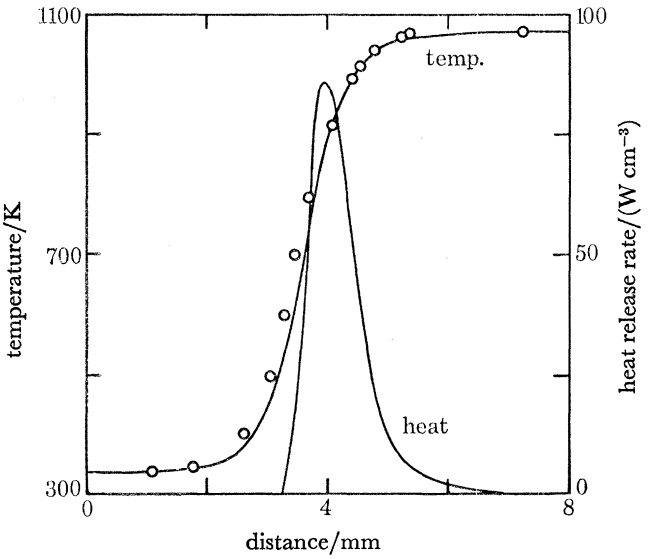

Figure 3. Comparison of computed temperature profile with observations of Dixon–Lewis *et al.* (1970) on flame L of table 1. o, Observed points; lines represent temperature profile and heat release rate profile computed with the use of reaction rate parameters given by set 2 in tables 3 and 4.

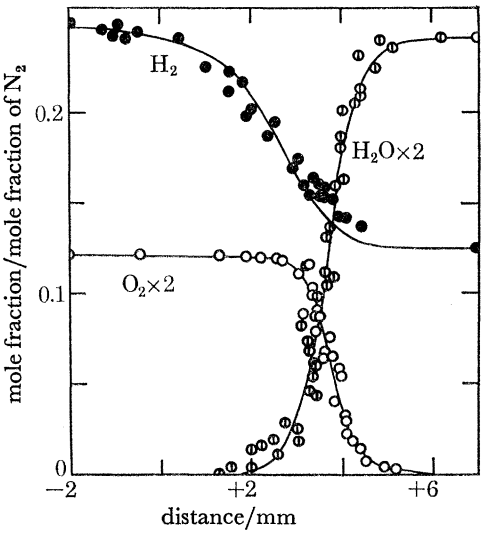

Figure 4. Ratios of mole fractions of hydrogen, oxygen and steam to mole fraction of nitrogen, to compare computed profiles with observations of Dixon-Lewis *et al.* (1970) on flame L of table 1. Points represent observations. Lines computed with the use of set 2 of reaction rate parameters from tables 3 and 4. Same distance zero as in figure 3.

(ii) Relative intensities of chemiluminescence in the burnt gas regions of flames K, L and M of table 1 when traces of sodium chloride are added to the gases entering the flames (Dixon-Lewis *et al.* 1962). These intensities are a relative measure of the square of the hydrogen atom concentration in the recombination region. The measurements, normalized with respect to the peak intensity in flame L (cf. Day *et al.* 1972), are shown by the points in figure 5.

(iii) Burning velocities of the three flames K, L and M (Day *et al.* 1972). These particular measurements form part of a larger series in which the dependence of the burning velocity on the ratio $X_{H_2,u}/X_{N_2,u}$ was examined in hydrogen–oxygen–nitrogen flames having $X_{O_2,u} = 0.0460$ and $T_u = 336$ K. The initial mole fractions, burning velocities and boundary temperatures for flames K, L and M are given in table 2, and the whole series of measured burning velocities is

shown by the points in figure 6. The burning velocities are quoted on the basis of gases at 291 K and 1 atm† pressure.

(iv) A profile of the ratio X_{CO_2}/X_{N_2} when a trace of carbon dioxide is added to the gases entering flame L (Dixon-Lewis, Sutton & Williams 1965; Dixon-Lewis 1972).

(v) Profiles of X_{HD}/X_{H_2} when traces of heavy water are added to flames K, L and M (Dixon-Lewis *et al.* 1962; Sutton 1963; Dixon-Lewis 1972).

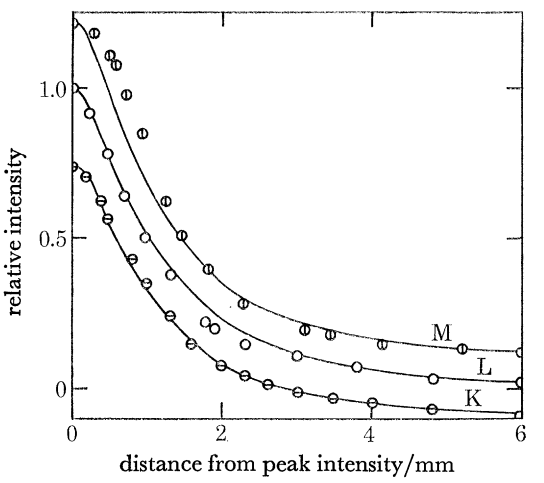

FIGURE 5. Comparison of computed relative chemiluminescent intensities with profiles observed by Dixon-Lewis *et al.* (1962) for flames K, L and M of table 1. Lines computed using set 2 of reaction rate parameters from tables 3 and 4. Observations: ○, flame L; ⊖, flame K (line and points lowered by 0.1 unit on intensity scale); ⊙, flame M (line and points raised by 0.1 unit on intensity scale).

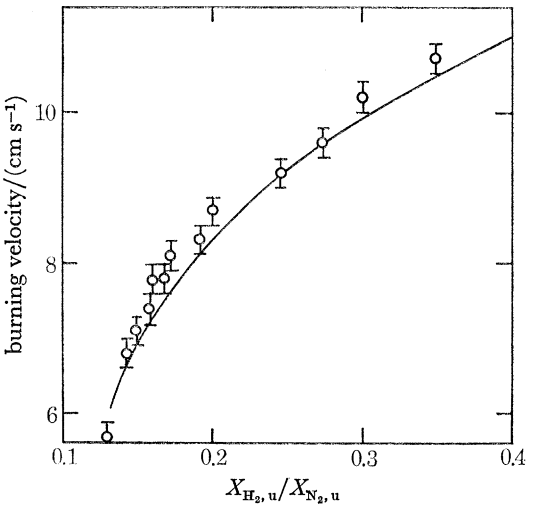

FIGURE 6. Burning velocities of hydrogen–oxygen–nitrogen flames having $X'_{O_2,u} = 0.0460$ and $T_u = 336$ K, showing dependence on the initial mole fraction ratio $X_{H_2,u}/X_{N_2,u}$, and comparing observed values of Day *et al.* (1972) with theoretical line calculated using set 2 of reaction rate parameters from tables 3 and 4. Burning velocities in this figure are on basis of gases at 291 K/1 atm.

TABLE 2. INITIAL COMPOSITIONS, FLAME TEMPERATURES AND BURNING VELOCITIES OF LOW TEMPERATURE FLAMES

(In all cases initial temperature $T_u = 336$ K.)

flame	$X_{H_2,u}/X_{N_2,u}$	$X_{H_2,u}$	$X_{N_2,u}$	$X_{O_2,u}$	T_b/K	S_u†/(cm s^{-1})
K	0.141	0.1181	0.8359	0.0460	1076.0	6.5 ± 0.2
L	0.246	0.1883	0.7657	0.0460	1078.0	9.2 ± 0.2
M	0.372	0.2587	0.6953	0.0460	1080.0	11.0 ± 0.2

† Quoted on basis of gases at 291 K and 1 atm pressure, for these three flames only.

(vi) Profiles of X_{HD}/X_{H_2} and X_{D_2}/X_{H_2} when a trace of deuterium is added to flame L (Dixon-Lewis *et al.* 1962; Dixon-Lewis 1972).

These data will now be considered in the light of information currently available from other sources.

† 1 atm ≈ 10^5 Pa.

(*b*) *Discussion of low temperature flame data in relation to reaction mechanism and rate parameters*

The results with the trace additions of carbon dioxide, heavy water and deuterium were analysed by Dixon-Lewis (1972) to give information about reaction (i) and the reactions

$$OH + HD \rightleftharpoons HOD + H, \qquad (iDa)$$

$$OH + CO \rightleftharpoons CO_2 + H. \qquad (xxi)$$

At 1050 K the ratios $k_1/k_{1Da} = 2.8$ and $k_1/k_{21} = 11.3 \pm 2.2$ were found. Additionally, the attack of hydrogen atoms on both carbon dioxide and heavy water was found to occur virtually entirely in the burnt gas recombination regions of the flames, where the relative hydrogen atom concentration profiles are known from the chemiluminescent intensity measurements already mentioned. Unfortunately, at the time of the analysis described by Dixon-Lewis (1972) information about the kinetic parameters controlling the main flame properties was insufficient to provide accurate calibrations of the hydrogen atom concentration profiles. The parameters used at that time gave a maximum hydrogen atom mole fraction of 1.07×10^{-3} in flame L, and the computations including the trace additives gave $k_1 = (2.7 \pm 0.4) \times 10^{12}$, $k_{1Da} = (9.6 \pm 0.5) \times 10^{11}$ and $k_{21} = (2.4 \pm 0.12) \times 10^{11}$, all at 1050 K. Comparison of both k_1 and k_{21} with results of other investigators at comparable temperatures suggested that both may be somewhat high; and for example, the more recent evaluation of Baulch & Drysdale (1974) gives $k_{21} = 1.75 \times 10^{11}$ at 1050 K. The possibility therefore now exists of reverting to the original purpose of some of the measurements with trace additives (Dixon-Lewis *et al.* 1962), namely, to use the reactions with the additives in order to calibrate the radical concentrations in the flames. The mean expression of Baulch & Drysdale (1974) for k_{21} would imply $X_{H,\,max} = 1.48 \times 10^{-3}$ in flame L, and this has been used as a calibration value.

To return now to the reaction mechanism, reaction ($-$iv) is always unimportant in the low temperature flames considered here, and in such flames effectively all the HO_2 formed in reaction (iv) proceeds to react with H, OH or O. For the mechanism given in § 1, the important kinetic parameters determining the flame structure and properties then become the rate coefficients k_2, k_4, k_{15} and k_{16} (and, to a lesser extent in rich flames, k_1 and k_3), and the ratios k_7/k_{12}, k_{7a}/k_{12}, k_{13}/k_{12} and k_{14}/k_{12}. It is possible to assign values to several of these parameters on the basis of information available from independent sources. Thus

(i) The ratios k_2/k_4 are reliably known at temperatures around 773 K from second explosion limit measurements in the hydrogen–oxygen system.

(ii) From the evaluations of Baulch *et al.* (1972) and Dixon-Lewis & Williams (1977), k_1 and k_3 were assigned the expressions

$$k_1 = 1.17 \times 10^9\, T^{1.3} \exp(-1825/T), \qquad (4)$$

$$k_3 = 1.8 \times 10^{10}\, T \exp(-4480/T). \qquad (5)$$

It should be noted in passing that equation (4) is entirely consistent with the new (calibration) value of $k_{21} = 1.75 \times 10^{11}$ cm^3 mol^{-1} s^{-1} at 1050 K and the ratio k_1/k_{21} derived directly from the measurements with trace additions of CO_2, D_2O and D_2 to flame L. Error limits of ± 0.1 are suggested for both values of $\lg k$ (Dixon-Lewis & Williams 1977).

(iii) Expressions for k_{15} and k_{16} have already been given in equations (2) and (3). The further assumption is made here that the chaperon efficiencies of molecular oxygen and nitrogen are

identical in each of the recombination steps. The expressions for k_{15} and k_{16} are of course still subject to test under the lower temperature flame conditions. In fact the expression (2*e*) for k_{15,H_2O} was constructed partly on the basis of the results in these flames. Error limits of $\pm 25\%$ over the temperature range 300–3000 K have been suggested for all the k_{15}. The expressions for k_{16}, which are of smaller importance, will be discussed later.

(iv) Information about k_4 at temperatures in the region of 1400 K may be obtained from analysis of the radical recombination in fuel-lean hydrogen–oxygen–nitrogen flames at low pressures. This will be discussed in §5. Further, there have recently been a number of measurements of k_4 at room temperature, in which the very sensitive absorption or resonance fluorescence of the Lyman α line has been used to study the decay of very low concentrations of hydrogen atoms ($< 4 \times 10^{-8}$ M) in the presence of 100–650 Pa of oxygen and 13–200 kPa of 'chaperon' gas. Under these conditions the decay was first order in hydrogen atom concentration, and was very much more rapid than in the absence of oxygen, thus implying no significant contribution from wall effects. The hydrogen atom concentrations were also small enough for the further reactions (vii) and (xii) of HO_2 to be unable to contribute significantly, at least at chaperon pressures above 40 kPa. The technique thus seems to be remarkably free from side effects, and should therefore give correspondingly reliable results. Using this technique with molecular hydrogen as chaperon gas, Bishop & Dorfman (1970) found $k_{4,H_2} = (17 \pm 4) \times 10^{15}$ cm^6 mol^{-2} s^{-1} at 298 K, and Wong & Davis (1974) obtained $k_{4,H_2} = (21.7 \pm 4.3) \times 10^{15}$. With a different technique using a discharge-flow system with e.s.r. detection, Moortgat & Allen (1972) found $k_{4,H_2} = 23.2 \times 10^{15}$. All these results are in good agreement with each other, and clearly the expression chosen for k_4 must be consistent with them. No information is available, however, which allows the temperature dependence of the chaperon efficiency of water vapour to be estimated relative to hydrogen. For this reason, and because water vapour is by far the most efficient chaperon in reaction (iv), it has been *assumed* here that the chaperon efficiences of N_2, O_2 and H_2O in the reaction remain constant at their known values at 773 K. In fact measurement has shown the assumption to be incorrect in the case of nitrogen (see Dixon-Lewis & Williams 1977).

It remains now to consider the ratios k_7/k_{12}, k_{7a}/k_{12}, k_{13}/k_{12} and k_{14}/k_{12}, and the rate coefficient k_2. Reactions (vii), (vii*a*) and (xii) are the various possible reactions of hydrogen atoms with HO_2, while reactions (xiii) and (xiv) are those of HO_2 with OH and O. Additionally, reactions (vii) and (vii*a*) are chain propagating steps; while (xii), (xiii) and (xiv) are chain terminating processes. The effect of varying the ratio $X_{H_2,u}/X_{N_2,u}$ on the burning velocities of the flames having $X_{O_2,u} = 0.0460$ and $T_u = 336$ K was measured by Day *et al.* (1972), and is shown in figure 6. The increased importance of reactions (xiii) and (xiv) at low $X_{H_2,u}/X_{N_2,u}$ ratios is reflected in the turn down of the burning velocity curve. From the magnitude of the negative curvature it is possible to achieve a separation of the ratios k_{13}/k_{12} and k_{14}/k_{12} from the others. It is not, however, easily possible to separate the effects of reactions (xiii) and (xiv) from each other. This latter separation involves consideration also of radical recombination results in fuel-lean hydrogen–oxygen–nitrogen flames at atmospheric pressure, again to be discussed in §5. It should be added that it is assumed here that reactions (xii), (xiii) and (xiv) all have zero activation energy. Their probable activation energies have been shown to be small (Dixon–Lewis & Williams 1977).

The lean flame recombination results at atmospheric pressure lead to $k_{13} = (8 \pm 4) \times 10^{12}$ cm^3 mol^{-1} s^{-1}. Values of k_{13} within this range were used in the present phase of calculation, and k_{14} was represented by the expression $k_{14} = a(k_7 + k_{12})$, where a is a constant which can be adjusted to fit the curvature in the burning velocity measurements. The value of a turns out to be about 0.1. The

form of the assumed expression rests on the basis that reaction (xiv) is the oxygen atom analogue of both reactions (vii) and (xii).

Because of the general similarity between the kinetic effects of reactions (vii) and (vii*a*), the distinction between these two reactions is also difficult to quantify; and rather than consider the ratios k_7/k_{12} and k_{7a}/k_{12} separately, it is probably preferable to consider the single ratio $(k_7+k_{7a})/k_{12}$, with the ratio k_{7a}/k_7 playing a subsidiary role. The earlier analyses of Day *et al.* (1972) and Dixon-Lewis *et al.* (1975*b*) both suggest that k_{7a}/k_7 is small, probably $\leqslant 0.1$. This ratio is assumed to remain constant over the whole flame, i.e. reactions (vii) and (vii*a*) are assumed to have the same activation energy.

TABLE 3. RATIOS OF RATE COEFFICIENTS AT 773 K

set	1	2	3
$(k_7+k_{7a})/k_{12}\,(=R)$	6.0	$12.0\exp(-540/T)$	$25.0\exp(-1100/T)$
R at 773 K	6.0	5.95	6.0
$(k_7+k_{7a})^2/k_2^2k_{10}$	3.20×10^{-4}	3.25×10^{-4}	3.20×10^{-4}
$(k_7+k_{7a})/k_2$	2.53×10^{4}	2.55×10^{4}	2.53×10^{4}
$k_2/k_{4,H_2}$	3.84×10^{-7}	3.84×10^{-7}	3.84×10^{-7}
k_{12}/k_2	4.22×10^{3}	4.30×10^{3}	4.22×10^{3}

With the aid of the relationships just discussed, the overall problem resolves itself essentially into determining matched values of the quantities $(k_7+k_{7a})/k_{12}$ and k_2 so as to reproduce the observed burning velocities and flame properties. Again, the earlier analysis of Day *et al.* (1972) suggested an average value of $(k_7+k_{7a})/k_{12}=6.5\pm1.0$ over the whole reaction zone. However, a more precisely defined value of $(k_7+k_{7a})/k_{12}$ at 773 K has since been obtained by Baldwin *et al.* (1974), who have re-examined their $H_2/N_2/O_2$ second explosion limit data from boric acid coated vessels. Depending on assumptions regarding the reaction between oxygen atoms and hydrogen peroxide in the systems, they found $(k_7+k_{7a})/k_{12}=5.9$ or 7.1 at 773 K, with estimated errors of $\pm25\%$ (R. R. Baldwin, private communication, 1978).

There have also been several measurements of the ratio $(k_7+k_{7a})/k_{12}$ at room temperature, and these have been discussed by Dixon-Lewis & Williams (1977). Published values of the ratio range from 2.4 ± 1.0 (Clyne & Thrush 1963), through a pair of values between 1 and 2 (Dodonov, Lavrovskaya & Talrose 1969; Bennett & Blackmore 1971) to approximately 0.6 (Westenberg & de Haas 1972). Taken in combination with the result of Baldwin *et al.* (1974), all these values imply that $(k_7+k_{7a})/k_{12}$ has a rather small activation energy, with extreme values of perhaps zero and 9 kJ mol^{-1}. Of the three expressions selected for further investigation, namely $(k_7+k_{7a})/k_{12}=6.0$, $12.0\exp(-540/T)$ and $25.0\exp(-1100/T)$, the second one corresponds closely with the median result of Clyne & Thrush (1963) at room temperature. In the following discussion, the three sets of parameters resulting from the use of these expressions will be referred to as 1, 2 and 3, respectively. All three sets give $(k_7+k_{7a})/k_{12}=6.0$ at 773 K.

Finally in connection with the reactions of HO_2 with H, OH and O, although the important parameters which determine the properties of these low temperature flames are the ratios such as $(k_7+k_{7a})/k_{12}$, the more refined quasi-steady state calculation of Dixon-Lewis *et al.* (1975*b*) takes account also of all the reverse reactions in the mechanism, and thus requires the absolute rate coefficients $k_7, k_{7a}, k_{12}, k_{13}$ and k_{14} as input data. The situation is again resolved by recourse to $H_2/N_2/O_2$ second limit results from boric acid coated vessels. Baldwin *et al.* (1974) find

$(k_7+k_{7a})^2/k_2^2 k_{10} = 2.48\times10^{-4}$ or 3.27×10^{-4} mol cm^{-3} s for $(k_7+k_{7a})/k_{12} = 7.1$ or 5.9 respectively, where reaction (x) is

$$HO_2+HO_2 = H_2O_2+O_2. \qquad (x)$$

By interpolating linearly within these ranges, the three selected expressions for $(k_7+k_{7a})/k_{12}$ lead at 773 K to the ratios given in the last four lines of table 3. The conversion from $(k_7+k_{7a})^2/k_2^2 k_{10}$ to $(k_7+k_{7a})/k_2$ assumes $k_{10} = 2.0\times10^{12}$ cm^3 mol^{-1} s^{-1} at 773 K. This is the same as the mean room temperature value found by Foner & Hudson (1962) and Paukert & Johnston (1972). i.e. it is assumed that $E_{10} = 0$. Confirmation that E_{10} is small is provided by the results of Tröe (1969), who examined the growth and decay of hydroperoxyl during the decomposition of hydrogen peroxide highly diluted with argon at high temperatures. Tröe's experiments were conducted in shock waves at temperatures between 950 and 1450 K, and if anything, the results suggest that k_{10} is a little less than 2×10^{12} in this temperature range (see also Dixon-Lewis & Williams 1977).

The important unknown parameters in the hydrogen–oxygen–nitrogen flames have now all been expressed at 773 K in terms of k_2 (table 3) Further, if an activation energy is assigned to reaction (ii) ($E_2 = 69.3$ kJ mol^{-1} has been used in this paper), then the constraints and assumptions outlined are such that the whole system becomes virtually completely defined once the pre-exponential factor A_2 is established. The full set of kinetic unknowns are A_2, the constant a in the expression for k_{14}, and the rather less important ratio k_{7a}/k_7. With an assumed small value for k_{7a}/k_7, the remaining two unknown parameters may be established from consideration, firstly, of the absolute values of the burning velocities and, secondly, of their variation with initial X_{H_2}/X_{N_2} ratio (figure 6). A check on the correctness of the whole series of assumptions is then provided by a comparison of the computed profiles with the requirements of the measurements outlined in §4(*a*).

(*c*) *Optimization of rate coefficients and comparison of computed profiles with experiment*

The first three groups of columns in table 4 give the three sets of kinetic parameters, corresponding with sets 1, 2 and 3 of table 3, which are capable of reproducing the observed burning velocities (table 2). The sensitivity to k_2 was such that simultaneous increases of 10% in its assumed value and the related values of k_4, k_7, k_{7a}, k_{12}, k_{13} and k_{14} caused a 6–7% increase in the computed burning velocity. The expressions for k_{4,H_2} in table 4 were based on a combination of the ratios $k_2/k_{4,H_2}$ at 773 K from table 3 with the result of Bishop & Dorfman (1970) at 298 K. They will be discussed further in §5(*a*). Constant chaperon efficiencies of 0.44, 0.35 and 6.5 were assumed for N_2, O_2 and H_2O respectively in reaction (iv), relative to $H_2 = 1.0$. The complete flame profiles were computed by the composite flux method with quasi-steady state assumptions to relate the concentrations of OH, O and HO_2 with the concentration of H atoms in the radical pools of the fuel-rich flames. Figures 7 and 8 show the profiles computed for flame L, with set 2 of rate parameters. In all the runs, the molecular interactions for the transport property calculations were represented by the Lennard-Jones (12:6) potential as in §3, except that for the runs of table 4 the molecular diameter σ_H was changed from 0.35 to 0.30 nm. This led to an increase of approximately 15% in the diffusion coefficient of H atoms in the flame gases. The change was made in order to bring the computed maximum H atom concentration of flame L into line with the calibration outlined earlier (giving $X_{H,\,max} = 1.48\times10^{-3}$). The sensitivity of $X_{H,\,max}$ and the overall computation to changes in the diffusion coefficient of H atoms will be discussed below.

For set 2 of rate parameters in table 4, the line in figure 6 shows the computed variation in burning velocity with initial X_{H_2}/X_{N_2} ratio. For the same conditions, the lines in figures 3 and 4

PHILOSOPHICAL TRANSACTIONS OF THE ROYAL SOCIETY A MATHEMATICAL, PHYSICAL & ENGINEERING SCIENCES

TABLE 4. RATE PARAMETERS USED IN COMPUTATION OF FLAMES K, L AND M

(Forward rate coefficients are expressed as $k = AT^B \exp(-C/T)$ in units of cm mol s.)

(*a*) *Parameters of expressions common to all sets*

reaction		A	B	C/K
(i)	$OH+H_2 \rightleftharpoons H_2O+H$	1.17×10^{9}	1.3	1825
(iii)	$O+H_2 \rightleftharpoons OH+H$	1.8×10^{10}	1.0	4480
(xv)	$H+H+H_2 \rightleftharpoons 2H_2$	9.2×10^{16}	−0.6	0
	$H+H+N_2 \rightleftharpoons H_2+N_2$	1.0×10^{18}	−1.0	0
	$H+H+O_2 \rightleftharpoons H_2+O_2$	1.0×10^{18}	−1.0	0
	$H+H+H_2O \rightleftharpoons H_2+H_2O$	6.0×10^{19}	−1.25	0
(xvi)	$H+OH+M \rightleftharpoons H_2O+M$			
	$M = H_2, N_2, O_2$	9.77×10^{17}	−0.71	0
	$M = H_2O$	4.89×10^{18}	−0.71	0
(xviii)	$H+O+M \rightleftharpoons OH+M$			
	$M = H_2, N_2, O_2$	6.2×10^{16}	−0.6	0
	$M = H_2O$	3.1×10^{17}	−0.6	0
(xviii)	$OH+OH \rightleftharpoons O+H_2O$	5.75×10^{12}	0	390

(*b*) *Other rate parameters and properties*

	set 1	set 2	set 3	set 4
σ_H/nm ...	0·3	0.3	0.3	0.3
$(k_7+k_{7a})/k_{12}$ ...	6.0	$12.0\exp(-540/T)$	$25.0\exp(-1100/T)$	4.5

reaction	A	B	C/K	A	B	C/K	A	B	C/K	A	B	C/K
(ii) $H+O_2 \rightleftharpoons OH+O$	1.52×10^{14}	0	8250	1.42×10^{14}	0	8250	1.30×10^{14}	0	8250	2.20×10^{14}	0	8250
(iv)† $H+O_2+H_2 \rightleftharpoons HO_2+H_2$	1.11×10^{18}	−0.72	0	1.03×10^{18}	−0.72	0	9.46×10^{17}	−0.72	0	1.60×10^{18}	−0.72	0
(vii) $H+HO_2 \rightleftharpoons OH+OH$	8.5×10^{13}	0	0	1.6×10^{14}	0	540	3.0×10^{14}	0	1100	1.38×10^{14}	0	0
(vii*a*) $H+HO_2 \rightleftharpoons O+H_2O$	4.6×10^{12}	0	0	1.0×10^{13}	0	540	1.9×10^{13}	0	1100	1.1×10^{13}	0	0
(xii) $H+HO_2 \rightleftharpoons H_2+O_2$	1.49×10^{13}	0	0	1.42×10^{13}	0	0	1.28×10^{13}	0	0	3.3×10^{13}	0	0
(xiii) $OH+HO_2 \rightleftharpoons H_2O+O_2$	8.5×10^{12}	0	0	8.5×10^{12}	0	0	8.5×10^{12}	0	0	8.5×10^{12}	0	0
(xiv)‡ $O+HO_2 \rightleftharpoons OH+O_2$ *a*	8.5×10^{12}	0	0	1.6×10^{13}	0	540	3.0×10^{13}	0	1100	1.38×10^{13}	0	0
(xiv)‡ $O+HO_2 \rightleftharpoons OH+O_2$ *b*	1.49×10^{12}	0	0	1.42×10^{12}	0	0	1.28×10^{12}	0	0	3.3×10^{12}	0	0
$10^3 X_{H,max}$ in flame L	1.434			1.475			1.510			1.379		

† Chaperon efficiencies relative to $H_2 = 1.0$ are 0.44, 0.35 and 6.5 for N_2, O_2 and H_2O, respectively.

‡ $k_{14} = k_{14a}+k_{14b}$.

show the appropriate computed profiles for flame L of tables 1 and 2, while those in figure 5 show the computed relative chemiluminescent intensity profiles for flames K, L and M. These relative intensity profiles were computed exactly as described by Day *et al.* (1972) with the assumption that, for equal concentrations of H and OH, reaction (xx) is 25 times as efficient as reaction (xix).

$$H + H + Na = H_2 + Na^*, \tag{xix}$$

$$H + OH + Na = H_2O + Na^*. \tag{xx}$$

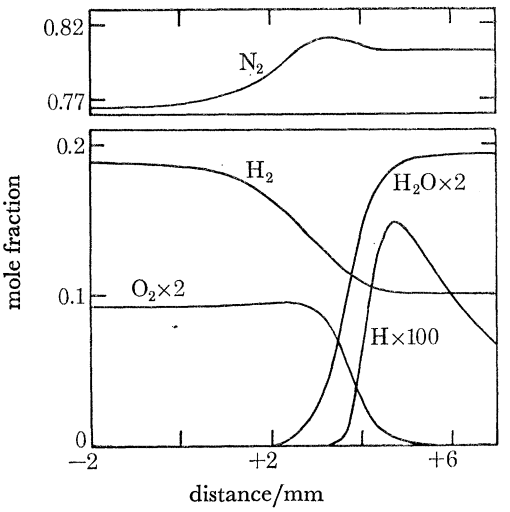

FIGURE 7. Computed mole fraction profiles of major species and hydrogen atoms in flame L of table 1. Reaction rate parameters as in set 2 of tables 3 and 4. Same distance zero as in figure 3.

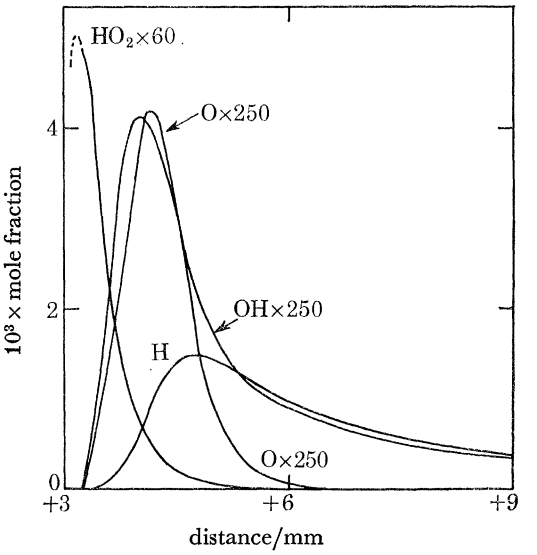

FIGURE 8. Computed mole fraction profiles of radical species in flame L of table 1. Reaction rate parameters as in set 2 of tables 3 and 4. Same distance zero as in figure 3.

Figures 3–6 show that set 2 of rate parameters gives reasonable agreement with experiment in all cases. Profiles calculated from sets 1 and 3 of rate parameters are further found to be almost identical with those from set 2, with negligible differences compared with the uncertainties of the measurements. The profile measurements in themselves do not therefore provide a basis for discrimination between the three sets.

In an attempt to provide further information, a fourth set of kinetic parameters was also briefly investigated, based upon the condition $(k_7 + k_{7a})/k_{12} = 4.5$ at all temperatures. Such a set of parameters is given as set 4 in table 4, in which the rate expressions for k_2 and k_4 have been altered together so as to reproduce the burning velocity of flame L while at the same time satisfying the other constraints governing them. The computed temperature profile and the mole fraction profiles are again not easily distinguished from those of set 2. The most notable difference between the results of the computations using sets 2 and 4 was that the maximum rate of heat release in flame L increased from 86.5 W cm^{-3} for set 2 to 100.2 W cm^{-3} for set 4. However, this difference is only observable experimentally by way of the temperature profile, and it is doubtful whether it is outside the precision of the measurements. It should be noted that, because of lack of sufficient information, the absolute values of k_7, k_{7a}, k_{12} and k_{14} are based on an estimated $(k_7 + k_{7a})^2/k_2^2 k_{10} = 4.22 \times 10^{-4}$ mol cm^{-3} s to correspond with $(k_7 + k_{7a})/k_{12} = 4.5$. This estimated

ratio was obtained by linear extrapolation of the results of Baldwin *et al.* (1974), quoted in §4(*b*). The ratios k_{7a}/k_7 and $k_{14}/(k_7+k_{12})$ in set 4 were made to retain approximately the same values as in sets 1, 2 and 3.

In addition to the four sets of rate parameters themselves, the maximum hydrogen atom mole fractions resulting from the computation of flame L are given in table 4 for each set. For set 2, the sensitivity of $X_{\mathrm{H,\,max}}$ to the value assumed for σ_{H} was also examined. The results are given in table 5. With the help of table 5, it is then possible to optimize the values of σ_{H} associated with the remaining sets of parameters, so as to give $X_{\mathrm{H,\,max}} = 1.48\times10^{-3}$. For sets 1 and 3, the optimizations give $\sigma_{\mathrm{H}} = 0.325$ and 0.275 nm, respectively. Except for set 3, the optimum values are all somewhat above that of $\sigma_{\mathrm{H}} = 0.271$ nm recommended by Svehla (1962). Within the range of required values of σ_{H} for sets 1 to 3, neither (i) the optimum values of the kinetic parameters, nor (ii) the computed temperature and stable species mole fraction profiles, nor (iii) the computed relative chemiluminescent intensity profiles are appreciably affected by the changes. For $\sigma_{\mathrm{H}} = 0.30$ nm in set 4 (leading to $X_{\mathrm{H,\,max}} = 1.38\times10^{-3}$) the relative chemiluminescent intensity profile was also indistinguishable from those of sets 1 to 3. Again therefore, these intensity profile measurements provide no really powerful means of discrimination between sets 1 to 4 of rate parameters.

TABLE 5. EFFECT OF LENNARD-JONES POTENTIAL PARAMETER σ_{H} ON MAXIMUM HYDROGEN ATOM MOLE FRACTION IN FLAME L, FOR SET 2 OF KINETIC PARAMETERS IN TABLE 4

σ_{H}/nm	0.30	0.325	0.35
$10^3 X_{\mathrm{H,\,max}}$ in flame L	1.48	1.52	1.56

5. RECOMBINATION IN NEAR-STOICHIOMETRIC AND LEAN FLAMES

(*a*) *Flames at lower temperatures* (*up to* 1550 K)

The decay of the free radical pool in the burnt gas of lean hydrogen flames is much more rapid than that in the fuel-rich flames, and Fenimore & Jones (1965) have drawn attention to the possible contribution of reaction (iv) to the recombination process in the lean situation. However, unlike the products of the recombination reactions (xv) and (xvi), HO_2 is not a stable molecule. As a result of this the further reactions of HO_2 must be considered in an analysis of lean flame recombination regions, and it is likely therefore that lean flame recombination measurements will provide further information about the reactions of HO_2. Using the complete reaction scheme given in §1, Dixon-Lewis *et al.* (1975*b*) showed that the formation of HO_2 and the competition of reactions (vii), (vii*a*), and (xii) to (xiv) with its redissociation are of major importance in determining the rate of the recombination. This applied particularly in the lower temperature lean flames for which measurements had previously been made by Kaskan (1958*b*). Unfortunately the attempt by Dixon-Lewis *et al.* to analyse Kaskan's results broke down because of uncertainties then associated with the calibration of his ultraviolet absorption measurements of the concentrations of hydroxyl radicals in the flames.

These difficulties have since been resolved, since W. E. Kaskan (private communication, 1974) kindly provided the information that the oscillator strength of the (0, 0) band of OH which he used in his original publications (Kaskan 1958*a*, *b*) was the early value of $f_{00} = 12.3\times10^{-4}$ due to Oldenberg & Rieke (1938). He also provided estimates of factors by which his published concentrations should be multiplied to allow for Doppler broadening of the emission lines from

the source lamp (1.1), and pressure broadening of the absorption lines in the flames (1.36 for gases at 1 atm and 1500 K, and 1.18 at 0.5 atm and 1500 K). Both these line broadening corrections have been applied in the present analysis. The source lamp correction assumed a lamp temperature of 400 K.

It still remains to consider the absorption coefficient of the OH radical. One approach to this is by way of the recombination results in the fuel-rich flames I and J of table 1. In these flames the recombination is mostly controlled by reactions (xv) and (xvi), whose rate coefficients have already been discussed in §3. By adjusting the calibration of the measured OH concentrations for these flames so that the gradients of the profiles of $[OH]^{-1}$ match the corresponding computed profiles, it is then possible to estimate a calibration factor for [OH]. This is, of course, performed after the appropriate line broadening corrections have been applied, and it is essentially a kinetic determination of the oscillator strength. Another approach, which also gives information about k_4 and k_{13}, is by way of the recombination data in lower temperature lean flames, as described below.

TABLE 6. PROPERTIES OF LOW TEMPERATURE, FUEL-LEAN HYDROGEN–OXYGEN–NITROGEN FLAMES IN RECOMBINATION REGION

(Flames are those for which OH concentrations are given by Kaskan (1958*b*).)

						approx. percentage primary recombination		
flame	p/atm	$(H_2/O_2)_u$	$(N_2/O_2)_a$	V_b†/(cm s^{-1})	approx. temp. range of recomb. K	(xv) H+H+M	(xvi) H+OH+M	(iv) H+O_2+M
N	0.45	1.00	3.76	18.8	1370–1410	v. small	0.6	99.4
O	0.45	1.60	3.76	11.9	1370–1435	v. small	1.6	98.4
P	1.0	1.00	3.76	33.4	1520–1530	v. small	0.7	99.3
Q	1.0	1.60	3.76	16.8	1500–1530	v. small	2.0	98.0

† V_b gives linear burnt gas velocity corrected to standard conditions of 298 K and p atm pressure.

If the rate parameters already given as set 2 in table 4 are used as kinetic data in recombination calculations with partial equilibrium assumptions, then table 6 shows the relative importance of reactions (xv), (xvi) and (iv) in the recombination zones of the four lean flames for which detailed results are given by Kaskan (1958*b*). As in table 1, the approximate percentages of primary removal by the three reactions are given for points lying roughly mid-way through the recombination zones. Again these percentages do not alter much over the whole region. However, the same is not true for the partitioning of the HO_2, formed in the forward reaction (iv), between its redissociation by reaction (−iv) on the one hand, and its reactions with H, OH and O on the other. Figures 9–12 show the fate of the HO_2 in the flames N, O, P and Q of table 6, the gas flow being from left to right in each case. In terms of concentrations of free electron spins as defined in the partial equilibrium calculation (Dixon-Lewis *et al.* 1975*a*), the reactions of HO_2 with H, OH and O are all recombination steps. At lower pressures these recombination steps are favoured relatively to reaction (−iv) by the increased mole fractions of the radical species (see also Dixon-Lewis, Isles & Walmsley 1973), and in this sense HO_2 formation at lower pressures is therefore a more efficient recombination agent than at higher pressures. Further, it is clear from figures 9 to 12 that, apart from HO_2, the only radical of real importance over the measured recombination regions is the hydroxyl radical. The recombination results in the lean flames at the two different pressures therefore provide a means of determining both k_4 and k_{13}, provided that the

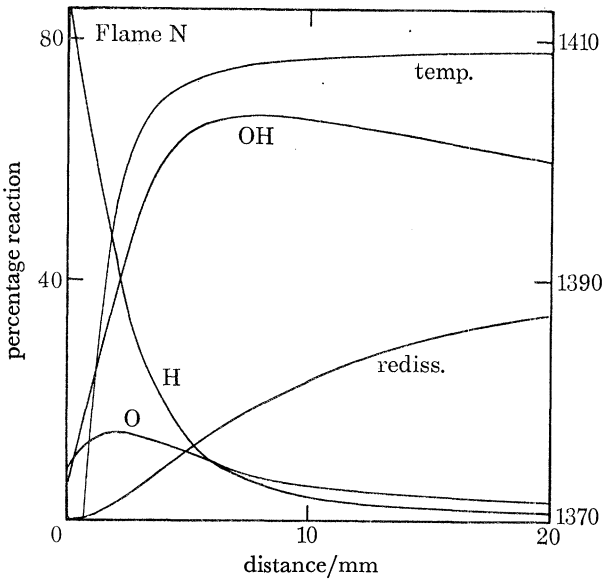

FIGURE 9. Partitioning of hydroperoxyl between redissociation and reactions with H, OH and O in recombination zone of flame N in table 6. Partial equilibrium assumptions employed in calculation using set 2 of reaction rate parameters from tables 3 and 4. Approximate range of measurements shown in figure 14 is from 1 to 16 mm on distance scale.

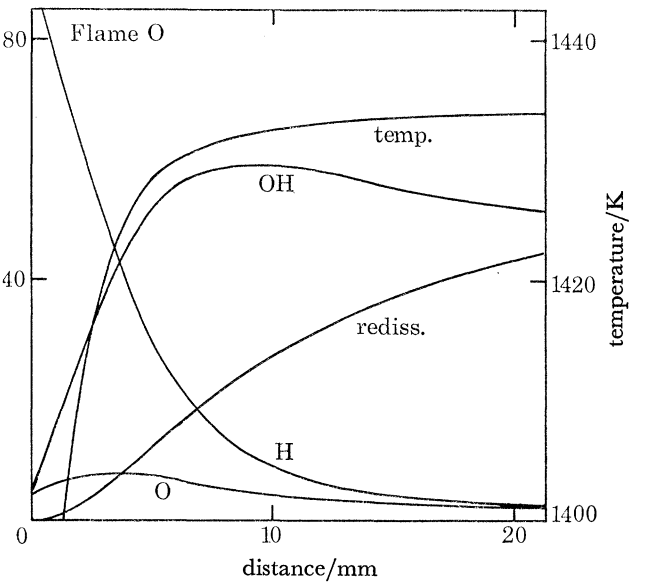

FIGURE 10. Partitioning of hydroperoxyl between redissociation and reactions with H, OH and O in recombination zone of flame O in table 6. Partial equilibrium assumptions employed in calculation using set 2 of reaction rate parameters from tables 3 and 4. Approximate range of measurements shown in figure 14 is from 0 to 20 mm on distance scale.

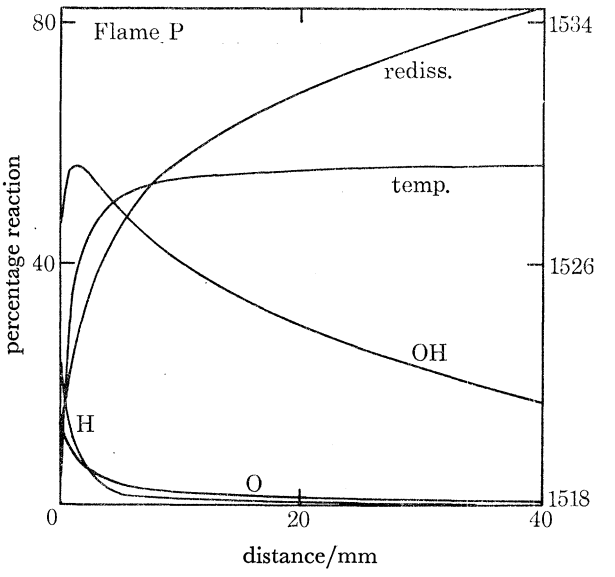

FIGURE 11. Partitioning of hydroperoxyl between redissociation and reactions with H, OH and O in recombination zone of flame P in table 6. Partial equilibrium assumptions employed in calculation using set 2 of reaction rate parameters from tables 3 and 4. Approximate range of measurements shown in figure 15 is from 0 to 16 mm on distance scale.

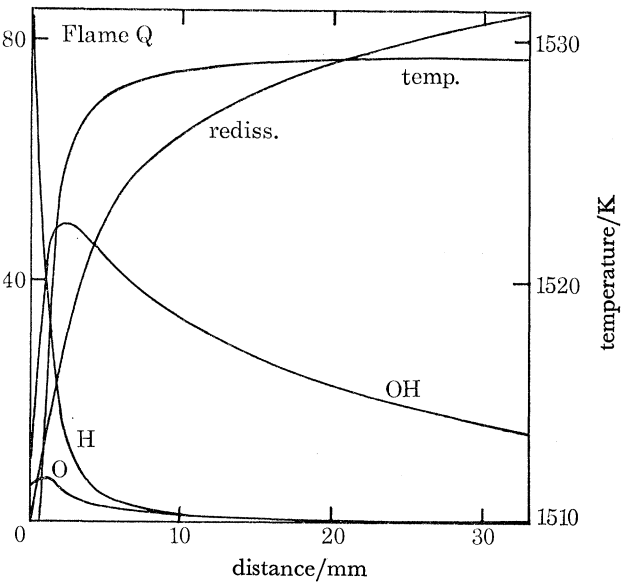

FIGURE 12. Partitioning of hydroperoxyl between redissociation and reactions with H, OH and O in recombination zone of flame Q in table 6. Partial equilibrium assumptions employed in calculation using set 2 of reaction rate parameters from tables 3 and 4. Approximate range of measurements shown in figure 15 is from 1 to 10 mm on distance scale.

appropriate absorption coefficient or f-number of OH is known. The absorption coefficient must also be chosen so that (i) the measured hydroxyl radical concentration profiles in the fuel-rich and near-stoichiometric flames H, I and J of table 1 are consistent with both the rate coefficients k_{15} and k_{16} already discussed in § 3, and the value of k_4 emerging from the analysis of the lean flame recombination results, and (ii) the values of k_4 derived here are consistent with the extrapolation of the expression combining the room temperature results of Bishop & Dorfman (1970) with the results of the analysis in § 4 relating to the main reaction zones of low temperature, fuel-rich flames. Optimization along these lines by iteration between flames H, I and J of table 1 on the one hand, and the flames of tables 2 and 6 on the other, led to a band oscillator strength $f_{00} = 9.5 \times 10^{-4}$ for OH, together with the expressions for k_4 and k_{13} given in set 2 of table 4.

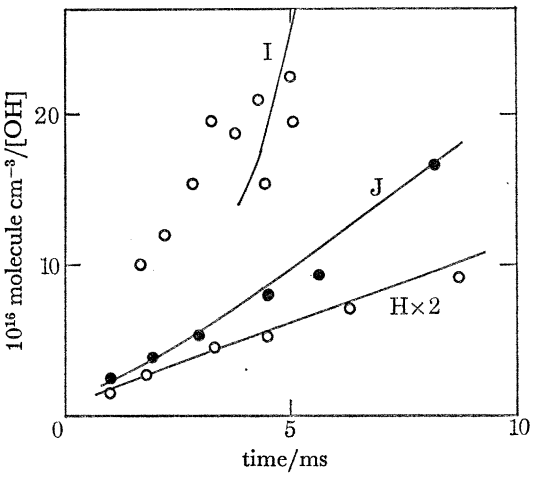

FIGURE 13. Recombination in fuel-rich hydrogen–oxygen–nitrogen flames. Comparison of measured points of Kaskan (1958*a*) with computed lines. Letters refer to flames of table 1. Reaction rate parameters as in set 2, tables 3 and 4.

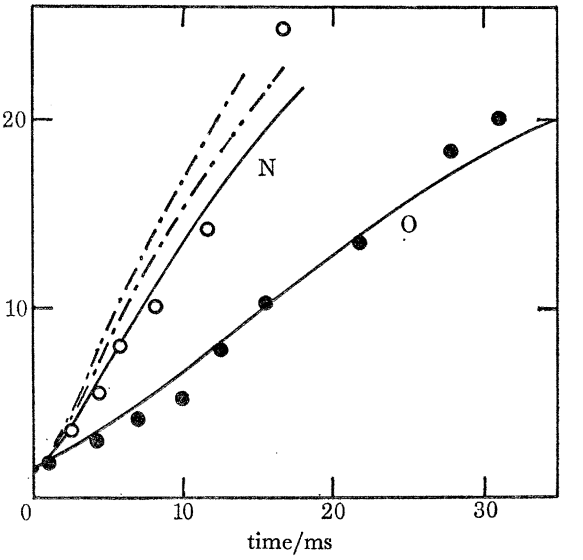

FIGURE 14. Recombination in fuel-lean hydrogen–oxygen–nitrogen flames. Comparison of measured points of Kaskan (1958*b*) with computed lines. Letters refer to flames of table 6. Solid lines refer to reaction rate parameters as in set 2, tables 3 and 4. Dot-dashed lines for flame N: upper line refers to rate parameters as in set 4, table 4; lower line also computed using set 4, but with $k_{13} = 4.0 \times 10^{12}$ cm^3 mol^{-1} s^{-1}.

Comparisons of theory and experiment on this basis for flames H, I, J, N, O, P and Q are provided by the curves of $[OH]^{-1}$ in figures 13–15. In these figures the points refer to observation, and the solid lines refer to calculations with partial equilibrium assumptions, in which set 2 of rate parameters was used. The agreement between theory and experiment is good, and the general precision as shown by the evenly dashed lines in figure 15 suggests that satisfactory agreement may be obtained by using any of the sets 1, 2 or 3 of rate parameters combined with $k_{13} = (8 \pm 4) \times 10^{12}$ cm^3 mol^{-1} s^{-1} at 1530 K.

If set 4 of rate parameters from table 4 is used unchanged for a similar calculation of the recombination zone profiles in flames N and P, the results are shown by the upper dot-dashed lines in figures 14 and 15. Owing to the higher value of k_4 compared with sets 1, 2 and 3, these lines have higher gradients than the solid lines for the corresponding flames, and the agreement with the

observed values is somewhat less good. This conclusion depends to some extent on the weighting given to the topmost observed value in flame N: this point corresponds with the lowest hydroxyl radical concentration in the whole series of measurements, and the determination of the fraction of incident light absorbed is consequently the least precise.

There are two ways in which the agreement between the theory and experiment may be improved in the case of the set 4 of rate parameters. The first of these involves a reduction in the

TABLE 7. PROPERTIES OF HIGHER TEMPERATURE, FUEL-LEAN HYDROGEN–OXYGEN–NITROGEN FLAMES IN RECOMBINATION REGION

(Flames are those for which H atom concentrations are given by Friswell & Sutton (1972).)

flame	p/atm	$(H_2/O_2)_u$	$(N_2/O_2)_u$	V_b†/(cm s^{-1})	approx. temp. range of recomb. K	approx. percentage recombination at ends of range of measurement by (xv) H+H+M	(xvi) H+OH+M	(iv) H+O$_2$+M
R	1.0	1.67	4.00	168	1800–2125	5.0–0.7	24–33	68–65
S	1.0	1.54	3.61	168	1875–2135	3.1–0.4	23–29	72–70
T	1.0	1.43	3.29	168	1890–2135	2.3–0.3	20–25	76–74
U	1.0	1.33	3.00	168	1900–2135	2.0–0.2	17–21	80–78

† V_b gives linear burnt gas velocity corrected to standard conditions of 298 K and p atm pressure.

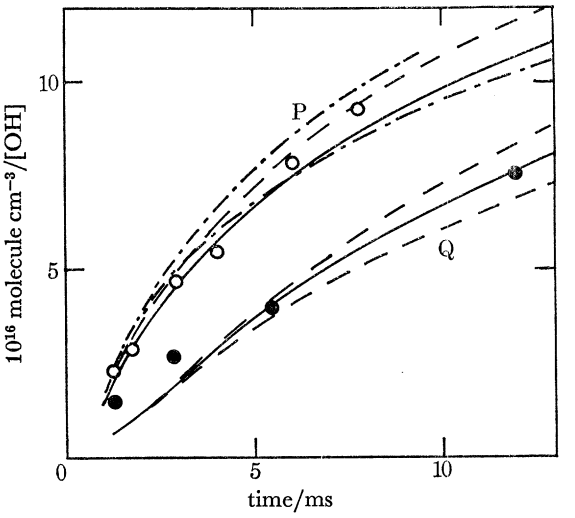

FIGURE 15. Recombination in fuel-lean hydrogen–oxygen–nitrogen flames. Comparison of measured points of Kaskan (1958*b*) with computed lines. Letters refer to flames of table 6. Solid lines refer to reaction rate parameters as in set 2, tables 3 and 4. Dashed lines also computed using set 2, but with $k_{13} = 4.0 \times 10^{12}$ (lower, flame Q only) and 1.2×10^{13} (upper) cm^3 mol^{-1} s^{-1} respectively. Dot-dashed lines for flame P: upper line refers to rate parameters as in set 4, table 4; lower line also computed using set 4, but with $k_{13} = 4.0 \times 10^{12}$ cm^3 mol^{-1} s^{-1}.

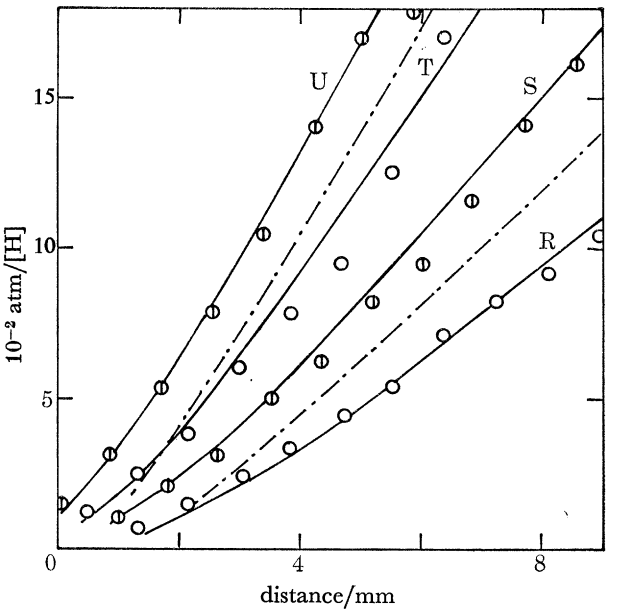

FIGURE 16. Recombination in fuel-lean hydrogen–oxygen–nitrogen flames. Comparison of measured points of Friswell & Sutton (1972) with computed lines. Letters refer to flames of table 7. Solid lines refer to reaction rate parameters as in set 2, tables 3 and 4. Dot-dashed lines for flames R and T computed using set 4, table 4.

value of k_{13}. The lower dot-dashed lines for flames N and P in figures 14 and 15 show the results of computations again for set 4, but with $k_{13} = 4.0 \times 10^{12}$ instead of 8.5×10^{12} cm^3 mol^{-1} s^{-1}. The agreement is slightly better than before, but it is still not as good as with sets 1–3.

The second possibility for improved agreement lies in the assumption of a higher transition probability associated with the ultraviolet absorption of OH. This would increase the value of each $[OH]^{-1}$, and so produce a steeper 'observed' curve of this reciprocal concentration. However, in this connection it should be noted that the value of $f_{00} = 9.5 \times 10^{-4}$, already used here for

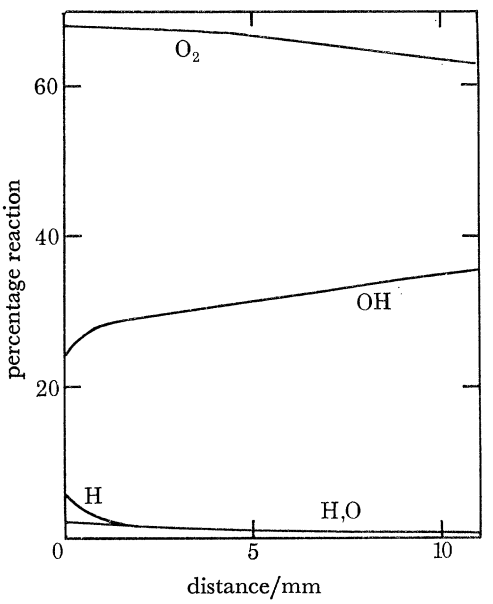

FIGURE 17. Approximate percentages of primary recombination by reactions (iv), (xv), (xvi) and (xvii) in flame R of table 7. Reactions are indicated by the species with which the hydrogen atom reacts in the primary recombination step above. Reaction rate parameters as in set 2, tables 3 and 4.

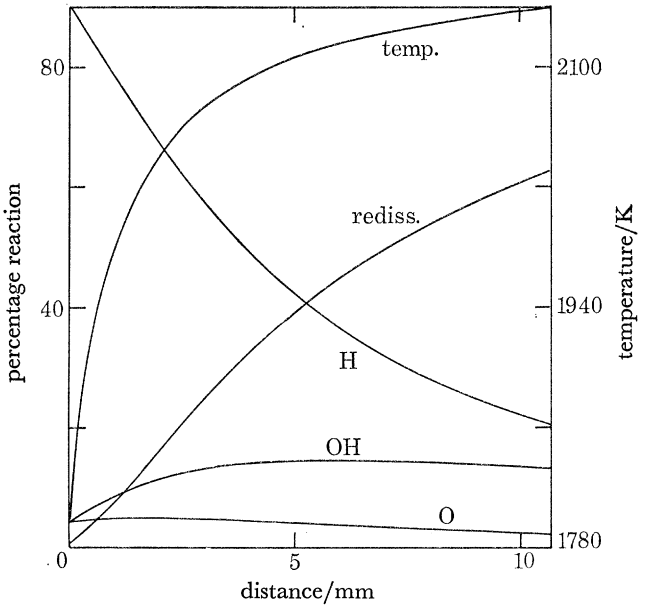

FIGURE 18. Partitioning of hydroperoxyl between redissociation and reactions with H, OH and O in recombination zone of flame R in table 7. Partial equilibrium assumptions employed in calculation using set 2 of reaction rate parameters from tables 3 and 4. Approximate range of measurements shown in figure 16 is from 0 to 7.5 mm on distance scale.

the calibration of Kaskan's measurements, is identical with a recent redetermination by Rouse & Engleman (1973), who used the same method as Oldenberg & Rieke (1938), as well as with Oldenberg & Rieke's original value when the latter is corrected for changes in the thermochemistry of OH and for vibration–rotation interaction. It is already some 6% higher than the mean of a number of other recent determinations from the radiative lifetime (Bennett & Dalby 1964; German & Zare 1969, 1970; De Zafra, Marshall & Metcalf 1971; Elmergreen & Smith 1972), and it is about 33% higher than the value found by Golden, del Greco & Kaufman (1963), who made another kinetic determination by generating OH in supposedly known concentration from $H + NO_2$ in a discharge-flow system.

Although the evidence from the recombination results in these lower temperature lean flames is not overwhelming, it does somewhat favour the sets 1, 2 and 3 of rate parameters as compared with set 4.

(*b*) *Higher temperature flames*

Friswell & Sutton (1972) have used the lithium/lithium hydroxide method to measure hydrogen atom concentrations in the burnt gas regions of four lean hydrogen–oxygen–nitrogen flames at temperatures in the region of 2100 K. The properties of the four flames are given in table 7, and the profiles of $[H]^{-1}$ are shown in figure 16. The points in figure 16 refer to the observations of Friswell & Sutton, while the solid lines have been computed on the basis of partial equilibrium assumptions, once more using set 2 of rate parameters from table 4. Agreement is again good.

In their own analysis of their results, Friswell & Sutton (1972) assumed that HO_2 in the recombination region was essentially held in partial equilibrium with H and O_2 by reactions (iv) and (−iv), and that the recombination was consequent upon the competition of reaction (xiii) alone with reaction (−iv). They then used the results to deduce a rate coefficient for reaction (xiii). For flame R of table 7, figure 17 shows the approximate percentages of primary recombination by reactions (iv), (xv), (xvi) and (xvii) at various positions in the burnt gas region, and figure 18 shows the fate of the HO_2 formed. The region of measurement extended from approximately zero to 8 mm on the distance scale. Over most of this region the major part of the HO_2 is removed by one or other of reactions (vii), (vii*a*) and (xii) with H atoms, and the assumptions of Friswell & Sutton are clearly incorrect. The results for flames S, T and U are similar to those for flame R. For set 2 of rate parameters, the approximate percentages of primary recombination by reactions (iv), (xv) and (xvi) are given for all the flames in table 7.

Bearing in mind that Friswell & Sutton (1972) quoted sodium D-line reversal temperatures of 2130 K in their flames, it is also instructive to compare the present computational results with those of the earlier, more exploratory approach by Dixon-Lewis *et al.* (1975*b*). At 2130 K, the expressions used for k_4 in the two analyses both give $k_{4,H_2} = 4.15 \times 10^{15}$ cm^6 mol^{-2} s^{-1}. However, the earlier work used $k_7 + k_{7a} = 3.02 \times 10^{14} \exp(-1100/T) = 1.8 \times 10^{14}$ at 2130 K, compared with 1.32×10^{14} used here. In the earlier work, the agreement between computation and experiment seemed to be improved when the temperatures in the calculation were raised some 20 or 30 K above those quoted by Friswell & Sutton, and indeed above those which can be shown by a thermal balance to apply for the adiabatic flames with $T_u = 298$ K. In terms of curve fitting, the effect of the increased temperature is partly to increase the rate of the redissociation reaction (−iv), thus compensating for the higher value of $(k_7 + k_{7a})$. In view of the dominance of reactions (vii) as consumers of HO_2 in the recombination zones of the hotter lean flames, as shown in figure 18, the comparison of the two analyses provides some slight evidence against set 3 of the rate parameters in table 4, for which $k_7 + k_{7a} = 3.2 \times 10^{14} \exp(-1100/T)$. It is possible that the analysis in these hotter flames could be further refined by more detailed measurement of the temperature profiles in the recombination regions, so that allowance could be made for temperature effects produced by heat losses from the combustion products. The analysis just discussed assumed an adiabatic system.

Lastly, in order to complete this part of the analysis, additional calculations were also performed using set 4 of the rate parameters of table 4. The results for flames R and T are shown by the dot-dashed lines in figure 16. The measurements are clearly incompatible with the combination of high absolute values of k_4, k_7 and k_{12} assumed in this set (for which $k_7 + k_{7a} + k_{12} = 1.82 \times 10^{14}$). The values of k_7 and k_{12}, it will be recalled from §4(*c*), are based on a linear extrapolation of the ratios $(k_7 + k_{7a})^2/k_2^2 k_{10}$ deduced by Baldwin *et al.* (1974) from their analyses of second explosion limit data in boric acid coated vessels at 773 K. Again therefore, so far as can

reasonably be estimated, the experimental evidence militates against the lower value of the ratio $(k_7+k_{7a})/k_{12}$ assumed in set 4. On the basis of the evidence, maximum error limits of $\pm 10\%$ around the optimum values of the ratio for sets 1, 2 and 3 are suggested.

6. Sensitivity analysis for the more important reaction parameters in flame L of table 1; approximate error limits for rate coefficients

Despite the predictive success of the flame model in the situations already examined, it follows from the complex nature of the flame mechanism that the sets 1, 2 and 3 of rate parameters given in table 4 are by no means unique. On the other hand, the number of experimental constraints is such that many of the rate coefficients can be defined within quite narrow limits from which internally consistent sets like those of table 4 may be drawn so as to satisfy the burning velocity and calibration requirements of flame L in table 1. The more important reaction parameters controlling flame L are the rate coefficients k_2 and k_{15}, and the ratio $(k_7+k_{7a})/k_{12}$. By starting from set 2 of rate parameters in table 4 and operating so as to satisfy the burning velocity requirement, the effect of moderate changes in both k_{15} and $(k_7+k_{7a})/k_{12}$ on the optimum values of the remaining two parameters may be found. These effects are given in table 8. The quoted changes are accompanied by alterations of up to 10% in $X_{\mathrm{H,\,max}}$ for flame L. These latter alterations are well within the error limits of $\pm 50\%$ suggested by Baulch & Drysdale (1974) for the calibration rate coefficient k_{21}.

Table 9 summarizes the forward rate parameters used in most of the remainder of the paper. With one or two minor differences which will be explained in § 7, these are the same as set 2 of rate parameters in table 4. Subject to the constraints on the rate coefficients indicated in table 8, the suggested error limits for the more important rate expressions are given in the final column of table 9. Such limits are not quoted for reactions (xiv) and (xvii). This is because the small quantifiable effects of these two reactions in the flames of figure 6 are too closely parallelled by the similar effects of reactions (xiii) and (xvi). Experimental errors, and errors in k_{13} and k_{16}, thus become of overriding importance. The sensitivities of several flame parameters and properties to the expressions assumed for k_{14}, k_{16} and k_{17} will be considered in § 9 (*b*) (ii).

7. Calculation of properties of hydrogen–air flames

In the preceding sections three sets of rate parameters have been deduced for the hydrogen–oxygen flame system which (i) differ only in detail, (ii) are capable of describing satisfactorily a wide variety of properties of the flames, and (iii) are consistent with a large number of other measurements on the hydrogen–oxygen system, including studies of explosion limits and slow reaction rates, and measurements in shock tubes and discharge-flow systems. To supplement these studies, an investigation of the burning velocities and properties of the whole flammable range of hydrogen–air mixtures, including faster and higher temperature flames, is described in the present section. Eight hydrogen–air flames at atmospheric pressure were studied, all with $T_{\mathrm{u}} = 298$ K, but having respectively $X_{\mathrm{H_2,\,u}} = 0.70$, 0.60, 0.50, 0.41, 0.30, 0.25, 0.20 and 0.15. Apart from the final flame temperatures, the only experimentally accessible quantities associated with these flames are (i) the burning velocities, and (ii) the compositions, including some radical concentration profiles, in the recombination regions. The radical recombination profiles have seldom been measured specifically for hydrogen–air flames. Because of the small thickness (< 1 mm) of the

main flame reaction zones, computation represents the only means by which the structures of these zones, and the flame mechanism, may be elucidated.

The calculations were carried out by the composite flux method of Dixon-Lewis *et al.* (1975*a*), with quasi-steady state assumptions. Dixon-Lewis *et al.* developed two different formulations of the calculation for hydrogen–oxygen systems, in which the overall, composite flux of free radicals was expressed alternatively in terms of either H or OH as the 'base' species. The formulation in terms of OH was thought likely to be more appropriate for the computation of lean flames, where the concentrations of OH and O may be much larger than the concentration of H atoms over

TABLE 8. SENSITIVITY OF BURNING VELOCITY OF FLAME L IN TABLE 1 TO PARAMETERS k_2, $(k_7+k_{7a})/_{12}$ AND k_{15}, BASED ON SET 2 OF PARAMETERS IN TABLES 3 AND 4

change (%)	parameter	*A*	*B*	*C*	*D*
+10	k_2 and k_4	+6.9	—	—	—
+20	k_{15}	−5.2	+ 7.5 (272)†	+7.0 (266)	—
−10	$(k_7+k_{7a})/k_{12}$	−8.3	+12.0 (276)	—	−28.5 (268)

A, Percentage increase in burning velocity; *B*, percentage increase in k_2 and k_4 to return burning velocity to measured value, with $(k_7+k_{7a})/k_{12}$ or k_{15} unchanged; *C*, percentage increase in $(k_7+k_{7a})/k_{12}$ to return burning velocity to measured value, with k_2 and k_4 unchanged; *D*, percentage increase in k_{15} to return burning velocity to measured value, with k_2 and k_4 unchanged.

† Numbers in parentheses are corresponding predicted burning velocities of 41% hydrogen–air flame (cm s^{-1}) (see §9(*b*) (ii)), for transport properties calculated with $\sigma_H = 0.30$ nm.

TABLE 9. RATE PARAMETERS USED IN COMPUTATION OF HYDROGEN–AIR FLAMES

(Forward rate coefficients are expressed as $k = AT^B \exp(-C/T)$ in cm mol s units.)

	reaction	*A*	*B*	*C*/K	error in lg *k*
(i)	$OH+H_2 \rightleftharpoons H_2O+H$	1.17×10^{9}	1.3	1825	±0.1
(ii)	$H+O_2 \rightleftharpoons OH+O$	1.42×10^{14}	0	8250	±0.1
(iii)	$O+H_2 \rightleftharpoons OH+H$	1.8×10^{10}	1.0	4480	±0.1
(iv)†	$H+O_2+H_2 \rightleftharpoons HO_2+H_2$	1.03×10^{18}	−0.72	0	±0.1
(vii)	$H+HO_2 \rightleftharpoons OH+OH$	1.4×10^{14}	0	540	±0.2‡
(vii*a*)	$H+HO_2 \rightleftharpoons O+H_2O$	1.0×10^{13}	0	540	
(xii)	$H+HO_2 \rightleftharpoons H_2+O_2$	1.25×10^{13}	0	0	±0.2‡
(xiii)	$OH+HO_2 \rightleftharpoons H_2O+O_2$	7.5×10^{12}	0	0	±0.2
(xiv)§	$O+HO_2 \rightleftharpoons OH+O_2$	(*a*) 1.4×10^{13}	0	540	—
		(*b*) 1.25×10^{12}	0	0	—
(xv)	$H+H+H_2 \rightleftharpoons H_2+H_2$	9.2×10^{16}	−0.6	0	±0.1
	$H+H+N_2 \rightleftharpoons H_2+N_2$	1.0×10^{18}	−1.0	0	±0.1
	$H+H+O_2 \rightleftharpoons H_2+O_2$	1.0×10^{18}	−1.0	0	—
	$H+H+H_2O \rightleftharpoons H_2+H_2O$	6.0×10^{19}	−1.25	0	±0.1
(xvi)	$H+OH+M \rightleftharpoons H_2O+M$				
	¶ $M = H_2, N_2, O_2$	9.77×10^{17}	−0.71	0	—
		$(1.6\times10^{22}$	−2.0	0	±0.2)
	¶ $M = H_2O$	4.89×10^{18}	−0.71	0	—
		$(8.0\times10^{22}$	−2.0	0)	—
(xvii)	$H+O+M \rightleftharpoons OH+M$				
	$M = H_2, N_2, O_2$	6.2×10^{16}	−0.6	0	—
	$M = H_2O$	3.1×10^{17}	−0.6	0	—
(xviii)	$OH+OH \rightleftharpoons O+H_2O$	5.75×10^{12}	0	390	±0.2
ratio	$(k_7+k_{7a})/k_{12}$	12.0	0	540	±0.05

† Chaperon efficiencies relative to $H_2 = 1.0$ are 0.44, 0.35 and 6.5 for N_2, O_2 and H_2O respectively.

‡ These error limits refer to the sum (k_7+k_{7a}). The ratio $(k_7+k_{7a})/k_{12}$ is more closely defined than this, as shown in the last line of the table.

§ $k_{14} = k_{14a}+k_{14b}$.

¶ Parameters in parentheses are to be preferred (see §9 (*b*) (ii)).

much of the flame. However, it was found that the computation of both the 20 and 25% hydrogen–air flames became excessively slow when the lean flame formulation (via OH) was used. The reason for this is that the lean flame formulation deals with the rates of reactions (i) and (iii) explicitly, and as a result 'stiffness' problems are introduced in the hot regions of the flames, with a consequent reduction of integration step size. The very appearance of these problems suggests approximate equilibration of one or both of reactions (i) and (iii), despite the low concentrations of molecular hydrogen in the regions considered. Retaining the formulation via OH, a further attempt was therefore made to start the integration through these flames in stages, by introducing

TABLE 10. COMPUTED PROPERTIES OF HYDROGEN–AIR FLAMES HAVING $T_u = 298$ K, AT ATMOSPHERIC PRESSURE

(Reaction rate parameters from table 9. Transport parameters as in text, with $\sigma_H = 0.35$ nm. Computations with quasi-steady state assumptions.)

$X_{H_2,u}$	0.70	0.60	0.50	0.41	0.30	0.25	0.20	0.15
$T_{b,\,undiss}$/K	1328.4	1644.4	1944.5	2207.8	2521.9	2204.1	1840.6	1472.3
$T_{b,\,equil}$/K	1328.4	1644.0	1940.6	2191.1	2400.5	2170.5	1835.6	1472.0
$S_{u,\,calc}$/(cm s^{-1})	78	163	229	254	200	143	87	33
$10^2\,X_{H,\,max}$ [a]	1.25	3.59	6.18	7.52	4.63	2.64	1.02	0.176
at T/K [a]	1199	1343	1457	1538	1556	1477	1392	1248
$10^5\,X_{O,\,max}$ [a]	6.56	45.0	171	458	1004	1019	677	221
at T/K [a]	1070	1172	1277	1384	1573	1559	1478	1316
$10^5\,X_{OH,\,max}$ [a]	5.20	33.5	158	600	1526	1337	793	264
at T/K [a]	1040	1247	1602	1767	1984	1854	1635	1391
$10^4\,X_{HO_2,\,max}$ [a]	3.4	5.16	5.88	6.09	6.50	7.49	6.11	2.68
at T/K [a, b]	435	363	345	346	341	324	375	528
max. heat release rate/kW cm^{-3}	1.62	6.22	12.84	17.61	14.37	9.97	4.72	0.99
at T/K [a]	940	948	960	980	980	956	1010	1058

(*a*) These maxima and temperatures are only approximate, particularly for HO_2.

(*b*) These temperatures represent approximately the start of the reaction zone, except for the flame with $X_{H_2,u} = 0.15$, for which start of reaction zone is at $T \approx 410$ K.

an initial region of integration with partial equilibrium assumptions on all of reactions (i), (ii) and (iii), and then transferring to the quasi-steady state type of integration at a later stage (see also §§2 and 8). 'Stiffness' problems again arose, and the approach was abandoned. After such a preliminary partial equilibrium calculation, however, the rich flame quasi-steady state formulation (via H atoms) led to a successful integration through the whole flame. The validity of the particular quasi-steady state assumptions involved in these cases will be discussed in §8. The lean flame formulation (via OH) was used successfully for the computation of the 15% hydrogen–air flame, and indeed it will be shown in §8 to be necessary for the computation of that flame.

The forward rate parameters employed in the computation of the hydrogen–air flames are given in table 9, and the expressions used for the independent equilibrium constants have already been listed in §3. The ratios $(k_7 + k_{7a})/k_{12}$, k_{13}/k_{12} and k_{14}/k_{12} are exactly the same as in set 2 of rate parameters in table 4. However, owing to a numerical oversight, the absolute values of k_7, k_{12}, k_{13} and k_{14} are slightly lower than in set 2. This will only affect the computed properties very marginally.

The input data for the transport property calculations are also given in §3, with $\sigma_H = 0.35$ nm. The effect of a small variation in σ_H (to 0.30 nm) on the properties of some of the flames is discussed in §9(*b*) (ii).

Table 10 summarizes a number of the more readily quantifiable flame properties which emerge from the calculation, and figures 19–34 inclusive show the temperature and stable species mole fraction profiles (odd numbered figures) and the radical mole fraction profiles (even numbered figures) in the eight flames. A comparison of the computed burning velocities with experiment will be deferred until after some of the more general features of the flame structures and properties have been discussed in § 9. First of all, however, it is necessary to examine in more detail the validity of the partial equilibrium and quasi-steady state assumptions.

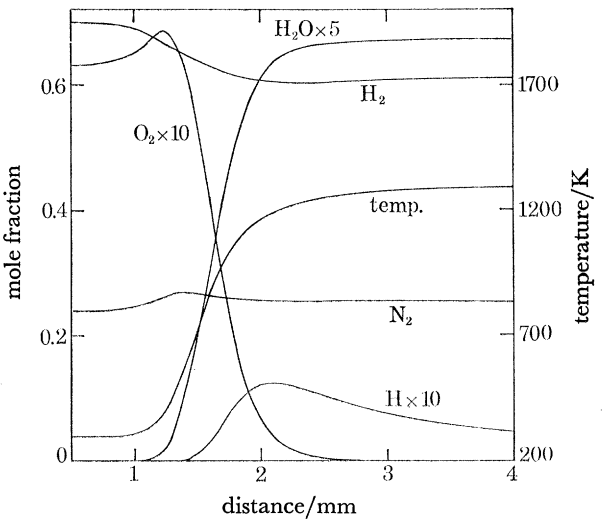

FIGURE 19. Computed temperature profile and mole fraction profiles for stable species and hydrogen atoms in 70% hydrogen–30% air flame at atmospheric pressure, with $T_u = 298$ K. Reaction rate parameters from table 9. Transport parameters as in text, with $\sigma_H = 0.35$ nm. Computed burning velocity $S_{u,calc} = 78$ cm s^{-1}, referred to unburnt gas at 298 K and 1 atm.

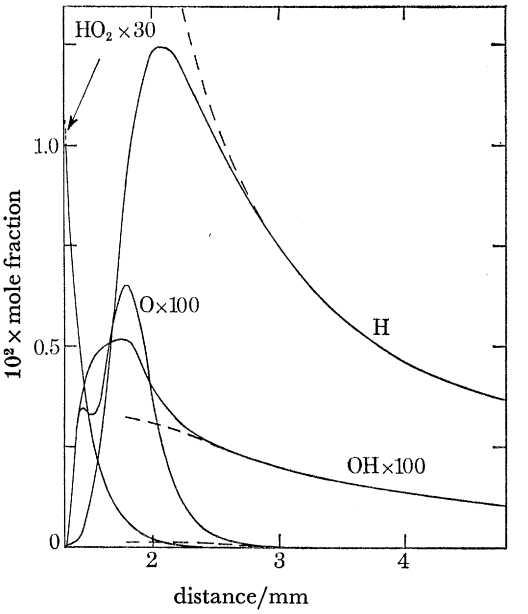

FIGURE 20. Computed mole fraction profiles for radical species in 70% hydrogen–30% air flame at atmospheric pressure, with $T_u = 298$ K. Reaction rate parameters from table 9. Transport parameters as in text, with $\sigma_H = 0.35$ nm. Same distance zero as in figure 19. Solid lines: calculation with quasi-steady state assumptions. Broken lines for H, O and OH: calculation with partial equilibrium assumptions.

8. Validity of partial equilibrium and quasi-steady state assumptions

(*a*) *Partial equilibrium*

The range of validity of the partial equilibrium assumptions in specific flames may be examined by comparison of the H, OH, O and O_2 mole fraction profiles calculated on this assumption with those computed over the whole flame by means of the quasi-steady state conditions. The partial equilibrium assumptions give a radical pool which continues to increase in size indefinitely on integration backwards from the hot boundary of the flame. It can also be shown that the quasi-steady state overall radical profile, represented in the rich flame formulation by $(X_H + 2X_O + X_{OH})$, approaches the similar partial equilibrium profile (i.e. $X_H + 2X_O + X_{OH}$ again) from underneath as the gases move from the cold to the hot side of the flame, and that the quasi-steady state molecular oxygen profile approaches the corresponding partial equilibrium profile

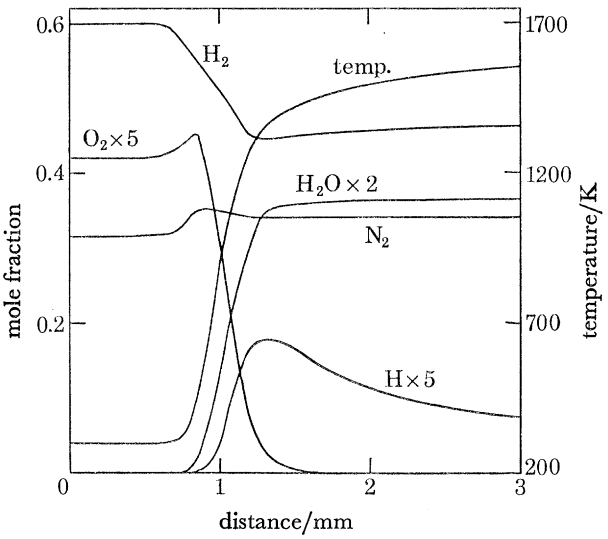

FIGURE 21. Computed temperature profile and mole fraction profiles for stable species and hydrogen atoms in 60% hydrogen–40% air flame at atmospheric pressure, with $T_u = 298$ K. Reaction rate parameters from table 9. Transport parameters as in text, with $\sigma_H = 0.35$ nm. Computed burning velocity $S_{u,calc} = 163$ cm s^{-1}, referred to unburnt gas at 298 K and 1 atm.

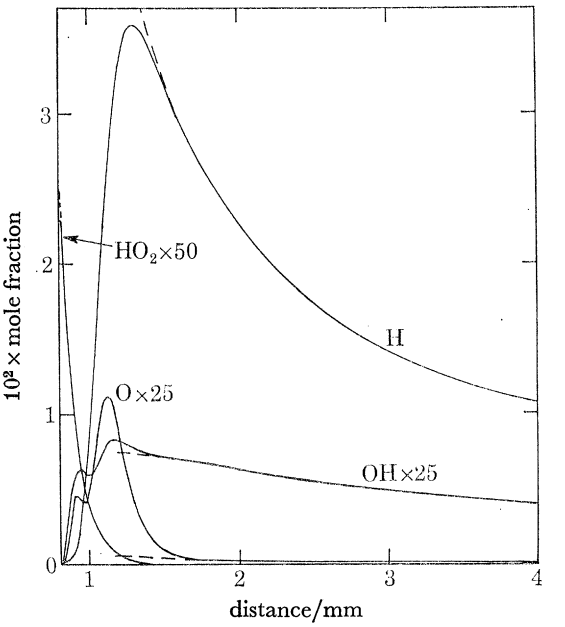

FIGURE 22. Computed mole fraction profiles for radical species in 60% hydrogen–40% air flame at atmospheric pressure, with $T_u = 298$ K. Reaction rate parameters from table 9. Transport parameters as in text, with $\sigma_H = 0.35$ nm. Same distance zero as in figure 21. Solid lines: calculation with quasi-steady state assumptions. Broken lines for H, O and OH: calculation with partial equilibrium assumptions.

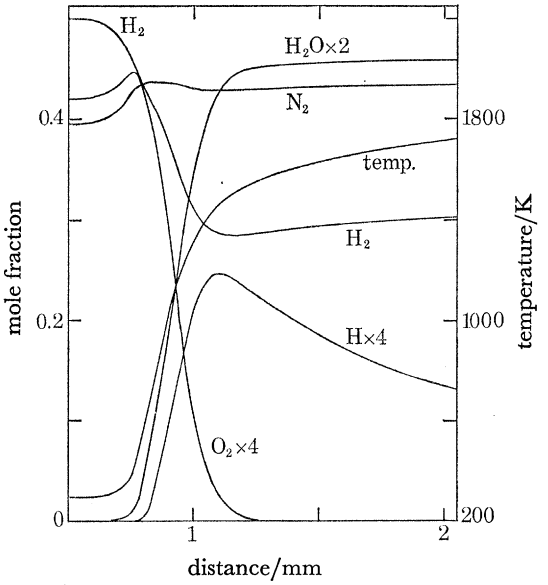

FIGURE 23. Computed temperature profile and mole fraction profiles for stable species and hydrogen atoms in 50% hydrogen–50% air flame at atmospheric pressure, with $T_u = 298$ K. Reaction rate parameters from table 9. Transport parameters as in text, with $\sigma_H = 0.35$ nm. Computed burning velocity $S_{u,calc} = 229$ cm s^{-1}, referred to unburnt gas at 298 K and 1 atm.

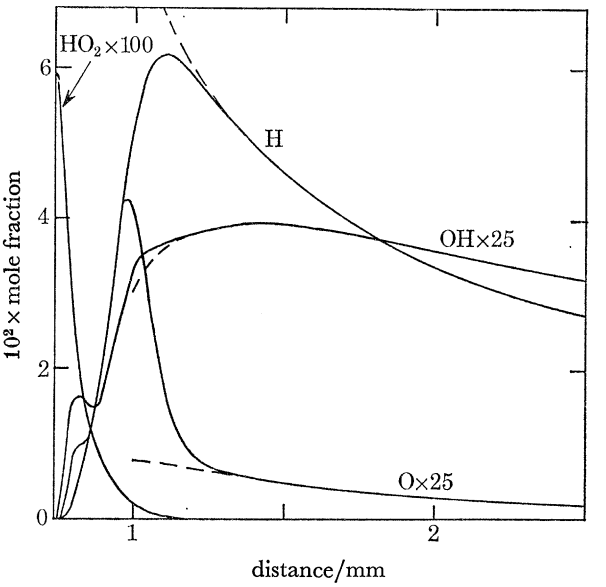

FIGURE 24. Computed mole fraction profiles for radical species in 50% hydrogen–50% air flame at atmospheric pressure, with $T_u = 298$ K. Reaction rate parameters from table 9. Transport parameters as in text, with $\sigma_H = 0.35$ nm. Same distance zero as in figure 23. Solid lines: calculation with quasi-steady state assumptions. Broken lines for H, O and OH: calculation with partial equilibrium assumptions.

PHILOSOPHICAL TRANSACTIONS OF THE ROYAL SOCIETY A MATHEMATICAL, PHYSICAL & ENGINEERING SCIENCES

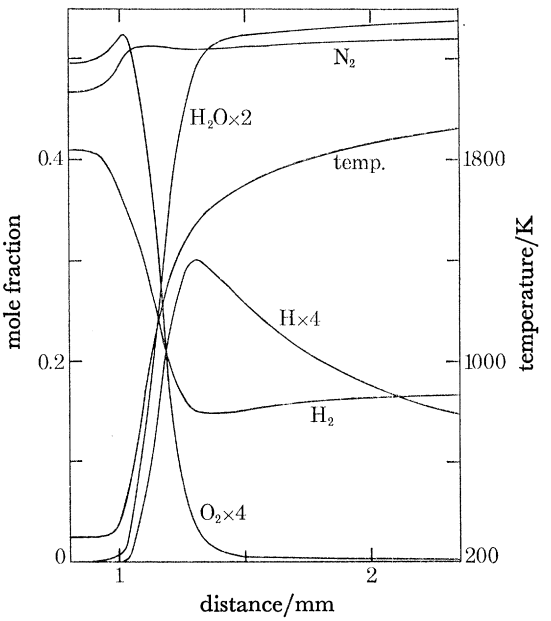

FIGURE 25. Computed temperature profile and mole fraction profiles for stable species and hydrogen atoms in 41% hydrogen–59% air flame at atmospheric pressure, with $T_u = 298$ K. Reaction rate parameters from table 9. Transport parameters as in text, with $\sigma_H = 0.35$ nm. Computed burning velocity $S_{u,calc} = 254$ cm s^{-1}, referred to unburnt gas at 298 K and 1 atm.

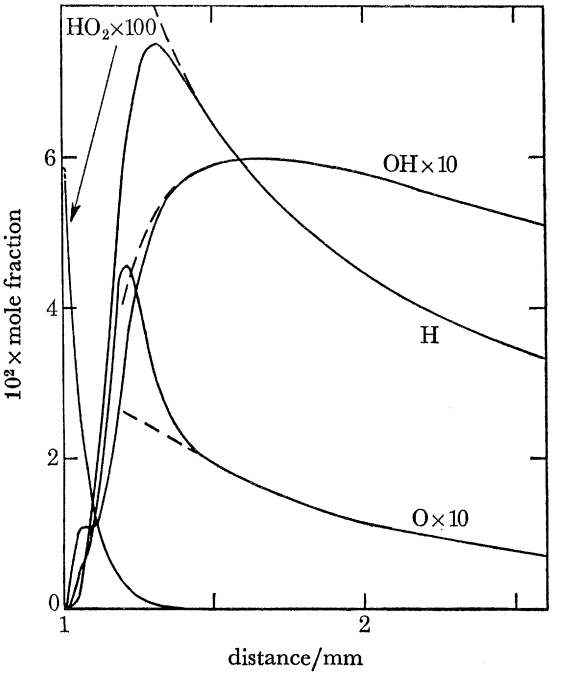

FIGURE 26. Computed mole fraction profiles for radical species in 41% hydrogen–59% air flame at atmospheric pressure, with $T_u = 298$ K. Reaction rate parameters from table 9. Transport parameters as in text, with $\sigma_H = 0.35$ nm. Same distance zero as in figure 25. Solid lines: calculation with quasi-steady state assumptions. Broken lines for H, O and OH: calculation with partial equilibrium assumptions.

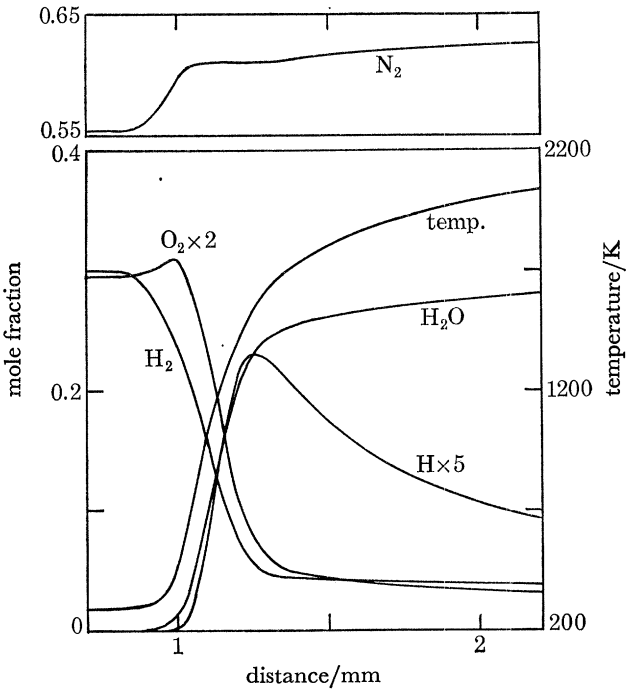

FIGURE 27. Computed temperature profile and mole fraction profiles for stable species and hydrogen atoms in 30% hydrogen–70% air flame at atmospheric pressure, with $T_u = 298$ K. Reaction rate parameters from table 9. Transport parameters as in text, with $\sigma_H = 0.35$ nm. Computed burning velocity $S_{u,calc} = 200$ cm s^{-1}, referred to unburnt gas at 298 K and 1 atm.

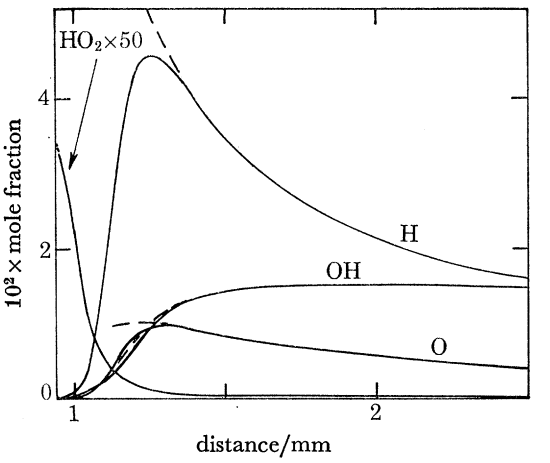

FIGURE 28. Computed mole fraction profiles for radical species in 30% hydrogen–70% air flame at atmospheric pressure, with $T_u = 298$ K. Reaction rate parameters from table 9. Transport parameters as in text, with $\sigma_H = 0.35$ nm. Same distance zero as in figure 27. Solid lines: calculations with quasi-steady state assumptions. Broken lines for H, O and OH: calculation with partial equilibrium assumptions.

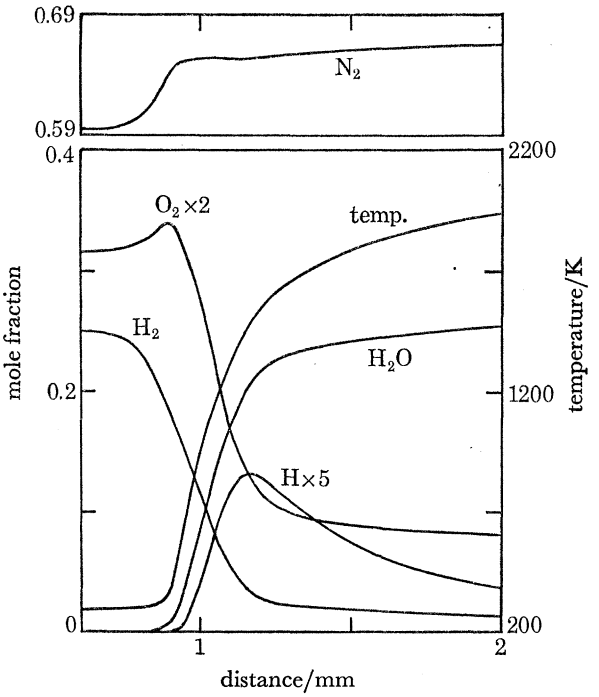

FIGURE 29. Computed temperature profile and mole fraction profiles for stable species and hydrogen atoms in 25% hydrogen–75% air flame at atmospheric pressure, with $T_u = 298$ K. Reaction rate parameters from table 9. Transport parameters as in text, with $\sigma_H = 0.35$ nm. Computed burning velocity $S_{u,calc} = 143$ cm s^{-1}, referred to unburnt gas at 298 K and 1 atm.

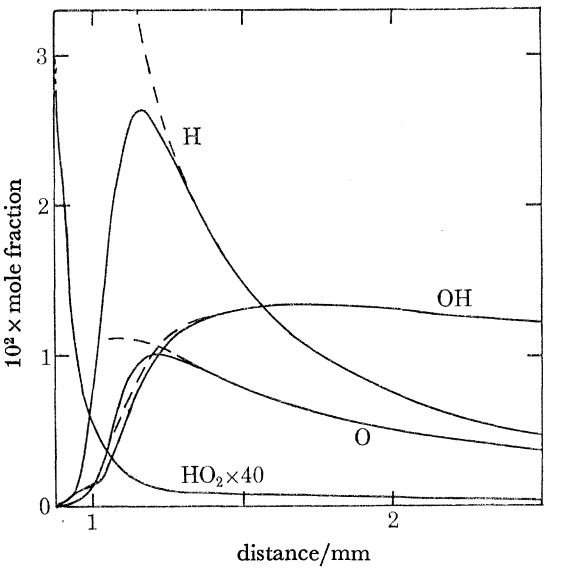

FIGURE 30. Computed mole fraction profiles for radical species in 25% hydrogen–75% air flame at atmospheric pressure, with $T_u = 298$ K. Reaction rate parameters from table 9. Transport parameters as in text, with $\sigma_H = 0.35$ nm. Same distance zero as in figure 29. Solid lines: calculation with quasi-steady state assumptions. Broken lines for H, O and OH: calculation with partial equilibrium assumptions.

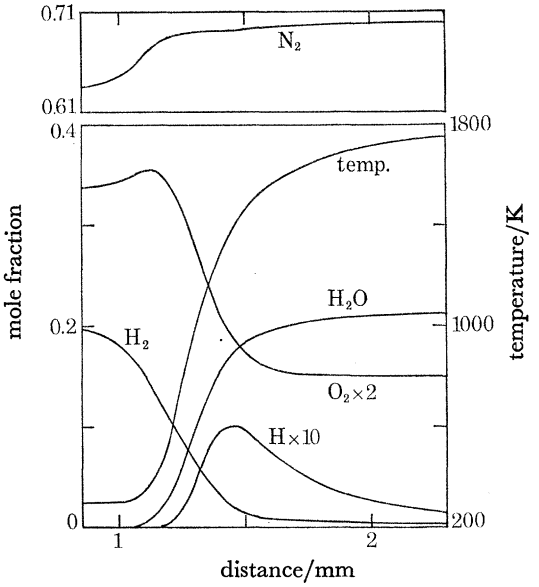

FIGURE 31. Computed temperature profile and mole fraction profiles for stable species and hydrogen atoms in 20% hydrogen–80% air flame at atmospheric pressure, with $T_u = 298$ K. Reaction rate parameters from table 9. Transport parameters as in text, with $\sigma_H = 0.35$ nm. Computed burning velocity $S_{u,calc} = 87$ cm s^{-1}, referred to unburnt gas at 298 K and 1 atm.

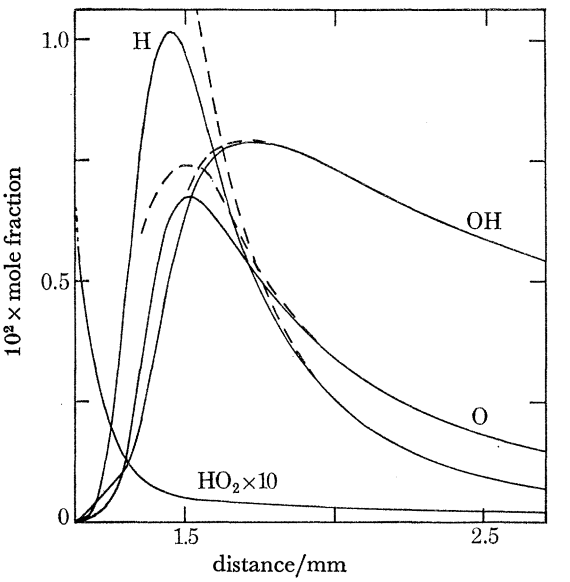

FIGURE 32. Computed mole fraction profiles for radical species in 20% hydrogen–80% air flame at atmospheric pressure, with $T_u = 298$ K. Reaction rate parameters from table 9. Transport parameters as in text, with $\sigma_H = 0.35$ nm. Same distance zero as in figure 31. Solid lines: calculation with quasi-steady state assumptions. Broken lines for H, O and OH: calculation with partial equilibrium assumptions.

PHILOSOPHICAL TRANSACTIONS OF THE ROYAL SOCIETY A MATHEMATICAL, PHYSICAL & ENGINEERING SCIENCES

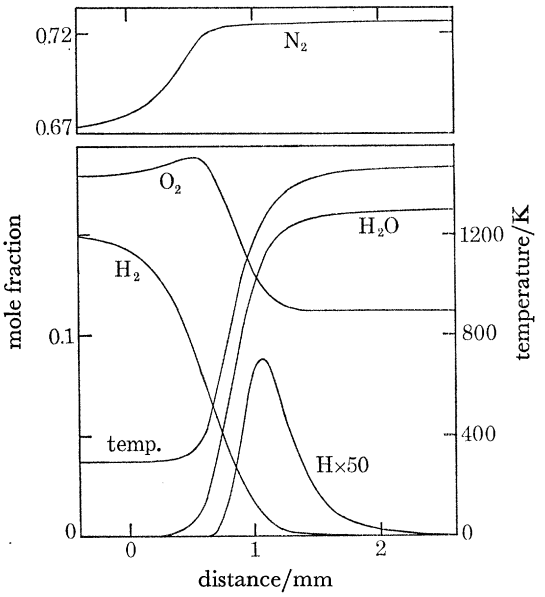

FIGURE 33. Computed temperature profile and mole fraction profiles for stable species and hydrogen atoms in 15% hydrogen–85% air flame at atmospheric pressure, with $T_u = 298$ K. Reaction rate parameters from table 9. Transport parameters as in text, with $\sigma_H = 0.35$ nm. Computed burning velocity $S_{u,\,calc} = 33$ cm s^{-1}, referred to unburnt gas at 298 K and 1 atm.

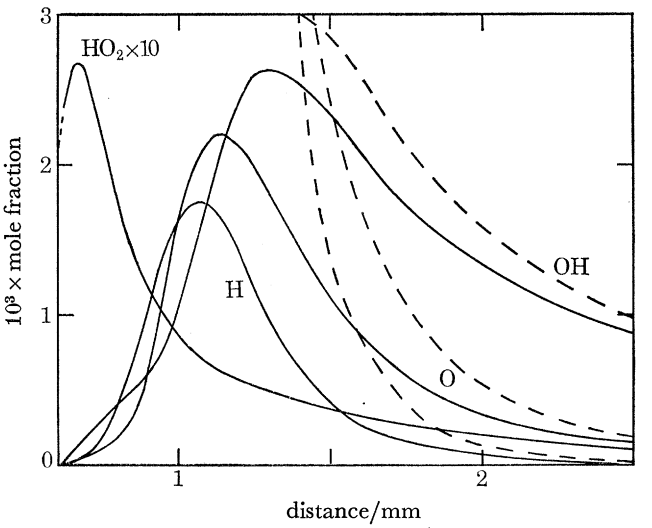

FIGURE 34. Computed mole fraction profiles for radical species in 15% hydrogen–85% air flame at atmospheric pressure, with $T_u = 298$ K. Reaction rate parameters from table 9. Transport parameters as in text, with $\sigma_H = 0.35$ nm. Same distance zero as in figure 33. Solid lines: calculation with quasi-steady state assumptions. Broken lines for H, O and OH: calculation with partial equilibrium assumptions.

from above. Therefore, for given recombination kinetics the partial equilibrium profile gives a maximum possible rate of rise of the overall radical concentration on moving backwards from the hot boundary. However, the distribution of the pool between H, OH and O may be such that, in sufficiently rich flames for example, the comparatively small quasi-steady state oxygen atom concentrations, and to a lesser extent the hydroxyl radical concentrations, appreciably overshoot their partial equilibrium values when the main reaction zone is reached. Attention has been drawn by Dixon-Lewis (1967) to the departure of the [H]/[OH] ratio from its partial equilibrium value in a fuel-rich hydrogen–oxygen–nitrogen flame, while Hamilton & Schott (1967) have shown the possibility of similar oxygen atom overshoots in hydrogen–oxygen shock tube kinetics, particularly in rich mixtures. Such hydroxyl radical or oxygen atom overshoots have been referred to as 'spikes' by Hamilton & Schott, and they are *kinetic* overshoots leading to super–partial equilibrium concentrations of the appropriate radicals. It therefore becomes necessary to distinguish two types of overshoot. The first is the general overshoot of the overall radical pool above full equilibrium. This will be referred to as *partial equilibrium overshoot*. The second is the *kinetic overshoot* of the type just described, which leads to concentrations of the appropriate radicals which are above the partial equilibrium values.

For flame L of table 1, figure 35 compares the radical profiles, the molecular oxygen profile and the temperature profile calculated by the partial equilibrium approach with those obtained from the full flame calculation based on the quasi-steady state conditions. For both atomic and molecular oxygen the concentrations in the reaction zone are clearly very far from those given by the partial equilibrium calculation. The quasi-steady state conditions lead to an oxygen atom

PHILOSOPHICAL TRANSACTIONS OF THE ROYAL SOCIETY A MATHEMATICAL, PHYSICAL & ENGINEERING SCIENCES

'spike' or kinetic overshoot with concentrations up to 40 or 50 times the partial equilibrium value. At a distance of 9.5 mm in figure 35, the quasi-steady state oxygen atom concentration is still some 25% above the partial equilibrium value; while even at much greater distances (20.0 mm) the low quasi-steady state molecular oxygen mole fraction of about 1.5×10^{-9} is still some twenty times above that at partial equilibrium. For OH, the partial equilibrium assumption has higher validity than for O or O_2, with the quasi-steady state conditions still, however, producing some overshoot above the partial equilibrium case when the main reaction zone is reached. The partial equilibrium assumptions can be said to be valid in the recombination zone of this flame for predicting the concentrations of those species which are present in significant amounts.

In similar manner to that just described for flame L, the broken lines in figures 20, 22, 24, 26, 28, 30, 32 and 34 show the radical profiles, calculated with partial equilibrium assumptions, for the hydrogen–air flames whose computed properties are given in table 10. The solid lines show the corresponding quasi-steady state profiles. Figures 20, 22, 24, 26 and 28 show that the hydroxyl radical and oxygen atom kinetic overshoots decrease steadily on moving towards stoichiometric

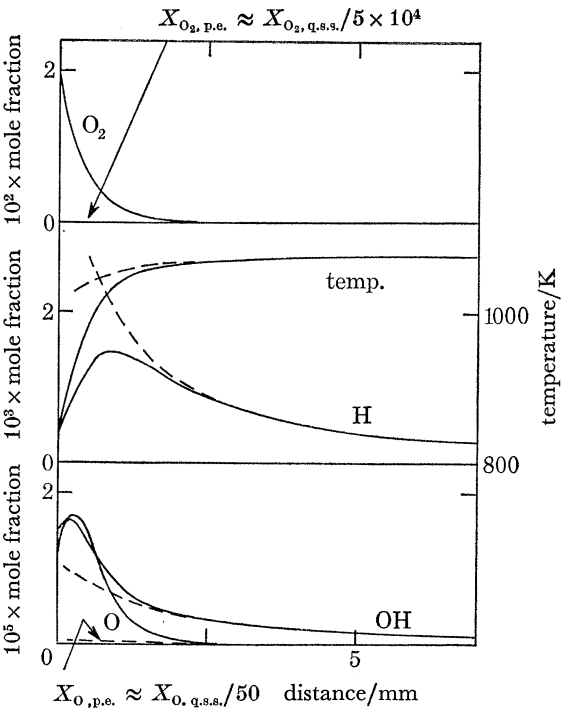

FIGURE 35. Computed quasi-steady state and partial equilibrium profiles for flame L of table 1, using set 2 of reaction rate parameters from tables 3 and 4. Solid lines: calculation with quasi-steady state assumptions. Broken lines: calculation with partial equilibrium assumptions.

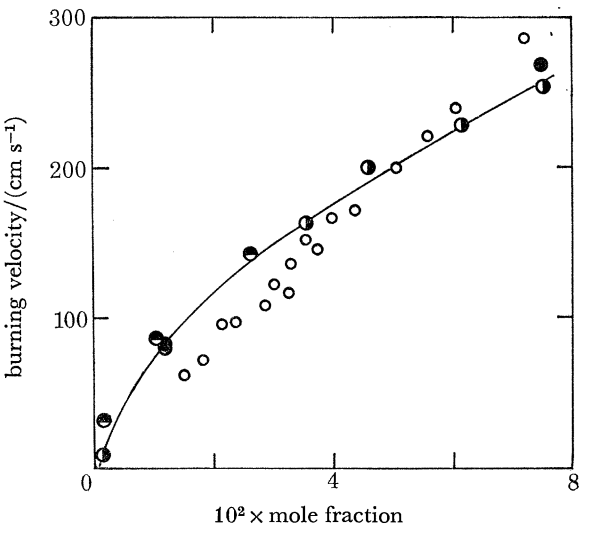

FIGURE 36. Burning velocities of hydrogen–air flames at atmospheric pressure, and flame L of table 1, plotted as a function of maximum hydrogen atom mole fraction. ○, Measurements of Padley & Sugden (1959), referred to burning velocities measured by Jahn (1934); ◑, computed for hydrogen-rich flames: ◓, computed for hydrogen-lean flames, both using quasi-steady state assumptions and reaction rate parameters from table 9, and transport parameters as in text, with $\sigma_H = 0.35$ nm; ●, computed for hydrogen–air flames containing 70 and 41% hydrogen, but without quasi-steady state assumptions, and with $\sigma_H = 0.30$ nm (see §9 (*b*) (ii) and table 14).

from the fuel-rich side. In the case of the hydroxyl radical there is no observable kinetic overshoot in the 41 % hydrogen–air flame, while the oxygen atom overshoot in this flame is by a factor of less than two. Observable oxygen atom kinetic overshoot has disappeared in the 30 % hydrogen–air flame. The disappearance of the kinetic overshoots or 'spikes' coincides with higher temperature levels and the appearance of higher partial equilibrium concentrations of hydroxyl radicals and oxygen atoms in the flames. At the same time it can be seen that in all the fuel-rich flames other than 70 % hydrogen–air, the partial equilibrium and quasi-steady state hydrogen atom profiles coincide almost right up to the peak in the quasi-steady state hydrogen atom mole fraction. Then, after the separation of the profiles, the hydrogen atom maxima are moderately sharp. The former statement implies the validity of the partial equilibrium assumptions in the recombination region. The latter also implies that extrapolation of measured hydrogen atom recombination profiles back into the flames by use of the partial equilibrium assumptions should give a good measure of the maximum concentration of hydrogen atoms. Such a back extrapolation was made for a number of fuel-rich $H_2/O_2/N_2$ flames by Padley & Sugden (1959), who plotted their maximum hydrogen atom concentrations against the burning velocities of the appropriate flames as measured by Jahn (1934). Figure 36 shows the computed data of table 10 and flame L of table 1 plotted in the same way, together with the results of Padley & Sugden. Despite some uncertainty about the measured burning velocities, which will be discussed in § 9, the two sets of results are in reasonable agreement.

Immediately on the fuel-lean side of stoichiometric in the 25 and 20 % hydrogen–air flames, the range of validity of the partial equilibrium approach is shown by the radical profiles of figures 30 and 32. Again the solid lines result from the quasi-steady state calculation (with rich flame formulation as indicated in § 7), and the broken lines refer to the calculation with partial equilibrium assumptions. The results for the two flames are similar to those for the 30 % hydrogen–air flame, in that (i) the two hydrogen atom profiles virtually coincide almost right up to the maximum in the quasi-steady state hydrogen atom mole fraction, and (ii) there is no observable kinetic overshoot in either the hydroxyl radical or oxygen atom profiles. One minor feature of the lean flame calculations, not observable with the fuel-rich mixtures, was that over an extended distance range (say 7 or 8 mm) in the burnt gases, the quasi-steady state calculation gave profiles for all the radicals which were very slightly steeper (1 or 2 %) than those resulting from the partial equilibrium calculation. It is unlikely that the difference is of much significance.

Lastly, figure 34 shows that in the 15 % hydrogen–air flame the partial equilibrium assumptions are not strictly valid in any of the burnt gas recombination region near the main reaction zone. It turns out that in this flame, where the concentrations of both atomic and molecular hydrogen in the recombination region are relatively much lower than in any of the other flames studied, reaction (ii) contributes to the burnt gas recombination by proceeding in the reverse direction on balance. The net reverse rate of reaction (ii) in the burnt gas region amounts to some 10 % of its simple overall backward rate given by $k_{-2}[\mathrm{OH}][\mathrm{O}]$. Even in the 20 % hydrogen–air flame the similar effect is much smaller (< 2 %). It is noteworthy that in both these flames (and in none of the others investigated) the molecular oxygen concentration sinks to slightly below its full equilibrium value at the end of the main reaction zone, and climbs back to full equilibrium in the recombination region.

To conclude this discussion of the partial equilibrium assumptions, it is now opportune to reconsider the validity of the computational approaches of §§ 3 and 5 in connection with the determination of recombination rate coefficients from measurements of hydrogen atom or

hydroxyl radical concentration decay profiles in the burnt gas regions of both rich and lean flames. Two points emerge:

(i) The *kinetic* overshoot phenomena in fuel-rich flames do not invalidate the partial equilibrium approach, since in those flames where the overshoot is important the concentrations of the overshooting species are too low to contribute appreciably to the overall radical concentrations. It is more likely that the conditions in many actual flames are such that the partial equilibrium approach will predict very slightly too rapid a recombination rate from a given set of rate coefficients. In some circumstances involving rich flames, however, oxygen atom overshoot may influence the accuracy of prediction of rates of oxygen atom reactions based on the partial equilibrium assumptions. This may need careful consideration, for example, before attempting to calculate nitric oxide formation by the Zeldovich mechanism.

(ii) The breakdown of the partial equilibrium assumptions in the recombination region of the 15% hydrogen–air flame must cast some doubt on the validity of the analysis of the lower temperature, lean flame recombination results in §5(*a*). However, in the analysis of §5(*a*) it is the gradient of the graph of $[OH]^{-1}$ which is compared with experiment. For a given concentration of the hydroxyl radical, figure 34 shows that in this respect both the quasi-steady state and partial equilibrium approaches give virtually the same gradients. Errors introduced should lie well within other uncertainties.

(*b*) *Quasi-steady state assumptions*

In the straightforward formulation of the hydrogen–oxygen flame problem without quasi-steady state assumptions, the stationary flame continuity equations governing the fluxes of hydroxyl radicals and oxygen atoms are

$$\begin{aligned} M_y(\mathrm{d}G_{OH}/\mathrm{d}y) = m_{OH}\rho_m^2\{&(k_{-1}X_H X_{H_2O} + k_2 X_H X_{O_2} + k_3 X_O X_{H_2} + 2k_7 X_H X_{HO_2} \\ &+ k_{-13} X_{H_2O} X_{O_2} + k_{14} X_O X_{HO_2} + \sum_M k_{-16,M} X_{H_2O} X_M \\ &+ \rho_m \sum_M k_{17,M} X_H X_O X_M + 2k_{-18} X_O X_{H_2O}) \\ &- (k_1 X_{OH} X_{H_2} + k_{-2} X_{OH} X_O + k_{-3} X_{OH} X_H + 2k_{-7} X_{OH}^2 \\ &+ k_{13} X_{OH} X_{HO_2} + k_{-14} X_{OH} X_{O_2} + \rho_m \sum_M k_{16,M} X_H X_{OH} X_M \\ &+ \sum_M k_{-17,M} X_{OH} X_M + 2k_{18} X_{OH}^2)\}, \end{aligned} \tag{4}$$

and

$$\begin{aligned} M_y(\mathrm{d}G_O/\mathrm{d}y) = m_O\rho_m^2\{&(k_2 X_H X_{O_2} + k_{-3} X_{OH} X_H + k_{7a} X_H X_{HO_2} + k_{-14} X_{OH} X_{O_2} \\ &+ \sum_M k_{-17,M} X_{OH} X_M + k_{18} X_{OH}^2) \\ &- (k_{-2} X_{OH} X_O + k_3 X_O X_{H_2} + k_{-7a} X_O X_{H_2O} + k_{14} X_O X_{HO_2} \\ &+ \rho_m \sum_M k_{17,M} X_H X_O X_M + k_{-18} X_O X_{H_2O})\}, \end{aligned} \tag{5}$$

where M_y represents the mass burning velocity of the one dimensional flame lying in the x, z plane, G_i represents the mass fraction of species i in the mass rate of flow, m_i is molecular mass, ρ_m represents molar density, and X is mole fraction.

Formally, equations (4) and (5) may be written as

$$\begin{aligned} M_y(\mathrm{d}G_i/\mathrm{d}y) &= \text{net mass chemical rate of formation of species,} \\ &= (\text{total mass chemical rate of formation}) - (\text{total mass chemical rate of removal}), \end{aligned} \tag{6}$$

and they provide differential equations governing the gradients of the fluxes of the species in the flame. The normal chemical quasi-steady state assumptions replace these differential equations by algebraic equations, by putting $M_y(\mathrm{d}G_i/\mathrm{d}y) = 0$ for the appropriate species. Their use in the flame calculation involves differentiation of the resulting algebraic equations to give new linear differential equations involving the mole fraction gradients of all the species present in the flame (Dixon-Lewis, Goldsworthy & Greenberg 1975*a*).

TABLE 11. RATIOS OF (|NET RATE OF FORMATION|/TOTAL RATE OF FORMATION) OF OH IN HYDROGEN–OXYGEN–NITROGEN FLAMES FOR WHICH THE COMPOSITE FLUX FORMULATION VIA H ATOMS WAS USED IN COMPUTATION

(Flames are identified either by letter (from table 1), or by value of $X_{\mathrm{H_2,u}}$ in the hydrogen–air system. Rate parameters from table 9. Transport parameters as in text, with $\sigma_{\mathrm{H}} = 0.35$ nm.)

approx. temp./K	flame L	0.70	0.60	0.50	0.41	0.30	0.25	0.20
500	—	< 0.010	0.035	0.080	0.12	0.15	0.097	0.003
600	0.005	0.006	0.014	0.022	0.061	0.063	0.081	0.053
700	0.001	0.002	0.002	0.002	0.006	0.030	0.030	0.034
800	0.001	< 0.001	0.003	0.008	0.012	0.004	0.003	0.015
900	< 0.001	< 0.001	0.003	0.008	0.014	0.017	0.014	0.011
1000	< 0.001	< 0.001	< 0.001	0.004	0.009	0.010	0.002	0.016
1200	—	< 0.001	0.002	0.007	0.014	0.014	0.009	0.003
1400	—	—	< 0.001	0.001	0.012	0.020	0.006	0.017
1600	—	—	< 0.001	< 0.001	0.002	0.011	0.007	0.003
1800	—	—	—	—	0.001	0.002	0.001	0.004
2000	—	—	—	—	—	< 0.001	< 0.001	—

TABLE 12. RATIOS OF (|NET RATE OF FORMATION|/TOTAL RATE OF FORMATION) OF O ATOMS IN HYDROGEN–OXYGEN–NITROGEN FLAMES FOR WHICH THE COMPOSITE FLUX FORMULATION VIA H ATOMS WAS USED IN COMPUTATION

(Flames are identified either by letter (from table 1), or by value of $X_{\mathrm{H_2,u}}$ in the hydrogen–air system. Rate parameters from table 9. Transport parameters as in text, with $\sigma_{\mathrm{H}} = 0.35$ nm.)

approx. temp./K	flame L	0.70	0.60	0.50	0.41	0.30	0.25	0.20
500	—	—	0.32	0.66	0.57	0.33	0.038	0.60
600	0.060	0.33	0.59	0.71	0.60	0.45	0.35	0.17
700	0.011	0.031	0.13	0.049	0.15	0.23	0.065	0.066
800	0.004	0.027	0.12	0.26	0.32	0.31	0.40	0.25
900	0.011	0.001	0.018	0.052	0.050	0.18	0.30	0.30
1000	< 0.001	0.010	0.031	0.044	0.040	0.058	0.059	0.093
1200	—	0.008	0.014	0.062	0.12	0.13	0.10	0.078
1400	—	—	0.024	0.035	0.019	0.063	0.055	0.038
1600	—	—	< 0.001	0.004	0.023	0.002	0.002	0.007
1800	—	—	—	—	0.004	0.005	0.005	0.004
2000	—	—	—	—	—	0.003	0.003	—

Following the solution of the equations with quasi-steady state assumptions it is possible to calculate all the flux gradients within the flame, including those for which the quasi-steady state assumptions are made, and hence (by equation (6)) to calculate the net rate of formation of each species. An estimate of the validity of the quasi-steady state assumptions may then be obtained by comparing the net rates of formation of the appropriate radicals with the total rates of formation (or removal) as implied in equations (4), (5) and (6). Tables 11 and 12 give such comparisons

for the hydroxyl radical and oxygen atom respectively, in those flames for which the fuel-rich quasi-steady state formulation was used. Table 13 gives a similar comparison for both hydrogen and oxygen atoms, from the fuel-lean formulation of the 15% hydrogen–air flame. In those flames for which the fuel-rich composite flux formulation was used, table 11 shows the quasi-steady state assumption for OH to be reasonably valid everywhere except at the extreme low temperature ends of some of the reaction zones. For oxygen atoms, however, table 12 shows the validity of the assumptions to be more questionable. In the 15% hydrogen–air flame, in the computation of which the lean flame formulation was used, the validity of both the quasi-steady state conditions is somewhat questionable (table 13), but the more so in the case of the oxygen atoms.

TABLE 13. RATIOS OF (|NET RATE OF FORMATION|/TOTAL RATE OF FORMATION) OF HYDROGEN AND OXYGEN ATOMS IN 15% HYDROGEN–AIR FLAME

(Rate parameters from table 9. Transport parameters as in text, with $\sigma_H = 0.35$ nm.)

approx. temp./K	H	O
500	0.24	0.71
600	0.17	0.13
700	0.14	0.038
800	0.087	0.21
900	0.038	0.24
1000	0.012	0.093
1200	0.078	0.069
1400	0.032	0.005
1440	0.046	0.020
1460	0.029	0.019
1470	0.004	0.005

Because of the uncertainty regarding the validity of the quasi-steady state approach when applied to oxygen atoms, a single calculation was performed for the 30% hydrogen–air flame, in which the quasi-steady state assumptions were applied only to the hydroxyl radical and HO_2. The general method of calculation is indicated in §2. The oxygen atom fluxes and concentrations were treated from first principles, with the flux gradients expressed explicitly by equation (5). The 30% hydrogen–air flame was chosen for investigation since it is the fuel-rich flame nearest to stoichiometric, and therefore having the highest oxygen atom concentrations of the fuel-rich flames studied. Because of the occurrence of polyhedral flame phenomena in the fuel-lean hydrogen–oxygen system, the computed properties of the lean flames are not so easily compared with experiment as the rich (see §9). The fuel-lean flame calculations were therefore considered to be somewhat less important than those for the rich flames.

In the case of the 30% hydrogen–air flame, the more precise treatment of the oxygen atom fluxes in the manner described caused an increase in the computed burning velocity, to about 210 cm s^{-1}. However, a quite independent method of calculation, but with the same input data and an entirely equivalent treatment of the transport processes, did not confirm this result. The latter calculation was performed by implicit finite difference solution of the time-dependent equations for the flame, without any quasi-steady state assumptions, and led to $S_u = 200$ cm s^{-1}. This is exactly the same burning velocity as that given in table 10. Similar treatments of the 20, 41 and 70% hydrogen–air flames by means of the time-dependent equations led to similar rather precise agreement with the results from the composite flux method. These treatments will be discussed further in §9 (*b*) (ii).

9. Discussion

(*a*) *Rates of heat release and radical production in the flames. General flame mechanism*

Figure 37 shows the heat release patterns at various temperatures in each of the hydrogen–air flames studied. Apart from the high magnitudes of these rates, which reach a maximum of 17.6 kW cm^{-3} (17.6 GW m^{-3}) in the 41 % hydrogen–air flame, the other striking feature is the small extent of the preheat zones in all the flames. In these zones, as well as in the early reaction zones, the transport processes ensure heating of the gases entering the flame, at the expense of dilution with reaction products. It is the increase in reaction rate due to this heating which is the

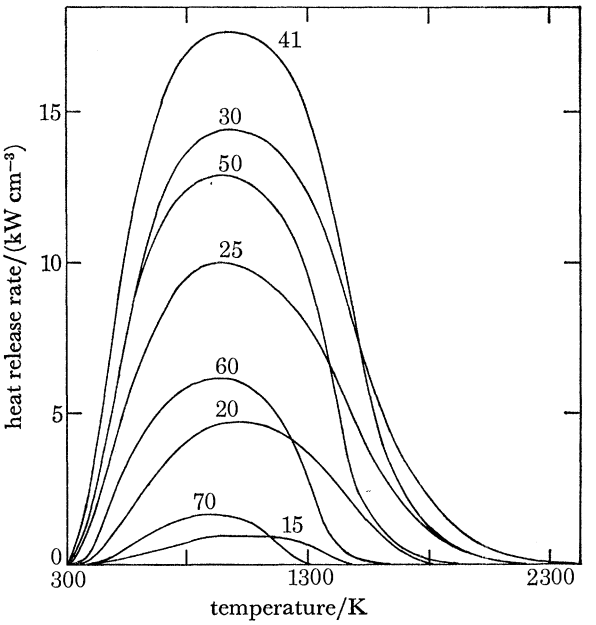

Figure 37. Computed heat release rates in hydrogen–air flames at atmospheric pressure. Numbers immediately above curves refer to percentage hydrogen in initial mixture at 298 K.

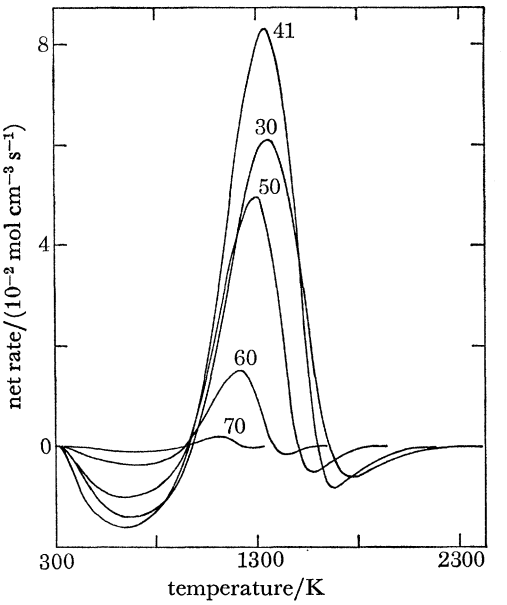

Figure 38. Computed rates of formation of radical pool, defined as $(X_H + 2X_O + X_{OH})$, where X is mole fraction, in fuel-rich hydrogen–air flames at atmospheric pressure. Numbers immediately above curves refer to percentage hydrogen in initial mixture at 298 K.

more important process for certain of the essential reactions in the flame, in particular for the high activation energy radical producing steps. Figures 38 and 39 show the overall chemical rates of production of radicals as a function of temperature in the hydrogen–air flames. The net chemical production of radicals occurs only in the higher temperature regions of the flames, starting at about 950 K (or a little above in leaner flames) and terminating slightly downstream of the maxima in the hydrogen atom mole fraction profiles (cf. table 10 and figures 19–34). Maximum production rates occur at temperatures between 1100 and 1350 K. The major heat releasing regions in the flames arise from the diffusion of the radicals *upstream* from these sources, and their subsequent reaction by lower activation energy steps.

Overall, the flames can be considered to consist effectively of *four* regions:

(i) A small preheat zone where a little heating occurs by thermal conduction alone.

(ii) The major heat release zone, where radicals produced in zone (iii), having diffused upstream, react with incoming gas by low activation energy steps. The gas in the early part of zone (ii) still also receives heat by thermal conduction.

(iii) A radical production zone where the temperature is high enough and the reactant concentrations are such that the system is effectively in a chain branching condition. In this zone the chain branching cycle moves towards partial equilibrium.

(iv) The radical recombination region, where the system decays towards full equilibrium, subject to the partial equilibrium conditions eventually achieved near the end of zone (iii).

There is, of course, some overlap between adjacent zones, so that their edges are not clearly defined.

It is important to note that this typical behaviour, with heat releasing reactions occurring at quite low temperatures, is contrary to that normally assumed for the purpose of obtaining analytical solutions to the flame problem. The global reaction models used for the latter purpose (see, for example, Zeldovich & Frank–Kamenetskii 1938*a*, *b*, *c*; Semenov 1940; Zeldovich & Semenov 1940; Zeldovich 1947) normally assume a single exothermic reaction of high activation energy to be driving the flame; they result in a preheat zone, with pure thermal conductive heating and no appreciable reaction, which extends up to very high temperatures. The real situation is more complex than this, and it is more difficult to uncouple the physical from the chemical processes.

The critical importance of the high temperature region in the real flame lies in the necessity for an adequate rate of production of radicals there.

(*b*) *Comparison of computed burning velocities of hydrogen–air flames with experiment*

(i) *Preliminary comparison*

Two earlier sets of measurements of the burning velocities of hydrogen–air mixtures at atmospheric pressure were made by Jahn (1934) and Scholte & Vaags (1959). Both sets of authors found the maximum burning velocity to occur at about 42% hydrogen, and to lie between 270 and 280 cm s^{-1}. The method of measurement used by Jahn was to divide the area of the schlieren cone of the flame into the volume flow rate of the gases entering it. Scholte & Vaags burned their flames as straight-sided cones on a constant velocity profile nozzle. They calculated the linear gas velocity, V, from the total volumetric gas flow and the area of the burner port, and then derived the burning velocity by measuring the cone half-angle, α, and using $S_u = V \sin \alpha$. For a 50% hydrogen–air flame with $T_u = 298$ K, both sets of investigators found a burning velocity of 250 (± 10) cm s^{-1}.

Three more recent measurements of the same hydrogen–air burning velocities, again with the use of burner methods, have given higher results. These measurements have used greater refinement, in that the gas velocities V approaching the flames have been measured directly by means of the powder particle tracking technique with stroboscopic illumination. All three investigations were carried out using nozzle burners, and again schlieren photography was used to define the flame cone half-angle, α. By this means, and using a nozzle of diameter 1 cm, Edmondson & Heap (1971) found $S_u = 296$ cm s^{-1} for the 50% hydrogen–air flame with $T_u = 295$ K. Using a conical flame of the same composition on a smaller nozzle of 4 mm diameter, Günther & Janisch (1971) found $S_u = 328$ cm s^{-1}; and from a button-shaped flame having the same initial conditions these authors (Günther & Janisch 1972) obtained $S_u = 305$ cm s^{-1}. The latter result was preferred because of the reduced curvature in the button-shaped flame.

In apparent support of the burning velocity of near 300 cm s^{-1}, Day *et al.* (1972) predicted by means of an earlier computation a burning velocity of 310 cm s^{-1} for the 50% hydrogen–air flame at atmospheric pressure (see also Dixon-Lewis 1970*b*). However, the present more refined

calculations predict lower burning velocities, and do not directly support the higher measured values. Figure 40 shows the whole range of burner measurements just discussed, together with the newly computed burning velocities from table 10. The theoretical curve shown in figure 40 correctly predicts the position of the maximum burning velocity, but it agrees with the older results of Jahn (1934) and Scholte & Vaags (1959) rather than with the newer and more refined measurements. The major change in the kinetic model as compared with the earlier calculation reported by Day *et al.* (1972) is the inclusion of the reverse reactions into the chemical mechanism.

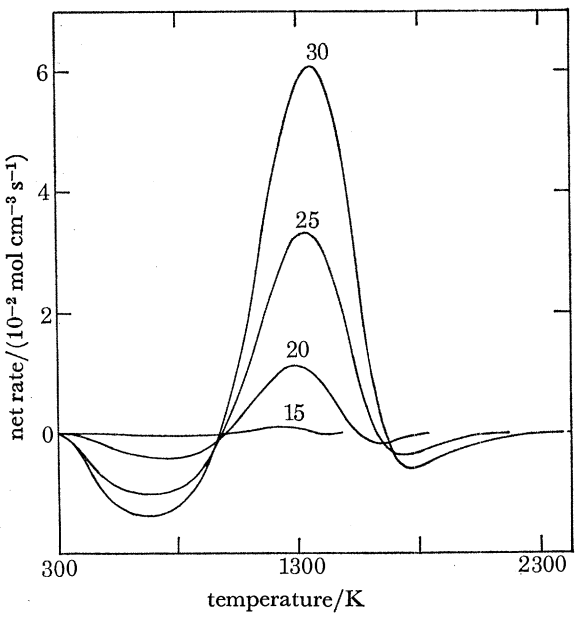

FIGURE 39. Computed rates of formation of radical pool, defined as $(X_H + 2X_O + X_{OH})$, where X is mole fraction, in fuel-lean hydrogen–air flames at atmospheric pressure. Numbers immediately above curves refer to percentage hydrogen in initial mixture at 298 K. The 30% hydrogen–air flame is included here to facilitate comparison.

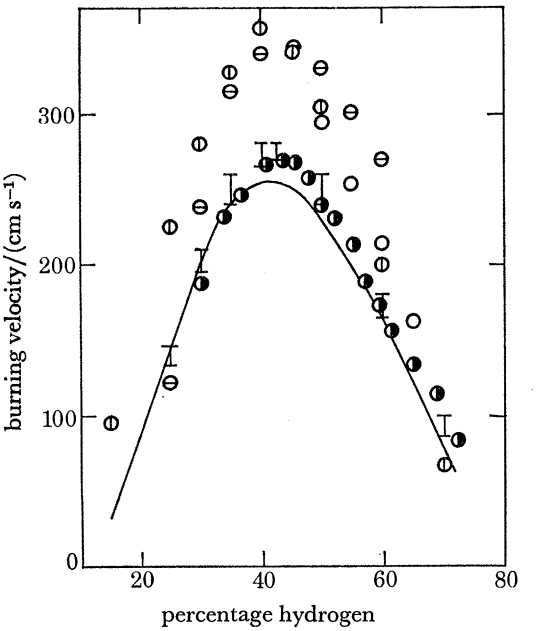

FIGURE 40. Burning velocities of hydrogen–air mixtures, comparing computed line with published measurements by burner methods. ◑, Jahn (1934); ⌶, Scholte & Vaags (1959); ○, Edmondson & Heap (1971); ⊖, Günther & Janisch (1971); ⊙, Günther & Janisch (1972). Reaction rate parameters for computations from table 9, and transport parameters as in text, with σ_H = 0.35 nm.

For both models, i.e. with and without reverse reactions, the rate parameters of the elementary steps were adjusted as in §4 by reference to the low temperature, very hydrogen-rich flames, in which the concentrations of OH and O are very small. As the concentrations of these species become larger in the hotter, less fuel-rich flames, the chain breaking reaction (−ii) may contribute appreciably to the chemistry, and so to the difference between the two predictions. At the cold end of the 50% hydrogen–air flame, reaction (−ii) contributes up to about 25% of the total rate of chain termination when the more refined model is used.

Returning to the comparison between theory and experiment illustrated in figure 40, the techniques used by Edmondson & Heap (1971) and Günther & Janisch (1972) for the measurement of the burning velocities have incorporated more refinements than the earlier approaches of Jahn (1934) and Schotle & Vaags (1959). For this reason the more recent values are to be preferred, and the problem arises of trying to explain the apparent differences between prediction

and measurement. These may be due either to purely numerical defects in the choice of rate parameters or to some more fundamental defect in the flame model, or they may be due to some defect in the method of comparison. Each of these possibilities will be considered in relation to the hydrogen-rich flames. On the lean side of stoichiometric the burning velocity measurement is complicated by the occurrence of cellular flame phenomena, and the differences associated with the flames containing 25% hydrogen or less will not be considered.

(ii) *Further consideration of reaction rate and diffusion parameters*

The assignment of rate parameters to the elementary reaction steps of the hydrogen–oxygen–nitrogen flame system, described in §§3–5, takes account of a wide variety of experimental data from flame and explosion limit studies, from shock tube studies, and from measurements at lower temperatures in fast flow systems. However, in terms of properties relating to the main reaction zones of the flames, discussion at that stage was restricted in §4 to the low temperature, hydrogen-rich systems. The approach to leaner flame conditions was limited in §5 to consideration of recombination, and effectively dealt only with reactions (iv) and (xiii). The weakest part of the analysis is probably that dealing with the partitioning of the hydroperoxyl radical between reactions (vii), (vii*a*), (xii), (xiii), (xiv) and (−iv); and in particular, reaction (xiv) has been assigned a slightly arbitrary rate expression based only on the curvature of the burning velocity plot in figure 6 (cf. §4(*b*)). Also, the rate coefficient k_{17}, which controls the rate of direct recombination of hydrogen and oxygen atoms, is arbitrarily defined; and in addition, although k_{16} has been assigned an expression which satisfactorily fits flame recombination data at temperatures between 1500 and 2000 K, its temperature dependence implied by equations (3*a*) and (3*b*) is probably too small. Using a discharge-flow system in conjunction with resonance fluorescence for the measurement of hydroxyl radical concentration, Zellner, Erler & Field (1977) have recently found $k_{16,\,N_2} = 1.7 \times 10^{17}$ cm^6 mol^{-2} s^{-1} at 300 K. In conjunction with the recombination results from flames and high temperature systems, this leads to $k_{16,\,N_2} = 1.6 \times 10^{22}\ T^{-2.0}$ cm^6 mol^{-2} s^{-1}. However, the sensitivity of the computed burning velocity to this change in k_{16} is found to be low. The use of the new expression for k_{16} instead of that given in table 9 leads to a reduction of only 1% in the computed burning velocities of both flame L of table 1 and the 41% hydrogen–air flame.

The occurrence of the maximum burning velocity on the fuel-rich side of stoichiometric is associated with the increase in the concentrations of OH and O as the stoichiometric composition is approached, and the consequent increased contribution from the chain breaking steps (xiii) and (xiv). The more or less correct prediction of the position of the maximum burning velocity therefore indicates that the partitioning of the HO_2 between its reactions with H atoms on the one hand, and with OH and O on the other, is not too seriously in error. On the other hand, inspection of figure 40 suggests that the rate parameters of table 9 predict burning velocities which become progressively lower than the measured values as the flames become leaner, and clearly this could be associated with the imprecision of the rate parameters for the reactions (xiv) and (xvii) of oxygen atoms. Accordingly, some fresh calculations were carried out in which $k_{14} = k_{17} = 0$. Using set 2 of parameter ratios from table 3, a similar procedure to that described in §4 was employed in order to derive a new set of rate parameters which satisfied the measured properties of flame L in table 1. As expected, a small reduction in k_2 and the other rate coefficients was necessary in order to compensate for the removal of the chain terminating effects of reactions (xiv) and (xvii). The revised expression for k_2 became $k_2 = 1.36 \times 10^{14} \exp(-8250/T)$ cm^3 mol^{-1} s^{-1}. The new rate parameters were next used to calculate the burning velocities of both

the 70 and the 30 % hydrogen–air flames. The burning velocity of the 70 % hydrogen–air flame was reduced by 1 % compared with table 10, and that of the 30 % hydrogen–air flame was increased by only 6 %, to 212 cm s^{-1}. In the context of the observed differences between theory and experiment, this increase is not significant. It must be concluded that imprecisions in k_{14} and k_{17} are not responsible for the observed differences, and indeed this conclusion is supported by recent independent measurements of k_{14}. Burrows, Harris & Thrush (1977) have found $k_{14} = (2.1 \pm 0.8) \times 10^{13}$ cm^3 mol^{-1} s^{-1} at 293 K. The parameters given in table 9 lead to $k_{14} = 3.5 \times 10^{12}$ at 300 K, and 9.5×10^{12} at 1000 K.

TABLE 14. EFFECTS OF LENNARD-JONES POTENTIAL PARAMETER σ_H, AND OF QUASI-STEADY STATE ASSUMPTIONS, ON COMPUTED PROPERTIES OF FIVE HYDROGEN–AIR FLAMES HAVING $T_u = 298$ K AT ATMOSPHERIC PRESSURE

(Reaction rate parameters from table 9).

	with q.s.s.				without q.s.s.			
r_H/nm =	0.35		0.30		0.35		0.30	
$X_{H_2,u}$	S_u/(cm s^{-1})	$10^2 X_{H,max}$	S_u/(cm s^{-1})	$10^2 X_{H,max}$	S_u/(cm s^{-1})	$10^2 X_{H,max}$	S_u/(cm s^{-1})	$10^2 X_{H,max}$
0.70	78	1.25	81	1.22	77	1.26	80	1.23
0.50	229	6.18	—	—	—	—	240	6.09
0.41	254	7.52	265	7.45	—	—	267	7.46
0.30	200	4.63	209	4.66	200	4.69	211	4.65
0.20	87	1.02	90	1.01	—	—	89	1.07

Another factor which may contribute to the lack of agreement is the use of possibly incorrect values for the diffusion parameters. In particular, the value used for σ_H in the hydrogen–air computations was higher than the optimum value of $\sigma_H = 0.30$ nm associated in §4 with the particular set of rate parameters used. For the hydrogen–air flames having $X_{H_2,u} = 0.70$, 0.50, 0.41, 0.30 and 0.20, the effects on the burning velocities and the maximum hydrogen atom mole fractions of a reduction in σ_H from 0.35 to 0.30 nm are given in table 14. The effects of the reduction on the maximum radical mole fractions are not large. Columns 2–5 of table 14 refer to calculations by the composite flux method, with the quasi-steady state assumptions. Columns 6–9 give values obtained by solution of the time-dependent equations, without the assumptions, and with an exactly equivalent formulation of the transport processes. The effect of the quasi-steady state assumptions can be seen to be negligible in all the flames, and indeed the only appreciable differences between the two treatments were in the heights of the HO_2 peaks, which occur right at the cold boundaries of the reaction zones (see even-numbered figures 20–34). The modification in σ_H leads to an increase of some 4 or 5 % in all the burning velocities. However, this increase again is not of sufficient magnitude to explain the observed differences between the computed and measured burning velocities.

Other attempts to resolve the problem by simple numerical adjustments of rate parameters while, by the use of table 8, keeping within the overall kinetic model and framework which takes account of the properties of the lower temperature flames of §4, were equally unsuccessful. Thus, with $\sigma_H = 0.30$ nm, set 2 of rate parameters leads to a computed burning velocity of 267 cm s^{-1} for the 41 % hydrogen–air flame (table 14); and specific excursions from this set, to correspond with the four permitted parameter changes considered in table 8, give burning velocities of 272, 266, 276 and 268 cm s^{-1} for the same flame (as shown in parentheses in the table).

PHILOSOPHICAL TRANSACTIONS OF THE ROYAL SOCIETY A MATHEMATICAL, PHYSICAL & ENGINEERING SCIENCES

These burning velocities are all within 3 % of the initial value. Taking full account of reasonable errors in the initial set 2 of rate parameters, it therefore still seems most likely that the reason for the observed departures of the predicted burning velocities of the hydrogen–air flames from the measured values should be sought in other directions. The comparison shown in figure 40 will next be discussed in relation to the measured burning velocities.

(iii) *Measured burning velocities*

A major problem in the comparison of theoretically predicted burning velocities with experiment is that the predictions strictly follow the definition of burning velocity by referring to planar flames in one-dimensional flow systems, whereas the measurements are made in flames which are frequently curved, and in flow systems which are not strictly one-dimensional. In particular, if the flow is diverging slightly, as it is in the reaction zones of all conical burner flames, then the equivalent gas velocity V (referred to unburnt gas density), which is used in the expression $S_u = V \sin \alpha$, will be slightly less for a plane near the hot side of the flame than it will be for the unburnt gas just entering it.

In § 9 (*a*) it was shown that the important, rate controlling process of radical production occurs in the hotter regions of flames. A natural corollary to this is that burning velocity measurements in flames which are not truly one-dimensional should be related to some position at the hot end of the flame. This is often not the approach which is used in experiments. Burning velocity measurements, even in systems which are not truly one-dimensional, are normally referred to a plane as near as possible to the cold side of the flame. This applies also to the measurements of Edmondson & Heap (1971) and Günther & Janisch (1971, 1972). Both of these pairs of authors measured the gas velocity V on approach to the flame and used this directly to derive the burning velocity.

With the help of the flame profiles shown in figures 21, 23, 25 and 27, it is possible to estimate the thickness of the flames containing 60, 50, 41 and 30 % hydrogen, from the point of first appreciable temperature rise to the position of maximum hydrogen atom concentration. These thicknesses are 0.6, 0.4, 0.35 and 0.35 mm, respectively. With the additional knowledge of the radius of the base of a conical flame at the position of first temperature rise, the approximate base radius at the position of maximum hydrogen atom concentration may be obtained, for not too large cone angles, by simple addition. Then for the same cone half-angle α, the areas of the slant faces of the two cones are proportional to the squares of their base radii, and multiplication of a reported, measured burning velocity by the appropriate area ratio calculated in this way should give a reasonable estimate of the burning velocity referred to the new plane. The procedure has been used on the conical flame results of Edmondson & Heap (1971), whose 'cold' flame radius was calculated to be 4.8 mm, and on the results of Günther & Janisch (1971), whose 'cold' flame radius was taken to be the same as their nozzle radius of 2 mm. Reductions in the burning velocities of Edmondson & Heap were of the order of 15–20 %, while for the results of Günther & Janisch on the smaller burner the reductions were of the order of 30–40 % depending on the flame. The revised burning velocities on this basis are shown in figure 41. They agree well between themselves and with the theoretically predicted values. Unfortunately, although Günther & Janisch (1972) mention some flow divergence and lateral expansion in their button-shaped flames, it is impossible to apply corrections to the results from these flames without reference to the original particle track photographs.

The methods of burning velocity measurement so far discussed have referred to stationary flames supported on burners. An alternative approach which has been widely employed is by the

study of the movement of non-stationary flames in initially quiescent gas mixtures. As is well known, the observed flame speed, S_s, in such cases includes a component due to movement of gas ahead of the flame. The derivation of burning velocities from such flame speeds requires careful analysis.

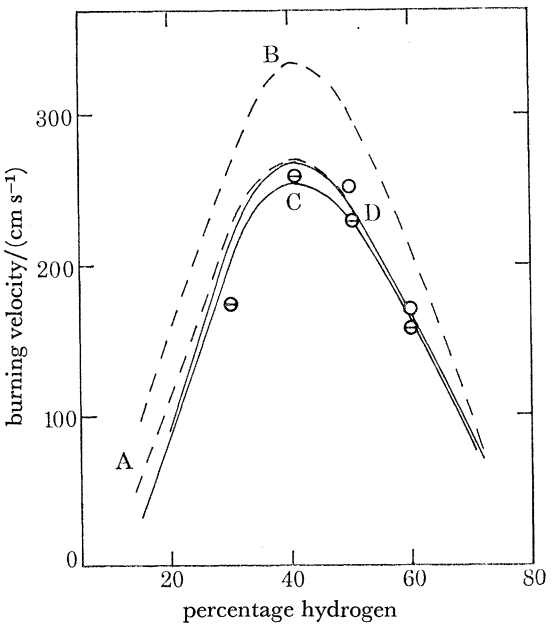

FIGURE 41. Comparison of computed and measured burning velocities of hydrogen–air mixtures. Measurements discussed in text. Points refer to adjustments to burner measurements to take approximate account of flow divergence up to the point of maximum H atom concentration: ○, Edmondson & Heap (1971); ⊖, Günther & Janisch (1971). Broken lines refer to derivations from single kernel flame speed measurements by Andrews & Bradley (1973) at 2.5 cm radius in constant volume bomb: curve A, derivation using 'thin flame' equation (7); curve B, derivation with allowance made by Andrews & Bradley for finite flame thickness (see text). Solid lines represent computed burning velocities: curve C, parameters as in table 10, with $\sigma_H = 0.35$ nm; curve D, same reaction rate parameters (from table 9), but with $\sigma_H = 0.30$ nm.

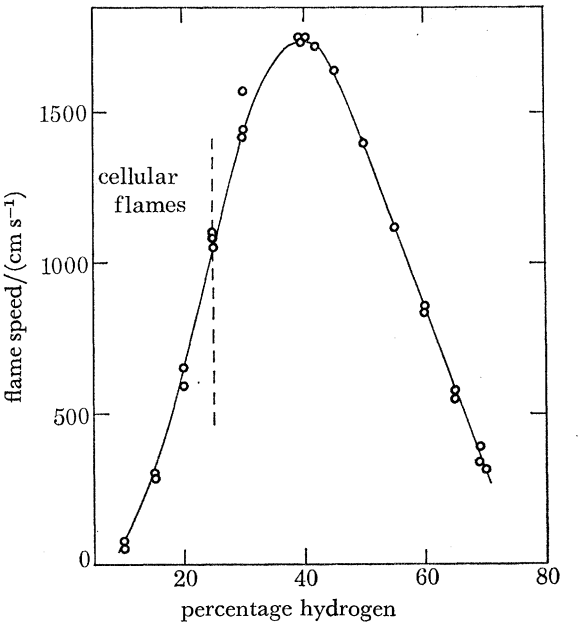

FIGURE 42. Flame speeds in hydrogen–air mixtures, as measured by Andrews & Bradley (1973) using single kernel method at 2.5 cm radius in constant volume bomb of 30 cm diameter and 30 cm length.

Andrews & Bradley (1972*a*) have critically reviewed both the stationary and non-stationary flame methods of measuring burning velocity, and have themselves used non-stationary flame methods (Andrews & Bradley 1972*b*, 1973) for the investigation of burning velocities in methane–air and hydrogen–air mixtures. In the case of the hydrogen–air mixtures attention was focused particularly (Andrews & Bradley 1973) on the determination of burning velocity from flame speeds measured in constant volume bomb explosions with single spark ignition at the centre. The hydrogen–air single kernel flame speeds measured by Andrews & Bradley (1973), at a flame radius of 2.5 cm in a cylindrical bomb of diameter 30 cm and length 30 cm, are shown in figure 42. The pressure rise is negligible at such an early stage in the explosion, and with the

assumptions of a uniformly expanding spherical flame front and an instantaneous change in gas density at the observed front from its unburnt value ρ_u to its ideal adiabatic burnt gas value ρ_b, the burning velocity can be derived by means of equation (7):

$$S_u = \frac{\rho_b}{\rho_u} S_s = \frac{\rho_b}{\rho_u} \frac{dr_b}{dt}, \tag{7}$$

where r_b is the measured radius of the core of burnt gas. Equation (7) follows directly from mass conservation considerations.

Burning velocities calculated according to equation (7) from the flame speeds of figure 42 are shown as the dotted curve A in figure 41. Curve A represents the minimum burning velocities which the hydrogen–air flames can have, consistent with the flame speed observations. On the hydrogen-rich side of stoichiometric it agrees fairly closely with the revised 'burner' values discussed above, and with the computed burning velocities (table 14). Nevertheless, there are still serious problems associated with the comparison.

Andrews & Bradley (1972*a*, *b*, 1973) have pointed out that because of the finite thickness of flame fronts in practice, equation (7) is not strictly valid, and to correct for this they have simply replaced ρ_b by a mean density $\overline{\rho_b}$ of burnt gas, given by

$$\overline{\rho_b} = 3r_b^{-3} \int_0^{r_b} \rho r^2 \, dr, \tag{8}$$

where r_b extends into the flame front itself. Because of the temperature variation in the flame, the value of $\overline{\rho_b}$ is greater than that of ρ_b, so that the replacement will lead to higher values of the burning velocity. For the planar flame front with $r = \infty$, $\overline{\rho_b} = \rho_b$.

There are two difficulties with this approach. First, the quantity $\overline{\rho_b}$ is not constant. Hence, since the mass, m_b, of the burnt gas core is given by

$$m_b = \tfrac{4}{3}\pi \overline{\rho_b} r_b^3, \tag{9}$$

the equation for the burning velocity more properly becomes

$$\begin{aligned} S_u &= \frac{1}{4\pi\rho_u r_b^2} \frac{dm_b}{dt} \\ &= \frac{1}{3\rho_u} \left\{ 3\overline{\rho_b} \frac{dr_b}{dt} + r_b \frac{d\overline{\rho_b}}{dt} \right\} \\ &= \frac{\overline{\rho_b} + \frac{1}{3} r_b (\partial \overline{\rho_b} / \partial r_b)}{\rho_u} S_s. \end{aligned} \tag{10}$$

The term $\partial\overline{\rho_b}/\partial r_b$ has a negative value which reduces the simple correction.

Secondly, and more seriously, it is not possible easily and precisely to define within the flame the plane that is responsible for the photographic record of a spherically expanding explosion wave. The available experimental evidence (Andrews & Bradley 1972*b*) suggests that the flame speed is independent of which section of the flame is optically visualized, and the theoretical results of Dixon-Lewis & Shepherd (1975) confirm that the temperature profiles in small, stationary cylindrical and spherical flames do not change appreciably with flame radius, at least at temperatures below 1000 K where refractive index changes are appreciable. On the other hand, because of the weighting given in equation (8) to the higher densities in the cooler parts of the burnt gas core near $r = r_b$, the mean density $\overline{\rho_b}$ changes very rapidly indeed depending on how much of the flame front itself is included in the core. Thus, if the profiles of the 41 % hydrogen–air

flame at $r_b \approx 2.5$ cm are the same as those in figures 25 and 26, then five assumed sets of correction data, appropriate to equation (10), are given in table 15. These correction data are calculated by graphical integration according to equation (8), and depend on the plane in the flame at which the outer integration limit r_b is assumed. In table 15, each of these assumed planes is separated from the next in the flame by only 0.1 mm; and if the flame speed associated with each plane is the same, then the whole correction procedure is clearly not meaningful. The method

TABLE 15. MEAN DENSITIES AND GRADIENTS OF MEAN DENSITIES IN EXPANDING BURNT GAS CORE OF 41 % HYDROGEN–AIR FLAME AT ATMOSPHERIC PRESSURE, UNDER SEVERAL ASSUMPTIONS REGARDING THE POSITION OF THE OUTER RADIUS r_b FOR A FIXED POSITION OF THE FLAME FRONT. $T_u = 298$ K

temp. at r_b / K	density at r_b / 10^{-4} g cm^{-3}	r_b / cm	$\overline{\rho_b}$ / 10^{-4} g cm^{-3}	$\partial\overline{\rho_b}/\partial r_b$† / 10^{-6} g cm^{-4}
300	13.50	2.51	1.342	−7.40
423	5.525	2.50	1.244	−3.45
979	2.449	2.49	1.2103	−2.36
1384	1.724	2.48	1.1996	−2.03
1563	1.522	2.47	1.1945	−1.78

† To calculate $\partial\overline{\rho_b}/\partial r_b$, values of $\overline{\rho_b}$ were calculated similarly for $r_b \approx 2.0$, 2.3, 2.7 and 3.0 cm.

therefore can only give a lower limit to the burning velocity with precision, by way of equation (7). It should be added that the adiabatic equilibrium burnt gas density for the 41 % hydrogen–air flame is $\rho_b = 1.131 \times 10^{-4}$ g cm^{-3}, so that if the conditions in the plane of maximum hydrogen atom concentration (corresponding with the last line in table 15) *control* the observed flame speed, the error introduced by using equation (7) is slightly less than 5 %. Andrews & Bradley (1973), on the other hand, introduced a maximum so-called density correction corresponding with the first line of table 15. Similar corrections which they applied to their whole series of hydrogen–air flame speed measurements led to the dotted curve B in figure 41. As already explained, however, this particular procedure is not meaningful.

The difficulty with the density correction would appear to be associated with the fact that the freely propagating flame is continuously increasing its area in such a way that the cool shells of the flame always have larger area than the hot. This is a different situation from that encountered in all stationary flames, for which stability considerations (towards perturbations) require the flow to be divergent on passing from the cold to the hot side of the flame. Although the position of first appreciable temperature rise conveniently defines a reference plane for measurement purposes, the chemical control of the flame is not exercised from there. It is exercised instead from the hot end of the flame. This, coupled with the much improved agreement between all the more precise burning velocity measurements when, as in figure 41, they are referred to a plane at the hot end of the flame, argues strongly for the siting of the reference plane in that region. By such means difficulties due to different flow configurations are avoided, and rationalization of the measurements is achieved for comparison with the theoretical predictions for one-dimensional flames.

The precise location of the correct reference plane for burning velocity measurements is a matter of some difficulty in theoretical terms, and for example the position of maximum rate of radical production might be used, or the position of maximum hydrogen atom concentration. In practical terms these difficulties are academic, since no theoretical plane can be defined in a flame for which full information is not available on the structure. For practical burning velocity

measurements, the closest easily measurable approximations to the correct reference plane will be (i) the beginning or end of the luminous zone when this is observable, or (ii) the plane at which appreciable yellow luminescence starts when a trace of a sodium salt is added to the entering gases.

These last conclusions have important implications for the technique of measuring burning velocities by burner methods. In any divergent flow situation, a stream tube corresponding with an area A_1 of flame front at the plane of first appreciable temperature rise will supply a larger area A_2 at the reference plane on the hot side of the flame. On this account, the mass flux across the reference plane is smaller than the approach mass flux of the unburnt gas at T_u in the ratio A_1/A_2, and this correction must be applied to gas velocities measured by the particle tracking technique before use of the expression $S_u = V \sin \alpha$. Burning velocities measured with the aid of the particle tracking technique, but without this area ratio correction, will be too high, and the absence of the correction is the reason for the high and inconsistent values quoted by Edmondson & Heap (1971) and Günther & Janisch (1971).

(iv) *Assessment of validity of the overall flame model*

Several assumptions which are additional to the choice of a specific series of elementary reactions are incorporated into the overall flame model from which the burning velocities and other properties are calculated. Perhaps the most fundamental of these is the assumption of a rapid interchange of translational and internal molecular energy, sufficiently so for the distribution of energy among the various degrees of freedom at any point in the flame to be represented by a single temperature. This assumption is implicit in the form of the equations used to describe the transport processes in the flame, and it is implicit also in the use of the Arrhenius form of expression to describe the change of reaction rate coefficient with temperature. However, because of relaxation problems, and in particular the problem of slow vibrational relaxation (for which Herzfeld & Litovitz (1959) quote collision numbers of the order of 10^3–10^6), it may be incorrect to use a single temperature to define both the translational and internal energy distributions at a point in faster flames, and the use of expressions which refer to systems in thermal equilibrium may not be valid. Their validity would seem to be particularly questionable when the very large magnitudes of the heat release rates in such flames are taken into account (cf. §9(*a*)). In the presence of the higher radical concentrations, for example, the possibility of kinetic repercussions such as a change in the partitioning of HO_2 between the low activation energy reactions (vii), (vii*a*), (xii), (xiii) and (xiv) as a result of a slow transfer of vibrational energy following the occurrence of reaction (iv) are not difficult to imagine.

The question next arises of the extent to which such thermal disequilibrium may affect the observed flame properties, and it was hoped to be able directly to resolve this problem in the case of the hydrogen–air flames by comparison of the computed and measured burning velocities. In the event, however, the attempt at comparison initially raised more questions than it answered, particularly as regards the burning velocity measurements. Nevertheless, the discussion in §9(*b*) (iii) has shown that the 'best' value of the burning velocity of the 41% hydrogen–air flame at atmospheric pressure is certainly not less than 270 cm s^{-1} (curve A of figure 41), and is probably about 5% greater than this. The supposed optimum value would be within the range of (285 ± 10) cm s^{-1}. If the closed vessel flame speed results for the 70% hydrogen–air flame are corrected to the plane of the maximum hydrogen atom concentration in the same way as was done for the flame containing 41% hydrogen, the resulting burning velocity is only 1.5% above

the 'thin' flame value obtained from equation (7). Within the limits of error of the flame speed measurement, it is here indistinguishable from the computed value.

The continuous lines C and D in figure 41 again show the computed burning velocities of the range of hydrogen–air flames, calculated with $\sigma_H = 0.35$ and 0.30 nm, respectively. Curve D agrees moderately well with the supposed optimum experimental curve on the fuel-rich side of stoichiometric, but it eventually becomes substantially lower even than the 'minimum' experimental curve A in lean flames. It has been shown that this last departure cannot be connected with inadequacies in the quasi-steady state assumptions; but it may be due to some other unlocated shortcoming in the kinetic model. A second possibility is that of unrealistically high measured burning velocities much on the lean side of stoichiometric, because of the appearance of cellular flame phenomena in that region. This second possibility makes the continued investigation of the kinetic model a doubtful proposition. The agreement in fuel-rich flames leads to the conclusion that thermal disequilibrium effects even in the faster flames do not cause departures of more than a small percentage from the computed burning velocities.

(*c*) *Flux profiles in the flames, and diffusion effects*

The discussion in §9(*a*) and (*b*) has centred essentially on the chemical and reaction kinetic aspects of the hydrogen–oxygen supported flames. In this final section of discussion attention will be directed towards the physical characteristics of the propagation mechanism. These have already been discussed briefly by Dixon-Lewis (1970*a*) and Day *et al.* (1972) in connection with the low temperature flames of table 2, but the same characteristics are shown also by the higher temperature hydrogen–air flames, both on the fuel-rich and fuel-lean sides of the stoichiometric composition.

(i) A curious feature of all the flames studied, as shown in the odd-numbered figures 19–33, is the *increase* in molecular oxygen concentration in the early part of the flame, and the early stage also at which the nitrogen mole fraction increases. Both effects are associated with the high diffusion coefficient of molecular hydrogen.

(ii) The contribution of *thermal diffusion* to the transport fluxes is a matter of considerable interest, since the temperature gradients in flames are quite high. In none of the hydrogen–air flames studied were the thermal diffusional fluxes of either molecular oxygen or steam found to be more than a small percentage of the ordinary diffusional fluxes. As an illustrative example, the magnitudes of the various fluxes of molecular oxygen in the 60% hydrogen–air flame are shown in figure 43. Positive values denote fluxes from left to right (or cold to hot in the flame) and vice versa. For molecular hydrogen the situation is different. Figures 44–46 show the various fluxes of molecular hydrogen in the flames containing initially 60, 41 and 15% hydrogen. Clearly the thermal diffusional flux is appreciable in all cases. However, in the 15% hydrogen–air flame, where the absolute concentrations of hydrogen are smaller than in the other two flames, the thermal diffusional flux is also relatively smaller; the same applies as between the flames containing 41 and 60% hydrogen. The relative magnitude of the thermal diffusional flux compared with ordinary diffusion decreases with decreasing absolute concentration of the light species.

(iii) Compared with ordinary diffusion, the contribution of thermal diffusion towards the fluxes of free radicals, in particular hydrogen atoms, is also small. The concentration effect here is aided by the fact that at the steepest gradient of $\ln(T)$ (near the start of the reaction zone) the radical concentrations are virtually zero. The fluxes of hydrogen atoms in the flames containing 41 and 15% hydrogen are shown in figures 47 and 48.

PHILOSOPHICAL TRANSACTIONS OF THE ROYAL SOCIETY A MATHEMATICAL, PHYSICAL & ENGINEERING SCIENCES

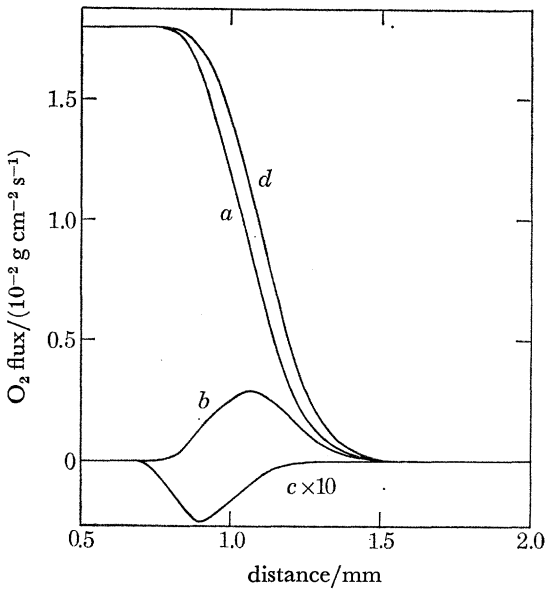

FIGURE 43. Molecular oxygen fluxes in 60% hydrogen–air flame. Curve *a*, convective flux, $M_y w_{O_2}$, where w is mass fraction; curve *b*, ordinary diffusional flux; curve *c*, thermal diffusional flux; curve *d*, overall flux, $M_y G_{O_2}$. Positive values denote fluxes from left to right (cold to hot in flame) and vice versa.

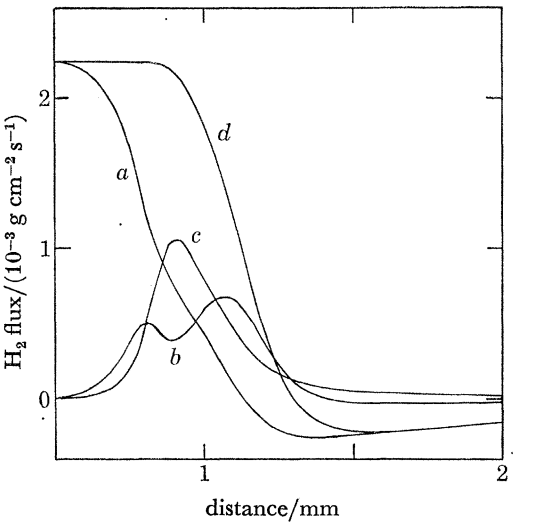

FIGURE 44. Molecular hydrogen fluxes in 60% hydrogen–air flame. Curve *a*, convective flux, $M_y(w_{H_2} - w_{H_2,b})$; curve *b*, ordinary diffusional flux; curve *c*, thermal diffusional flux; curve *d*, overall flux, $M_y(G_{H_2} - G_{H_2,b})$. Positive values denote fluxes from left to right (cold to hot in flame) and vice versa.

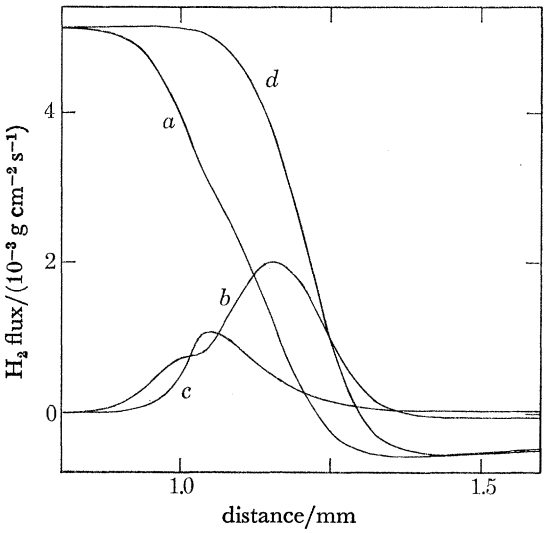

FIGURE 45. Molecular hydrogen fluxes in 41% hydrogen–air flame. Curve *a*, convective flux, $M_y(w_{H_2} - w_{H_2,b})$; curve *b*, ordinary diffusional flux; curve *c*, thermal diffusional flux; curve *d*, overall flux, $M_y(G_{H_2} - G_{H_2,b})$. Positive values denote fluxes from left to right (cold to hot in flame) and vice versa.

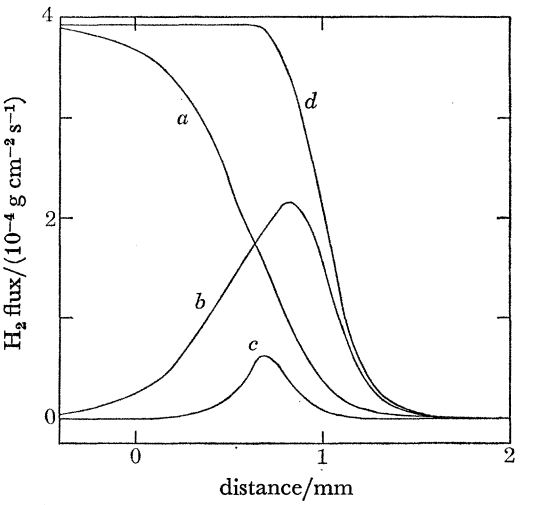

FIGURE 46. Molecular hydrogen fluxes in 15% hydrogen–air flame. Curve *a*, convective flux, $M_y w_{H_2}$; curve *b*, ordinary diffusional flux; curve *c*, thermal diffusional flux; curve *d*, overall flux, $M_y G_{H_2}$. Positive values denote fluxes from left to right (cold to hot in flame) and vice versa.

(iv) Despite the comparatively small magnitude of the flux, thermal diffusion of hydrogen atoms does have a significant effect on the burning velocity of hydrogen–air flames. G. Tsatsaronis (private communication, 1977) has obtained solutions to the time-dependent equations for the 20, 30 and 41 % hydrogen–air flames, in which only thermal diffusion of molecular hydrogen, oxygen, nitrogen and steam were considered. Table 16 compares the results of these calculations with the results of table 14 for the same flames. In obtaining the results of table 14, the thermal diffusion of all the radicals as well as the molecular species was considered. The comparison clearly shows that neglect of the thermal diffusion of hydrogen atoms causes an increase in the maximum hydrogen atom mole fraction, and approximately a 5 or 6 % increase in burning velocity. Although of small magnitude compared with ordinary diffusion, the effect of thermal diffusion, which produces a positive flux of hydrogen atoms, is to take the place of some of the convective flux of the alternative computations.

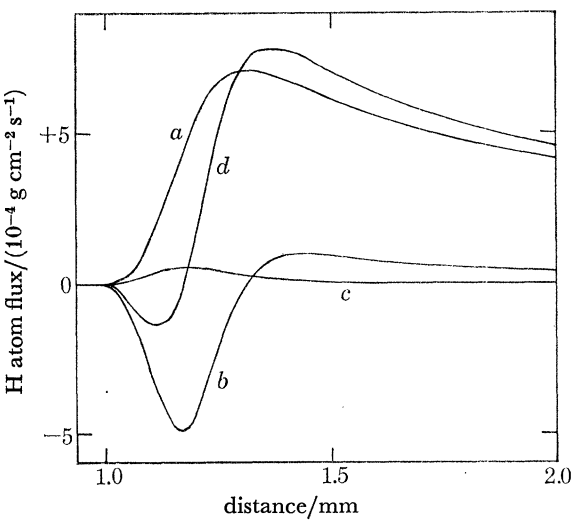

FIGURE 47. Atomic hydrogen fluxes in 41 % hydrogen–air flame. Curve *a*, convective flux, $M_y w_H$; curve *b*, ordinary diffusional flux; curve *c*, thermal diffusional flux; curve *d*, overall flux, $M_y G_H$. Positive values denote fluxes from left to right (cold to hot in flame) and vice versa.

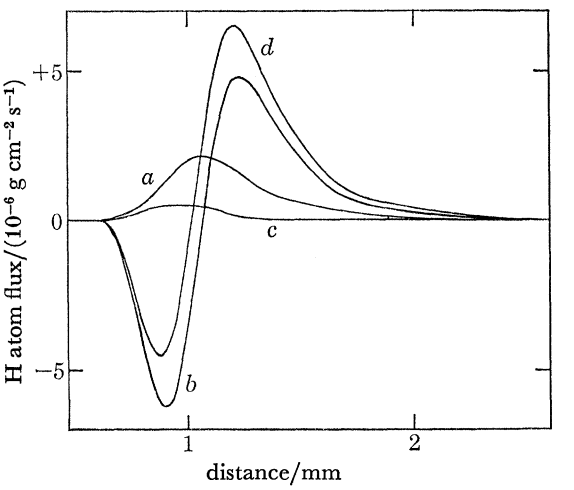

FIGURE 48. Atomic hydrogen fluxes in 15 % hydrogen–air flame. Curve *a*, convective flux, $M_y w_H$; curve *b*, ordinary diffusional flux; curve *c*, thermal diffusional flux; curve *d*, overall flux, $M_y G_H$. Positive values denote fluxes from left to right (cold to hot in flame) and vice versa.

(v) The negative slopes of the overall flux curves *d* for hydrogen atoms early in the reaction zones (figures 47 and 48) correspond with the chemical removal of hydrogen atoms in these regions (cf. figures 38 and 39). The hydrogen atoms are formed chemically only at higher temperatures, as already discussed in § 9 (*a*), and they arrive in the cooler regions by diffusion against the gas flow. Because of the simultaneous occurrence of the low activation energy, heat releasing, chain propagating steps at the lower temperatures, the effect of increasing the diffusion coefficient of hydrogen atoms (by decreasing σ_H) is to *increase* the burning velocity in all the hydrogen–air flames, while not appreciably affecting the burning velocities of the lower temperature $H_2/O_2/N_2$ flames discussed in § 4. These effects are contrary to that obtained using a simpler reaction mechanism which did not include the formation and subsequent low temperature reactions of the hydroperoxyl radical (Dixon-Lewis 1967). In that computation, and in other computations using similar simple reaction mechanisms (see, for example, Giddings & Hirschfelder 1957), the

effect of increasing the diffusion coefficient of hydrogen atoms was to *decrease* the burning velocity. The effect of varying the diffusion velocity of the radical species thus appears to depend on some of the detail of the reaction mechanism.

(vi) An interesting additional feature of the hydrogen atom flux curves is provided by the relative magnitudes of the convective and diffusional fluxes in the positive direction, towards the burnt gas in the two flames of figures 47 and 48. Radical diffusion in the positive direction represent a diffusional loss to the main flame zone, and at low burning velocities this loss becomes relatively larger compared with the convective flux. The phenomenon may have some relevance to the occurrence of flammability limits.

TABLE 16. EFFECT OF THERMAL DIFFUSION OF HYDROGEN ATOMS ON COMPUTED PROPERTIES OF THREE HYDROGEN–AIR FLAMES HAVING $T_u = 298$ K AT ATMOSPHERIC PRESSURE

(Reaction rate parameters from table 9.)

	Thermal diffusion of H included				Thermal diffusion of H neglected			
σ_H/nm =	0.35		0.30		0.35		0.30	
$X_{H_2,u}$	S_u/(cm s^{-1})	$10^2 X_{H,max}$	S_u/(cm s^{-1})	$10^2 X_{H,max}$	S_u/(cm s^{-1})	$10^2 X_{H,max}$	S_u/(cm s^{-1})	$10^2 X_{H,max}$
0.41	—	—	267	7.46	266	—	282	—
0.30	200	4.69	211	4.65	212	4.80	224	—
0.20	—	—	89	1.07	91	—	95	—

10. CONCLUSIONS

Structure measurements in several low temperature, fuel-rich hydrogen–oxygen–nitrogen flames have been considered together with recombination data from a wider range of flames, and information obtained from studies of other aspects of the hydrogen–oxygen reaction system, in order to derive a reasonable set of rate parameters for the flame reactions. Three sets of such parameters are given as sets 1, 2 and 3 in table 4. The reaction mechanism and one set of the rate parameters (§7 and table 9) were then used to calculate the properties of the whole composition range of hydrogen–air premixed flames. Computation of all the flame properties was carried out initially by the composite flux method of Dixon–Lewis *et al.* (1975*a*). Partial equilibrium assumptions on reactions (i), (ii) and (iii) may be employed to relate the concentrations of H, OH, O and O_2 in calculations where only the concentration profiles in the recombination regions of the flames are required. In the calculation of the complete flame properties, quasi-steady state assumptions must be used to relate the concentrations either of O, OH and HO_2 with that of H (rich flame formulation), or of H, O and HO_2 with that of OH (lean flame formulation). The following features emerge:

(*a*) The partial equilibrium assumptions lead to a radical pool which continues to increase in size indefinitely on integration backwards from the hot boundary of a flame. With the quasi-steady state assumption, on the other hand, the overall radical pool, represented by $(X_H + 2X_O + X_{OH})$, rises to a maximum and then decreases to zero again on the cold side of the flame. For all except the lower temperature 15% hydrogen–air flame, and to some extent the 70% hydrogen–air flame, the partial equilibrium and quasi-steady state profiles were indistinguishable almost up to the maxima in the latter. The partial equilibrium assumptions are valid over the whole of the region of coincidence, for those species having significant concentrations.

(*b*) On continuing the integration further backwards into the main reaction zones of the flames,

the quasi-steady state overall radical profiles fall below those calculated with partial equilibrium assumptions, as already implied. On the other hand, in fuel-rich flames the distribution of the pool between H, OH and O in this region becomes such that the comparatively small quasi-steady state oxygen atom concentration, and to a lesser extent also the hydroxyl radical concentration, appreciably overshoot their partial equilibrium values. This is the phenomenon of *kinetic overshoot*. It is observable only in sufficiently fuel-rich flames, and for example, there is no observable hydroxyl radical kinetic overshoot in hydrogen–air flames containing less than 41 % hydrogen at atmospheric pressure, and no oxygen atom kinetic overshoot in those with less than 30 % hydrogen.

(*c*) It was found that the quasi-steady state assumptions were not strictly valid over the whole of the reaction zones of the flames studied, at least not for oxygen atoms. However, the effect of this departure from the assumed conditions on the computed flame properties was found to be negligible.

(*d*) The general pattern of flame structure which emerges from the calculations is one in which radicals are produced by chain branching reactions in the hotter regions of the flames, while the major heat releasing reactions occur at lower temperatures. Ahead of the reaction zone there is only a very small preheat region where heating occurs purely by thermal conduction. At the low temperature end of the reaction zone, radicals diffusing upstream from the high temperature source meet and react exothermally with incoming molecular oxygen by low activation energy steps. The behaviour is different from that of flame models which assume a single global reaction with high activation energy.

(*e*) The comparison of the computed burning velocities with measured values is not straightforward. This is because the computation refers to a strictly one-dimensional flow system, whereas measurements are carried out only on flames which approximate more or less to this state. Thus, for example, stability considerations alone dictate that stationary flames shall propagate in a flow which diverges towards the hot side of the flame. The problem then arises of defining, if this is possible, a controlling reference plane in the flame, so that measured burning velocities are independent of the specific system in which they are measured, and so that hopefully they are also representative of the true one-dimensional flow situation. Having regard to the flame mechanism as discussed in § 9 and summarized in the preceding paragraph, it becomes most logical to choose a plane towards the hot end of the flame for this purpose. In the present case the plane was chosen at which the hydrogen atom concentration is a maximum. On this basis, the computed burning velocities of the hydrogen–air flames agree with experiment for compositions near the rich flammability limit, but become gradually lower than experiment as the composition moves towards stoichiometric and into the lean flame region. At the maximum burning velocity (41 % hydrogen–air flame) the predicted values given in parentheses in table 8 are between 3 and 7 % below the middle of the optimum measured range of (285 ± 10) cm s^{-1}.

(*f*) For the reaction mechanism which includes participation of the hydroperoxyl radical, an increase in the diffusion coefficient of hydrogen atoms results in an increase in computed burning velocity of all the hydrogen–air flames at atmospheric pressure. A reduction in σ_H from 0.30 nm as used in table 8 to the value of 0.27 nm recommended by Svehla (1962) would increase all the computed burning velocities of the 41 % hydrogen–air flame by 2.5 %.

(*g*) Other conditions being equal in hydrogen–air flames near stoichiometric, calculations in which thermal diffusion of hydrogen atoms is considered give burning velocities some 5 or 6 % lower than similar calculations where such thermal diffusion is neglected.

It is a pleasure to thank British Gas for their support of this work. I also wish to thank Dr Ing. G. Tsatsaronis for his collaboration in obtaining solutions of the time-dependent equations for some of the hydrogen–air flames.

References

Andrews, G. E. & Bradley, D. 1972*a* *Combust. Flame* **18**, 133.
Andrews, G. E. & Bradley, D. 1972*b* *Combust. Flame* **19**, 275.
Andrews, G. E. & Bradley, D. 1973 *Combust. Flame* **20**, 77.
Baldwin, R. R., Fuller, M. E., Hillman, J. S., Jackson, D. & Walker, R. W. 1974 *J. chem. Soc., Faraday Trans.* I, **70**, 635.
Baulch, D. L., Drysdale, D. D., Horne, D. G. & Lloyd, A. C. 1972 *Evaluated kinetic data for high temperature reactions*, vol. 1. London: Butterworths.
Baulch, D. L. & Drysdale, D. D. 1974 *Combust. Flame* **23**, 215.
Bennett, J. E. & Blackmore, D. R. 1971 *Thirteenth Symposium* (*Int.*) *on Combustion*, p. 51. Pittsburgh: Combustion Institute.
Bennett, R. G. & Dalby, F. W. 1964 *J. chem. Phys.* **40**, 1414.
Bishop, W. P. & Dorfman, L. M. 1970 *J. chem. Phys.* **52**, 3210.
Burrows, J. P., Harris, G. W. & Thrush, B. A. 1977 *Nature, Lond.* **267**, 233.
Clyne, M. A. A. & Thrush, B. A. 1963 *Proc. R. Soc. Lond.* A **275**, 559.
Day, M. J., Dixon-Lewis, G. & Thompson, K. 1972 *Proc. R. Soc. Lond.* A **330**, 199.
Day, M. J., Thompson, K. & Dixon-Lewis, G. 1973 *Fourteenth Symposium* (*Int.*) *on Combustion*, p. 47. Pittsburgh: Combustion Institute.
Del Greco, F. P. & Kaufman, F. 1963 *Ninth Symposium* (*Int.*) *on Combustion*, p. 659. New York: Academic Press.
De Zafra, R. L., Marshall, A. & Metcalf, H. 1971 *Phys. Rev.* A **3**, 1557.
Dixon-Lewis, G. 1967 *Proc. R. Soc. Lond.* A **298**, 495.
Dixon-Lewis, G. 1968 *Proc. R. Soc. Lond.* A **307**, 111.
Dixon-Lewis, G. 1970*a* *Proc. R. Soc. Lond.* A **317**, 235.
Dixon-Lewis, G. 1970*b* *Combust. Flame* **15**, 197.
Dixon-Lewis, G. 1972 *Proc. R. Soc. Lond.* A **330**, 219.
Dixon-Lewis, G., Goldsworthy, F. A. & Greenberg, J. B. 1975*a* *Proc. R. Soc. Lond.* A **346**, 261.
Dixon-Lewis, G., Greenberg, J. B. & Goldwsorthy, F. A. 1975*b* *Fifteenth Symposium* (*Int.*) *on Combustion*, p. 717. Pittsburgh: Combustion Institute.
Dixon-Lewis, G., Isles, G. L. & Walmsley, R. 1973 *Proc. R. Soc. Lond. A* **331**, 571.
Dixon-Lewis, G. & Shepherd, I. G. 1975 *Fifteenth Symposium* (*Int.*) *on Combustion*, p. 1483. Pittsburgh: Combustion Institute.
Dixon-Lewis, G., Sutton, M. M. & Williams, A. 1962 *Disc. Faraday Soc.* **33**, 205.
Dixon-Lewis, G., Sutton, M. M. & Willlams, A. 1965 *Trans. Faraday Soc.* **61**, 255.
Dixon-Lewis, G., Sutton, M. M. & Williams, A. 1970 *Proc. R. Soc. Lond.* A **317**, 227.
Dixon-Lewis, G. & Williams, D. J. 1977 *Comprehensive chemical kinetics* (ed. C. H. Bamford & C. F. H. Tipper), vol. 17, p. 1. Amsterdam: Elsevier.
Dodonov, A. F., Lavrovskaya, G. K. & Talrose, V. L. 1969 *Kinet. Katal.* **10**, 701.
Eberius, K. H., Hoyermann, K. & Wagner, H. Gg. 1969 *Ber. Bunsenges. phys. Chem.* **73**, 962.
Edmondson, H. & Heap, M. P. 1971 *Combust. Flame* **16**, 161.
Elmergreen, B. G. & Smith, W. H. 1972 *Astrophys. J.* **178**, 557.
Fenimore, C. P. & Jones, G. W. 1965 *Tenth Symposium* (*Int.*) *on Combustion*, p. 489. Pittsburgh: Combustion Institute.
Foner, S. N. & Hudson, R. L. 1962 *Adv. Chem. Ser.* **36**, 34.
Friswell, N. J. & Sutton, M. M. 1972 *Chem. Phys. Lett.* **15**, 108.
Gay, A. & Pratt, N. H. 1971 *Proc. 8th Shock Tube Symp.*, paper 39. London: Chapman & Hall.
German, K. R. & Zare, R. N. 1969*a* *Phys. Rev.* **186**, 9.
German, K. R. & Zare, R. N. 1969*b* *Phys. Rev. Lett.* **23**, 1207.
German, K. R. & Zare, R. N. 1970 *Bull. Am. Phys. Soc.* **15**, 82.
Getzinger, R. W. & Blair, L. S. 1969 *Combust. Flame* **13**, 271.
Giddings, J. C. & Hirschfelder, J. O. 1957 *Sixth Symposium* (*Int.*) *on Combustion*, p. 199. New York: Reinhold.
Golden, D. M., del Greco, F. P. & Kaufman, F. 1963 *J. chem. Phys.* **39**, 3034.
Günther, R. & Janisch, G. 1971 *Chemie-Ingr-Tech.* **43**, 975.
Günther, R. & Janisch, G. 1972 *Combust. Flame* **19**, 49.
Halstead, C. J. & Jenkins, D. R. 1969 *Twelfth Symposium* (*Int.*) *on Combustion*, p. 979. Pittsburgh: Combustion Institute.

PHILOSOPHICAL TRANSACTIONS OF THE ROYAL SOCIETY A MATHEMATICAL, PHYSICAL & ENGINEERING SCIENCES

Halstead, C. J. & Jenkins, D. R. 1970 *Combust. Flame* **14**, 321.
Ham, D. O., Trainor, D. W. & Kaufman, F. 1970 *J. chem. Phys.* **53**, 4395.
Ham, D. O., Trainor, D. W. & Kaufman, F. 1973 *J. chem. Phys.* **58**, 4599.
Hamilton, C. W. & Schott, G. L. 1967 *Eleventh Symposium* (*Int.*) *on Combustion*, p. 635. Pittsburgh: Combustion Institute.
Herzfeld, K. F. & Litovitz, T. A. 1959 *Absorption and dispersion of ultrasonic waves*. New York: Adademic Press Inc.
Hurle, I. R. 1967 *Eleventh Symposium* (*Int.*) *on Combustion*, p. 827. Pittsburgh: Combustion Institute.
Jacobs, T. A., Giedt, R. R. & Cohen, N. 1967 *J. chem. Phys.* **47**, 54.
Jahn, G. 1934 *Der Zundvorgang in Gasgemischen*. Berlin: Oldenbourg.
JANAF 1971 *Thermochemical Tables*, 2nd ed. National Bureau Standards Publication NSRDS-NBS37, Washington, D.C.
Kaskan, W. E. 1958*a* *Combust. Flame* **2**, 229.
Kaskan, W. E. 1958*b* *Combust. Flame* **2**, 286.
Larkin, F. S. & Thrush, B. A. 1964 *Disc. Faraday Soc.* **37**, 112.
Larkin, F. S. & Thrush, B. A. 1965 *Tenth Symposium* (*Int.*) *on Combustion*, p. 397. Pittsburgh: Combustion Institute.
Moortgat, G. K. & Allen, E. R. 1972 Paper presented at 163rd *Am. chem. Soc. National Meeting*, Boston.
Olderberg, O. & Rieke, F. F. 1938 *J. chem. Phys.* **6**, 439.
Padley, P. J. & Sugden, T. M. 1959 *Seventh Symposium* (*Int.*) *on Combustion*, p. 235. London: Butterworths.
Paukert, T. T. & Johnston, H. S. 1972 *J. chem. Phys.* **56**, 2824.
Rink, J. P. 1962 *J. chem. Phys.* **36**, 262.
Rouse, P. E. & Engleman, R. 1973 *J. quant. Spectrosc. radiat. Transfer*, **13**, 1503.
Scholte, T. G. & Vaags, P. B. 1959 *Combust. Flame* **3**, 495.
Semenov, N. 1940 *Prog. Phys. Sci. USSR* **24**, 433.
Sutton, E. A. 1962 *J. chem. Phys.* **36**, 2923.
Sutton, M. M. 1963 M.Sc. thesis, University of Leeds.
Svehla, R. A. 1962 *NASA tech. rep.* R-**132**.
Tröe, J. 1969 *Ber. Bunsenges. phys. Chem.* **73**, 946.
Walkauskas, P. & Kaufman, F. 1975 *Fifteenth Symposium* (*Int.*) *on Combustion*, p. 691. Pittsburgh: Combustion Institute.
Westenberg, A. A. & de Haas, N. 1972 *J. phys. Chem.* **76**, 1586.
Wong, W. & Davis, D. D. 1974 *Int. J. chem. Kinet.* **6**, 401.
Zeldovich, Y. B. 1947 *Zh. tekh. Fiz.* **17**, 3.
Zeldovich, Y. B. & Frank-Kamenetskii, D. A. 1938*a* *Dokl. Akad. Nauk SSSR* **19**, 693, 699.
Zeldovich, Y. B. & Frank-Kamenetskii, D. A. 1938*b* *Zh. fiz. Khim.* **12**, 100.
Zeldovich, Y. B. & Frank-Kamenetskii, D. A. 1938*c* *Acta phys.-chim. URSS* **9**, 341.
Zeldovich, Y. B. & Semenov, N. 1940 *Zh. éksp. teor. Fiz.* **10**, 1116, 1427.
Zellner, R., Erler, K. & Field, D. 1977 *Sixteenth Symposium* (*Int.*) *on Combustion*, p. 939. Pittsburgh: Combustion Institute.

PHILOSOPHICAL TRANSACTIONS OF THE ROYAL SOCIETY A MATHEMATICAL, PHYSICAL & ENGINEERING SCIENCES